

Drivers of plant nutrient acquisition and allocation strategies and their influence
on plant responses to environmental change

by

Evan A. Perkowski, B.S.

A Dissertation

In

Biological Sciences

Submitted to the Graduate Faculty
of Texas Tech University in
Partial Fulfillment of
the Requirements for
the Degree of

Doctor of Philosophy

Approved

Nicholas G. Smith, Ph.D.
Chair of Committee

Aimée T. Classen, Ph.D.

Natasja van Gestel, Ph.D.

Lindsey C. Slaughter, Ph.D.

Dylan W. Schwilk, Ph.D.

Mark Sheridan, Ph.D.
Dean of the Graduate School

May 2023

Copyright 2023, Evan A. Perkowski

Acknowledgements

Placeholder for text

Table of Contents

Acknowledgements	ii
Abstract	vii
List of Tables	viii
List of Figures	x
1. Introduction	1
2. Structural carbon costs to acquire nitrogen are determined by nitrogen and light availability in two species with different nitrogen acquisition strategies	8
2.1 Introduction	8
2.2 Methods	12
2.2.1 <i>Experiment setup</i>	12
2.2.2 <i>Plant measurements and calculations</i>	13
2.2.3 <i>Statistical analyses</i>	14
2.3 Results	16
2.3.1 <i>Carbon costs to acquire nitrogen</i>	16
2.3.2 <i>Whole plant nitrogen biomass</i>	19
2.3.3 <i>Root carbon biomass</i>	21
2.3.4 <i>Root nodule biomass</i>	23
2.4 Discussion	27
2.4.1 <i>Carbon costs to acquire nitrogen increase with light availability and decrease with fertilization</i>	27
2.4.2 <i>Modeling implications</i>	29
2.4.3 <i>Study limitations</i>	31
2.4.4 <i>Conclusions</i>	33
3. Soil nitrogen availability modifies leaf nitrogen economies in mature temperate deciduous forests: a direct test of photosynthetic least-cost theory	35
3.1 Introduction	35

3.2 Methods	39
3.2.1 <i>Study site description</i>	39
3.2.2 <i>Experimental design</i>	40
3.2.3 <i>Leaf gas exchange and trait measurements</i>	40
3.2.4 A_{net}/C_i curve-fitting and parameter estimation	43
3.2.5 Proportion of leaf nitrogen allocated to photosynthesis and structure	45
3.2.6 Tradeoffs between nitrogen and water use	46
3.2.7 Soil nitrogen availability and pH	47
3.2.8 Statistical analyses	49
3.3 Results	51
3.3.1 Leaf N content	51
3.3.2 Net photosynthesis and leaf biochemistry	54
3.3.3 Leaf N allocation	57
3.3.4 Tradeoffs between nitrogen and water use	60
3.4 Discussion	63
3.4.1 Soil nitrogen availability modifies tradeoffs between nitrogen and water use	64
3.4.2 Soil pH did not modify tradeoffs between nitrogen and water usage	66
3.4.3 Species identity explains a large amount of variation in leaf and whole plant traits	67
3.4.4 Implications for photosynthetic least-cost theory model development	68
3.4.5 Conclusions	70
4. The relative cost of resource use for photosynthesis drives variance in leaf nitrogen content across a climate and soil resource availability gradient	71
4.1 Introduction	71
4.2 Methods	77
4.2.1 Site descriptions and sampling methodology	77

4.2.2	<i>Leaf trait measurements</i>	77
4.2.3	<i>Site climate data</i>	83
4.2.4	<i>Site edaphic characteristics</i>	83
4.2.5	<i>Plant functional group assignments</i>	85
4.2.6	<i>Data analysis</i>	86
4.3	Results	89
4.3.1	<i>Cost to acquire nitrogen relative to water (β)</i>	89
4.3.2	<i>Leaf $C_i:C_a$</i>	92
4.3.3	<i>Leaf nitrogen content</i>	96
4.3.4	<i>Structural equation model</i>	100
4.4	Discussion	103
4.4.1	<i>Negative effects of leaf $C_i:C_a$ on N_{area} are driven by reductions in M_{area}, not N_{mass}</i>	103
4.4.2	<i>Soil nitrogen availability increases N_{area} through changes in the cost to acquire nitrogen</i>	105
4.4.3	<i>Soil moisture increases N_{area} by facilitating increases in soil nitrogen availability</i>	106
4.4.4	<i>Indirect effects of climate on N_{area} are mediated through changes in leaf $C_i:C_a$ and β</i>	107
4.4.5	<i>Species identity traits modify effects of the environment on β, leaf $C_i:C_a$, and N_{area}</i>	107
4.4.6	<i>Next steps for optimality model development</i>	109
4.4.7	<i>Conclusions</i>	110
5.	Optimal resource investment to photosynthetic capacity maximizes nutrient allocation to whole plant growth under elevated CO₂	111
5.1	Introduction	111
5.2	Methods	116
5.2.1	<i>Seed treatments and experimental design</i>	116
5.2.2	<i>Growth chamber conditions</i>	117
5.2.3	<i>Leaf gas exchange measurements</i>	119

5.2.4 <i>Leaf trait measurements</i>	120
5.2.5 <i>A/C_i curve fitting and parameter estimation</i>	122
5.2.6 Stomatal limitation	122
5.2.7 <i>Proportion of leaf nitrogen allocated to photosynthesis and structure</i>	123
5.2.8 <i>Whole plant traits</i>	125
5.2.9 <i>Statistical analyses</i>	127
5.3 Results	129
5.3.1 <i>Leaf nitrogen and chlorophyll content</i>	129
5.3.2 <i>Leaf biochemistry and stomatal conductance</i>	133
5.3.3 <i>Leaf nitrogen allocation</i>	137
5.3.4 <i>Whole plant traits</i>	141
5.3.5 <i>Nitrogen fixation</i>	145
5.4 Discussion	149
5.4.1 <i>Soil nitrogen fertilization has divergent effects on leaf and whole plant acclimation responses to CO₂</i>	150
5.4.2 <i>Implications for future model development</i>	154
5.4.3 <i>Study limitations and future directions</i>	155
5.4.4 <i>Conclusions</i>	157
6. Conclusions	159
References	161

Abstract

List of Tables

2.1 Analysis of variance results exploring species-specific effects of light availability, nitrogen fertilization, and their interactions on carbon costs to acquire nitrogen (N_{cost}), whole-plant nitrogen biomass (N_{wp}), and root carbon biomass (C_{bg})	17
2.2 Analysis of variance results exploring effects of light availability, nitrogen fertilization, and their interactions on <i>G. max</i> root nodule biomass and the ratio of root nodule biomass to root biomass* . . .	24
2.3 Slopes of the regression line describing the relationship between each dependent variable and nitrogen fertilization at each light level* . .	25
3.1 Effects of soil N availability, soil pH, and species on leaf N content per unit leaf area (N_{area}), leaf N content per unit leaf mass (N_{mass}), and leaf mass per unit leaf area (M_{area})	52
3.2 Effects of soil N availability, soil pH, species, and N_{area} on leaf biochemistry	55
3.3 Effects of soil N availability, soil pH, and species on the proportion of leaf nitrogen content allocated to photosynthesis, Rubisco, bioenergetics, and structure	58
3.4 Effects of soil N availability, soil pH, species, and N_{area} on tradeoffs between nitrogen and water use	61

4.1	Site locality information, sampling year(s), 2006-2020 mean annual precipitation (MAP; mm), mean annual temperature (MAT; °C), and water holding capacity (WHC; mm)*	81
4.2	Effects of soil moisture, soil nitrogen availability, and plant functional group on β	90
4.3	Effects of soil moisture, soil nitrogen availability, and plant functional group on χ^*	94
4.4	Effects of soil nitrogen fertilization, inoculation, and CO ₂ treatments on N_{area} , N_{mass} , and M_{area}	98
4.5	Structural equation model results investigating direct effects of climatic and soil resource availability on N_{area} , N_{mass} , M_{area} , leaf $C_{\text{i}}:C_{\text{a}}$, and β	101
5.1	Effects of soil nitrogen fertilization, inoculation, and CO ₂ treatments on N_{area} , N_{mass} , M_{area} , and Chl_{area}	131
5.2	Effects of soil nitrogen fertilization, inoculation, and CO ₂ on leaf biochemistry	135
5.3	Effects of soil N availability, soil pH, species, and N_{area} on leaf nitrogen allocation	139
5.4	Effects of soil N availability, soil pH, species, and N_{area} on total leaf area, whole plant biomass, and carbon costs to acquire nitrogen . .	143
5.5	Effects of soil N availability, soil pH, species, and N_{area} on root nodule biomass and plant investments in symbiotic nitrogen fixation	147

List of Figures

2.1 Relationships between soil nitrogen fertilization and light availability on carbon costs to acquire nitrogen in <i>G. hirsutum</i> and <i>G. max</i>	18
2.2 Relationships between soil nitrogen fertilization and light availability on whole-plant nitrogen biomass in <i>G. hirsutum</i> and <i>G. max</i>	20
2.3 Relationships between soil nitrogen fertilization and light availability on root carbon biomass in <i>G. hirsutum</i> and <i>G. max</i>	22
2.4 Effects of shade cover and nitrogen fertilization on root nodule biomass and the ratio of root nodule biomass to root biomass in <i>G. max</i>	26
3.1 Effects of soil N availability and species on leaf N content per unit leaf area, leaf nitrogen content per unit leaf biomass, and leaf mass per leaf area	53
3.2 Effects of soil N availability, species, and leaf N content leaf biochemistry	56
3.3 Effects of soil N availability, species, and leaf N content on the fraction of leaf nitrogen allocated to photosynthesis and structure	59
3.4 Effects of soil N availability, species, and leaf N content on tradeoffs between nitrogen and water use	62
4.1 Maps that detail site locations along 2006-2020 mean annual precipitation and mean annual temperature gradients in Texas, USA.	82

4.2 Effects of soil nitrogen availability and soil moisture on the unit cost ratio β	91
4.3 Effects of 4-day mean vapor pressure deficit, 2-day soil moisture (per water holding capacity), and soil nitrogen availability on leaf $C_i:C_a$	95
4.4 Effects of leaf $C_i:C_a$, soil nitrogen availability, and soil moisture on leaf nitrogen content per unit leaf area, leaf nitrogen content per unit leaf biomass, and leaf mass per area	99
4.5 Structural equation model results exploring direct and indirect drivers of N_{area}	102
5.1 Effects of CO_2 , fertilization, and inoculation on leaf nitrogen per unit leaf area, leaf nitrogen content, leaf mass per unit leaf area, and chlorophyll content per unit leaf area	132
5.2 Effects of CO_2 , fertilization, and inoculation on maximum rate of Rubisco carboxylation, the maximum rate of RuBP regeneration, and the ratio of the maximum rate of RuBP regeneration to the maximum rate of Rubisco carboxylation leaf mass per unit leaf area, dark respiration, stomatal conductance, and stomatal limitation	136
5.3 Effects of CO_2 , fertilization, and inoculation on the relative fraction of leaf nitrogen allocated to photosynthesis and the fraction of leaf nitrogen allocated to structure	140
5.4 Effects of CO_2 , fertilization, and inoculation on total leaf area, total biomass, and structural carbon costs to acquire nitrogen	144

5.5 Effects of CO ₂ , fertilization, and inoculation on nodule biomass, nodule: root biomass, and percent nitrogen fixed from the atmo- sphere.	148
--	-----

1 Chapter 1

2 Introduction

3 Photosynthesis represents the largest carbon flux between the atmosphere
4 and biosphere, and is regulated by complex ecosystem carbon and nutrient cy-
5 cles (Hungate et al. 2003; IPCC 2021). As a result, the inclusion of robust,
6 empirically tested representations of photosynthetic processes is critical in order
7 for terrestrial biosphere models to accurately and reliably simulate carbon and
8 nutrient fluxes between the atmosphere and terrestrial biosphere (Wieder et al.
9 2015; Smith and Dukes 2013; Prentice et al. 2015; Oreskes et al. 1994). Despite
10 evidence that the inclusion of coupled carbon and nutrient cycles can improve
11 model uncertainty, widespread divergence in predicted carbon and nutrient fluxes
12 is still apparent across model products (Arora et al. 2020; Friedlingstein et al.
13 2014; Davies-Barnard et al. 2020). Divergence in predicted carbon and nutrient
14 fluxes across terrestrial biosphere models may be due to an incomplete under-
15 standing of how plants acclimate to changing environments (Smith and Dukes
16 2013; Davies-Barnard et al. 2020), as terrestrial biosphere models are sensitive to
17 the formulation of photosynthetic processes (Ziehn et al. 2011; Bonan et al. 2011;
18 Booth et al. 2012; Smith et al. 2016; Smith et al. 2017; Rogers et al. 2017).

Many terrestrial biosphere models predict leaf-level photosynthesis through linear relationships between area-based leaf nitrogen content and the maximum rate of Ribulose-1,5-bisphosphate carboxylase/oxygenase ("Rubisco"), following from the idea that large fractions of leaf nitrogen content are allocated to the construction and maintenance of Rubisco and other photosynthetic enzymes (Evans

24 1989). The inclusion of coupled carbon and nutrient cycles in terrestrial biosphere
25 models (Shi et al. 2016; Braghieri et al. 2022) allows for the prediction of leaf ni-
26 trogen content through soil nitrogen availability, which causes models to indirectly
27 predict photosynthetic processes through shifts in soil nitrogen availability (Smith
28 et al. 2014; Lawrence et al. 2019). While these patterns are commonly observed
29 in ecosystems globally (Brix 1971; Evans 1989; Liang et al. 2020; Firn et al. 2019),
30 this formulation of photosynthetic processes does not allow for the prediction of
31 leaf and whole plant acclimation responses to changing environments (Smith and
32 Dukes 2013; Rogers et al. 2017; Harrison et al. 2021), and suggests that con-
33 stant leaf nitrogen-photosynthesis relationships are ubiquitous across ecosystems.
34 Incorporating leaf and whole plant acclimation schemes in terrestrial biosphere
35 models is important (Smith and Dukes 2013), particularly because recent work
36 indicates that variance in leaf nitrogen content and leaf photosynthesis across en-
37 vironmental gradients may be better explained as an integrated product of leaf
38 acclimation responses to changing climates and soil nitrogen availability than soil
39 nitrogen availability alone (Dong et al. 2017; Dong et al. 2020; Smith et al. 2019;
40 Querejeta et al. 2022; Dong et al. 2022; Westerband et al. 2023).

41 Photosynthetic least-cost theory (Prentice et al. 2014; Wang et al. 2017;
42 Smith et al. 2019; Scott and Smith 2022; Harrison et al. 2021) provides a con-
43 temporary framework for predicting leaf and whole plant acclimation responses
44 to environmental change. The theory, which unifies photosynthetic optimal coor-
45 dination (Chen et al. 1993; Maire et al. 2012) and least-cost (Wright et al. 2003)
46 theories, posits that plants optimize photosynthetic processes by minimizing the
47 summed cost of nitrogen and water use (referred to here and in the rest of this dis-

48 sertation as β). The minimized summed cost of nitrogen and water use is dictated
49 by the ratio of intercellular CO₂ to atmospheric CO₂ (referred to here and in the
50 rest of this dissertation as leaf C_a:C_a, or χ), which is determined by factors that
51 influence leaf nitrogen demand, such as CO₂, temperature, vapor pressure deficit,
52 and light availability (Prentice et al. 2014; Smith et al. 2019; Stocker et al. 2020;
53 Wang et al. 2017). Photosynthetic processes are optimized such that nitrogen
54 is allocated to photosynthetic enzymes in to allow net photosynthesis rates to be
55 equally co-limited by the maximum rate of Rubisco carboxylation and the max-
56 imum rate of Ribulose-1,5-bisphosphate (RuBP) regeneration (Chen et al. 1993;
57 Maire et al. 2012). The theory indicates that costs of nitrogen and water use
58 are substitutable such that, in a given environment, optimal photosynthesis rates
59 can be achieved by sacrificing inefficient use of a relatively more abundant (and
60 less costly to acquire) resource for more efficient use of a relatively less abundant
61 (and more costly to acquire) resource. These predictions imply that acclimation
62 responses to changing environments may be partially driven by trade-offs between
63 nitrogen and water use, though empirical tests of the theory are sparse.

64 Optimality models leveraging patterns expected from photosynthetic least-
65 cost theory have been developed for both C₃ (Wang et al. 2017; Smith et al. 2019;
66 Stocker et al. 2020) and more recently for C₄ species (Scott and Smith 2022). Such
67 models show broad agreement with patterns observed across environmental gradi-
68 ents (Paillassa et al. 2020; Querejeta et al. 2022; Smith et al. 2019; Westerband
69 et al. 2023), and are capable of reconciling dynamic leaf nitrogen-photosynthesis
70 relationships and acclimation responses to elevated CO₂, temperature, light avail-
71 ability, and vapor pressure deficit (Dong et al. 2017; Dong et al. 2020; Dong et al.

72 2022; Dong et al. 2022; Smith and Keenan 2020; Luo et al. 2021; Peng et al. 2021;
73 Querejeta et al. 2022; Westerband et al. 2023). Current versions of optimality
74 models that invoke patterns expected from photosynthetic least-cost theory hold
75 β constant across growing environments. As growing evidence suggests that costs
76 of nitrogen use change across resource availability and climatic gradients in species
77 with different nutrient acquisition strategies (Fisher et al. 2010; Brzostek et al.
78 2014; Allen et al. 2020; Terrer et al. 2018), one might expect that β should
79 dynamically change across environments and in species with different acquisition
80 strategies. However, manipulative experiments that test mechanisms underlying
81 nitrogen-water use trade-offs and leaf nitrogen-photosynthesis relationships pre-
82 dicted from theory across soil resource availability and climatic gradients are rare.
83 Furthermore, no study has related shifts in β to nitrogen-water use trade-offs or
84 leaf nitrogen-photosynthesis relationships. Understanding the dynamic nature of
85 β across different environmental contexts and impacts of β on patterns expected
86 from theory are critical for further optimality model development, and is the cen-
87 tral motivation for the experiments presented in this dissertation.

88 In this dissertation, I use four experiments to quantify nutrient acquisition
89 and allocation responses under different environmental conditions and in species
90 with different nutrient acquisition strategies. These experiments provide impor-
91 tant empirical data needed to evaluate patterns expected from photosynthetic
92 least-cost theory and test mechanisms that drive such patterns. In the first ex-
93 perimental chapter, I re-analyze data from a greenhouse experiment that grew
94 *Glycine max* L. (Merr) and *Gossypium hirsutum* seedlings under full-factorial
95 combinations of four light treatments and four fertilization treatments. This re-

96 analysis examined the effect of soil nitrogen availability and light availability on
97 structural carbon costs to acquire nitrogen in a species capable of forming associa-
98 tions with symbiotic nitrogen-fixing bacteria (*G. max*) and a species not capable
99 of forming such associations (*G. hirsutum*). I find strong evidence suggesting that
100 increasing light availability increases structural carbon costs to acquire nitrogen
101 and that increasing soil nitrogen fertilization decreases structural carbon costs to
102 acquire nitrogen.

103 In the second experimental chapter, I measure leaf physiological traits in
104 the upper canopy of mature trees growing in a 9-year nitrogen-by-pH field manip-
105 ulation experiment to assess whether changes in soil nitrogen availability or soil
106 pH modify nitrogen-water use trade-offs expected from photosynthetic least-cost
107 theory. I find strong nitrogen-water use trade-offs in response to increasing soil ni-
108 trogen availability, indicated by a strong negative relationship between leaf $C_i:C_a$
109 (referred to here and in the rest of this dissertation as χ) and leaf nitrogen content,
110 as well as a strong increase in leaf nitrogen content per unit leaf χ with increas-
111 ing soil nitrogen availability. Interestingly, I also find a null effect of soil pH on
112 nitrogen-water use trade-offs. These patterns provide strong support for patterns
113 expected from photosynthetic least-cost theory across soil nitrogen availability
114 gradients, and indicate that previous studies which note strong nitrogen-water
115 use trade-offs in response to soil pH may be driven by covariation between soil
116 nitrogen availability and soil pH (Paillassa et al. 2020; Westerband et al. 2023).

117 In the third experimental chapter, I leverage a broad precipitation and soil
118 nutrient availability gradient in Texan grasslands to investigate primary drivers of
119 leaf nitrogen content. In this chapter, I directly quantify β and χ using leaf $\delta^{13}\text{C}$ to

120 examine primary drivers of leaf nitrogen content and find that leaf nitrogen content
121 is driven through a negative relationship with χ . I also show that soil nitrogen
122 availability is negatively associated with β , and that β is positively associated
123 with χ . I show strong support for patterns expected from theory, showing for
124 the first time that positive effects of increasing soil nitrogen availability on leaf
125 nitrogen content are mediated by changes in β .

126 In the fourth experimental chapter, I use reach-in growth chambers to
127 quantify leaf and whole plant acclimation responses to CO₂ across a soil nitro-
128 gen fertilization gradient, while also manipulating nutrient acquisition strategy
129 by controlling whether seedlings were able to form associations with symbiotic
130 nitrogen-fixing bacteria. Specifically, I measure leaf physiological and whole plant
131 growth responses of 7-week *G. max* seedlings grown under one of two CO₂ treat-
132 ments, one of nine fertilization treatments, and one of two inoculation treatments
133 in a full factorial design. I find a down-regulation in leaf nitrogen content and
134 leaf photosynthesis under elevated CO₂, a pattern that is not modified across
135 the fertilization gradient or between inoculation treatments. However, I also find
136 strong stimulation in total leaf area and whole plant growth under elevated CO₂
137 that are enhanced with increasing fertilization. There was no observable effect of
138 inoculation in modifying whole plant growth responses to CO₂, which I speculate
139 is the result of a down-regulation in plant investments to nitrogen fixation with
140 increasing fertilization. Results from this experiment provide strong evidence sug-
141 gesting that leaf acclimation responses to CO₂ were controlled by optimal resource
142 investment to photosynthetic capacity, following patterns expected from photo-
143 synthetic least-cost theory, and suggest divergent roles of soil nitrogen fertilization

144 in modifying leaf and whole plant acclimation responses to CO₂.

145 Throughout the four experimental chapters, I find strong and consistent
146 patterns supportive of patterns expected from photosynthetic least-cost theory.
147 Specifically, I find strong nitrogen-water use trade-offs in response to changing
148 climates and soil resources, that shifts in soil nitrogen availability have strong
149 negative impacts on costs of nitrogen acquisition, and therefore tend to increase
150 β , and that constant leaf nitrogen-photosynthesis relationships only occur in sys-
151 tems where nitrogen is limiting. In a final conclusion chapter, I summarize ma-
152 jor findings from each of the four experimental chapters and synthesize common
153 mechanisms that drive leaf and whole plant responses to changing environmen-
154 tal conditions. I conclude this dissertation with brief dialogue on lessons learned
155 throughout experimental chapters, and propose future experiments that will tar-
156 get additional uncertainties in photosynthetic least-cost theory responses across
157 environmental gradients.

158

Chapter 2

159

Structural carbon costs to acquire nitrogen are determined by
160 nitrogen and light availability in two species with different nitrogen
161 acquisition strategies

162 2.1 Introduction

163

Carbon and nitrogen cycles are tightly coupled in terrestrial ecosystems.

164

This tight coupling influences photosynthesis (Walker et al. 2014; Rogers et al.

165

2017), net primary productivity (LeBauer and Treseder 2008; Thomas et al. 2013),

166

decomposition (Cornwell et al. 2008; Bonan et al. 2013; Sulman et al. 2019), and

167

plant resource competition (Gill and Finzi 2016; Xu-Ri and Prentice 2017). Ter-

168

restrial biosphere models are beginning to include connected carbon and nitrogen

169

cycles to improve the realism of their simulations (Fisher et al. 2010; Brzostek

170

et al. 2014; Wieder et al. 2015; Shi et al. 2016; Zhu et al. 2019). Simula-

171

tions from these models indicate that coupling carbon and nitrogen cycles can

172

drastically influence future biosphere-atmosphere feedbacks under global change,

173

such as elevated carbon dioxide or nitrogen deposition (Thornton et al. 2007;

174

Goll et al. 2012; Wieder et al. 2015; Wieder et al. 2019). Nonetheless, there

175

are still limitations in our quantitative understanding of connected carbon and

176

nitrogen dynamics (Thomas et al. 2015; Meyerholt et al. 2016; Rogers et al.

177

2017; Exbrayat et al. 2018; Shi et al. 2019), forcing models to make potentially

178

unreliable assumptions.

179

Plant nitrogen acquisition is a process in terrestrial ecosystems by which

180

carbon and nitrogen are tightly coupled (Vitousek and Howarth 1991; Delaire

181

et al. 2005; Brzostek et al. 2014). Plants must allocate photosynthetically de-

182 rived carbon belowground to produce and maintain root systems or exchange with
183 symbiotic soil microbes in order to acquire nitrogen (Högberg et al. 2008; Hög-
184 berg et al. 2010). Thus, plants have an inherent carbon cost associated with
185 acquiring nitrogen, which can include both direct energetic costs associated with
186 nitrogen acquisition and indirect costs associated with building structures that
187 support nitrogen acquisition (Gutschick 1981; Rastetter et al. 2001; Vitousek
188 et al. 2002; Menge et al. 2008). Model simulations (Fisher et al. 2010; Brzostek
189 et al. 2014; Shi et al. 2016; Allen et al. 2020) and meta-analyses (Terrer et al.
190 2018) suggest that these carbon costs vary between species, particularly those
191 with different nitrogen acquisition strategies. For example, simulations using iter-
192 ations of the Fixation and Uptake of Nitrogen (FUN) model indicate that species
193 that acquire nitrogen from non-symbiotic active uptake pathways (e.g. mass flow)
194 generally have larger carbon costs to acquire nitrogen than species that acquire
195 nitrogen through symbiotic associations with nitrogen-fixing bacteria (Brzostek
196 et al. 2014; Allen et al. 2020).

197 Carbon costs to acquire nitrogen likely vary in response to changes in soil
198 nitrogen availability. For example, if the primary mode of nitrogen acquisition
199 is through non-symbiotic active uptake, then nitrogen availability could decrease
200 carbon costs to acquire nitrogen as a result of increased per-root nitrogen up-
201 take (Franklin et al. 2009; Wang et al. 2018). However, if the primary mode of
202 nitrogen acquisition is through symbiotic active uptake, then nitrogen availabil-
203 ity may incur additional carbon costs to acquire nitrogen if it causes microbial
204 symbionts to shift toward parasitism along the parasitism–mutualism continuum
205 (Johnson et al. 1997; Hoek et al. 2016; Friel and Friesen 2019) or if it reduces

206 the nitrogen acquisition capacity of a microbial symbiont (van Diepen et al. 2007;
207 Soudzilovskaia et al. 2015; Muñoz et al. 2016). Species may respond to shifts in
208 soil nitrogen availability by switching their primary mode of nitrogen acquisition
209 to a strategy with lower carbon costs to acquire nitrogen in order to maximize
210 the magnitude of nitrogen acquired from a belowground carbon investment and
211 outcompete other individuals for soil resources (Rastetter et al. 2001; Menge et al.
212 2008).

213 Environmental conditions that affect demand to acquire nitrogen to sup-
214 port new and existing tissues could also be a source of variance in plant carbon
215 costs to acquire nitrogen. For example, an increase in plant nitrogen demand could
216 increase carbon costs to acquire nitrogen if this increases the carbon that must be
217 allocated belowground to acquire a proportional amount of nitrogen (Kulmatiski
218 et al. 2017; Noyce et al. 2019). This could be driven by a temporary state of
219 diminishing return associated with investing carbon toward building and main-
220 taining structures that are necessary to support enhanced nitrogen uptake, such
221 as fine roots (Matamala and Schlesinger 2000; Norby et al. 2004; Arndal et al.
222 2018), mycorrhizal hyphae (Saleh et al. 2020), or root nodules (Parvin et al. 2020).
223 Alternatively, if the environmental factor that increases plant nitrogen demand
224 causes nitrogen to become more limiting in the system (e.g. atmospheric CO₂;
225 Luo et al. (2004), LeBauer and Treseder (2008), Vitousek et al. (2010), Liang
226 et al. (2016)), species might switch their primary mode of nitrogen acquisition to
227 a strategy with lower relative carbon costs to acquire nitrogen in order to gain a
228 competitive advantage over species with either different or more limited modes of
229 nitrogen acquisition (Ainsworth and Long 2005; Taylor and Menge 2018).

230 Using a plant economics approach, I examined the influence of plant ni-
231 trogen demand and soil nitrogen availability on plant carbon costs to acquire
232 nitrogen. This was done by growing a species capable of forming associations
233 with nitrogen-fixing bacteria (*Glycine max* L. (Merr)) and a species not capable
234 of forming these associations (*Gossypium hirsutum* L.) under four levels of light
235 availability (plant nitrogen demand proxy) and four levels of soil nitrogen fertil-
236 ization (soil nitrogen availability proxy) in a full-factorial, controlled greenhouse
237 experiment. I used this experimental set-up to test the following hypotheses:

- 238 1. An increase in plant nitrogen demand due to increasing light availability will
239 increase carbon costs to acquire nitrogen through a proportionally larger
240 increase in belowground carbon than whole-plant nitrogen acquisition. This
241 will be the result of an increased investment of carbon toward belowground
242 structures that support enhanced nitrogen uptake, but at a lower nitrogen
243 return.
- 244 2. An increase in soil nitrogen availability will decrease carbon costs to acquire
245 nitrogen as a result of increased per root nitrogen uptake in *G. hirsutum*.
246 However, soil nitrogen availability will not affect carbon costs to acquire
247 nitrogen in *G. max* because of the already high return of nitrogen supplied
248 through nitrogen fixation.

249 2.2 Methods

250 2.2.1 *Experiment setup*

251 *Gossypium hirsutum* and *G. max* were planted in individual 3 liter pots
252 (NS-300; Nursery Supplies, Orange, CA, USA) containing a 3:1 mix of unfertil-
253 ized potting mix (Sungro Sunshine Mix #2, Agawam, MA, USA) to native soil
254 extracted from an agricultural field most recently planted with *G. max* at the
255 USDA-ARS Laboratory in Lubbock, TX, USA (33.59°N, -101.90°W). The field
256 soil was classified as Amarillo fine sandy loam (75% sand, 10% silt, 15% clay).
257 Upon planting, all *G. max* pots were inoculated with *Bradyrhizobium japonicum*
258 (Verdesian N-Dure™ Soybean, Cary, NC, USA) to stimulate root nodulation. In-
259 dividuals of both species were grown under similar, unshaded, ambient greenhouse
260 conditions for 2 weeks to germinate and begin vegetative growth. Three blocks
261 were set up in the greenhouse, each containing four light treatments created us-
262 ing shade cloth that reduced incoming radiation by either 0 (full sun), 30, 50,
263 or 80%. Two weeks post-germination, individuals were randomly placed in the
264 four light treatments in each block. Individuals received one of four nitrogen fer-
265 tilization doses as 100ml of a modified Hoagland solution (Hoagland and Arnon
266 1950) equivalent to either 0, 70, 210, or 630 ppm N twice per week within each
267 light treatment. Nitrogen fertilization doses were received as topical agents to
268 the soil surface. Each Hoagland solution was modified to keep concentrations of
269 other macro- and micronutrients equivalent (Supplementary Table S1). Plants
270 were routinely well watered to eliminate water stress.

271 2.2.2 *Plant measurements and calculations*

272 Each individual was harvested after 5 weeks of treatment, and biomass
273 was separated by organ type (leaves, stems, and roots). Nodules on *G. max*
274 roots were also harvested. Except for the 0% shade cover and 630 ppm N treat-
275 ment combination, all treatment combinations in both species had lower average
276 dry biomass:pot volume ratios than the 1:1 ratio recommended by Poorter et al.
277 (2012) to minimize the likelihood of pot volume-induced growth limitation (Sup-
278 plementary Tables S2, S3; Supplementary Fig. S1). All harvested material was
279 dried, weighed, and ground by organ type. Carbon and nitrogen content (g g^{-1})
280 was determined by subsampling from ground and homogenized biomass of each
281 organ type using an elemental analyzer (Costech 4010; Costech, Inc., Valencia,
282 CA, USA). We scaled these values to total leaf, stem, and root carbon and ni-
283 trogen biomass (g) by multiplying dry biomass of each organ type by carbon or
284 nitrogen content of each corresponding organ type. Whole-plant nitrogen biomass
285 (g) was calculated as the sum of total leaf (g), stem (g), and root (g) nitrogen
286 biomass. Root nodule carbon biomass was not included in the calculation of root
287 carbon biomass; however, relative plant investment toward root or root nodule
288 standing stock was estimated as the ratio of root biomass to root nodule biomass
289 (g g^{-1}), following similar metrics to those adopted by Dovrat et al. (2018) and
290 Dovrat et al. (2020).

291 Carbon costs to acquire nitrogen (N_{cost} ; gC gN^{-1}) were estimated as the
292 ratio of total root carbon biomass (C_{bg} ; gC) to whole-plant nitrogen biomass
293 (N_{wp} ; gN). This calculation quantifies the relationship between carbon spent on
294 nitrogen acquisition and whole-plant nitrogen acquisition by using root carbon

295 biomass as a proxy for estimating the magnitude of carbon allocated toward ni-
296 trogen acquisition. This calculation therefore assumes that the magnitude of root
297 carbon standing stock is proportional to carbon transferred to root nodules or my-
298 corrhizae, or lost through root exudation or turnover. The assumption has been
299 supported in species that associate with ectomycorrhizal fungi (Hobbie 2006; Hob-
300 bie and Hobbie 2008), but is less clear in species that acquire nitrogen through
301 non-symbiotic active uptake or symbiotic nitrogen fixation. It is also unclear
302 whether relationships between root carbon standing stock and carbon transfer to
303 root nodules are similar in magnitude to carbon lost through exudation or when
304 allocated toward other active uptake pathways. Thus, because of the way mea-
305 surements were calculated, proximal values of carbon costs to acquire nitrogen are
306 underestimates.

307 2.2.3 *Statistical analyses*

308 I explored the effects of light and nitrogen availability on carbon costs to ac-
309 quire nitrogen using separate linear mixed-effects models for each species. Models
310 included shade cover, nitrogen fertilization, and interactions between shade cover
311 and nitrogen fertilization as continuous fixed effects, and also included block as a
312 random intercept term. Three separate models for each species were built with
313 this independent variable structure for three different dependent variables: (i)
314 carbon costs to acquire nitrogen (gC gN^{-1}); (ii) whole plant nitrogen biomass (de-
315 nominator of carbon cost to acquire nitrogen; gN); and (iii) belowground carbon
316 biomass (numerator of carbon cost to acquire nitrogen; gC). I constructed two
317 additional models for *G. max* with the same model structure described above to

318 investigate the effects of light availability and nitrogen fertilization on root nodule
319 biomass (g) and the ratio of root nodule biomass to root biomass (unitless).

320 I used Shapiro–Wilk tests of normality to determine whether species spe-
321 cific linear mixed-effects model residuals followed a normal distribution. None of
322 our models satisfied residual normality assumptions when models were fit using
323 untransformed data (Shapiro–Wilk: $p < 0.05$ in all cases). I attempted to satisfy
324 residual normality assumptions by first fitting models using dependent variables
325 that were natural-log transformed. If residual normality assumptions were still
326 not met (Shapiro–Wilk: $p < 0.05$), then models were fit using dependent variables
327 that were square root transformed. All residual normality assumptions were satis-
328 fied when models were fit with either a natural-log or square root transformation
329 (Shapiro–Wilk: $p > 0.05$ in all cases). Specifically, I natural-log transformed *G.*
330 *hirsutum* carbon costs to acquire nitrogen and *G. hirsutum* whole-plant nitrogen
331 biomass. I also square root transformed *G. max* carbon costs to acquire nitrogen,
332 *G. max* whole-plant nitrogen biomass, root carbon biomass in both species, *G.*
333 *max* root nodule biomass, and the *G. max* ratio of root nodule biomass to root
334 biomass. I used the ‘lmer’ function in the ‘lme4’ R package (Bates et al. 2015) to
335 fit each model and the ‘Anova’ function in the ‘car’ R package (Fox and Weisberg
336 2019) to calculate Wald’s χ^2 to determine the significance ($\alpha = 0.05$) of each fixed
337 effect coefficient. Finally, I used the ‘emmeans’ R package (Lenth 2019) to conduct
338 post-hoc comparisons of our treatment combinations using Tukey’s tests. Degrees
339 of freedom for all Tukey’s tests were approximated using the Kenward–Roger ap-
340 proach (Kenward and Roger 1997). All analyses and plots were conducted in R
341 version 4.0.1 (R Core Team 2021).

342 2.3 Results

343 2.3.1 *Carbon costs to acquire nitrogen*

344 Carbon costs to acquire nitrogen in *G. hirsutum* increased with increasing
345 light availability ($p < 0.001$; Table 2.1; Fig. 2.1) and decreased with increasing
346 nitrogen fertilization ($p < 0.001$; Table 2.1; Fig. 2.1). There was no interaction
347 between light availability and nitrogen fertilization ($p = 0.486$, Table 2.1; Fig.
348 2.1).

349 Carbon costs to acquire nitrogen in *G. max* also increased with increasing
350 light availability ($p < 0.001$, Table 2.1; Fig. 2.1) and decreased with increasing
351 nitrogen fertilization ($p < 0.001$; Table 2.1; Fig. 2.1). There was no interaction
352 between light availability and nitrogen fertilization ($p = 0.261$, Table 2.1; Fig.
353 2.1).

Table 2.1. Analysis of variance results exploring species-specific effects of light availability, nitrogen fertilization, and their interactions on carbon costs to acquire nitrogen (N_{cost}), whole-plant nitrogen biomass (N_{wp}), and root carbon biomass (C_{bg})

	df	N_{cost}			N_{wp}			C_{bg}		
		Coefficient	χ^2	p	Coefficient	χ^2	p	Coefficient	χ^2	p
<i>G. hirsutum</i>										
Intercept		1.594	-	-	-3.232	-	-	0.432	-	-
Light (L)	1	-1.09E-02	56.494	<0.001	-6.41E-03	91.275	<0.001	-2.62E-03	169.608	<0.001
Nitrogen (N)	1	-1.34E-03	54.925	<0.001	1.83E-03	118.784	<0.001	1.15E-04	2.901	0.089
L*N	1	3.88E-06	0.485	0.486	-1.34E-05	10.721	0.001	-1.67E-06	3.140	0.076
<i>G. max</i>										
Intercept		1.877	-	-	0.239	-	-	0.438	-	-
Light (L)	1	-7.67E-03	174.156	<0.001	-6.72E-04	39.799	<0.001	-2.55E-03	194.548	<0.001
Nitrogen (N)	1	-2.35E-04	21.948	<0.001	1.55E-04	70.771	<0.001	2.52E-04	19.458	<0.001
L*N	1	-2.89E-06	1.262	0.261	-6.32E-07	1.435	0.231	-3.16E-06	10.803	0.001

354 *Significance determined using Wald's χ^2 tests ($P = 0.05$). P -values < 0.05 are in bold and p -values between 0.05 and
 355 0.1 are italicized. Negative coefficients for light treatments indicate a positive effect of increasing light availability
 356 on all response variables, as light availability is treated as percent shade cover in all linear mixed-effects models.

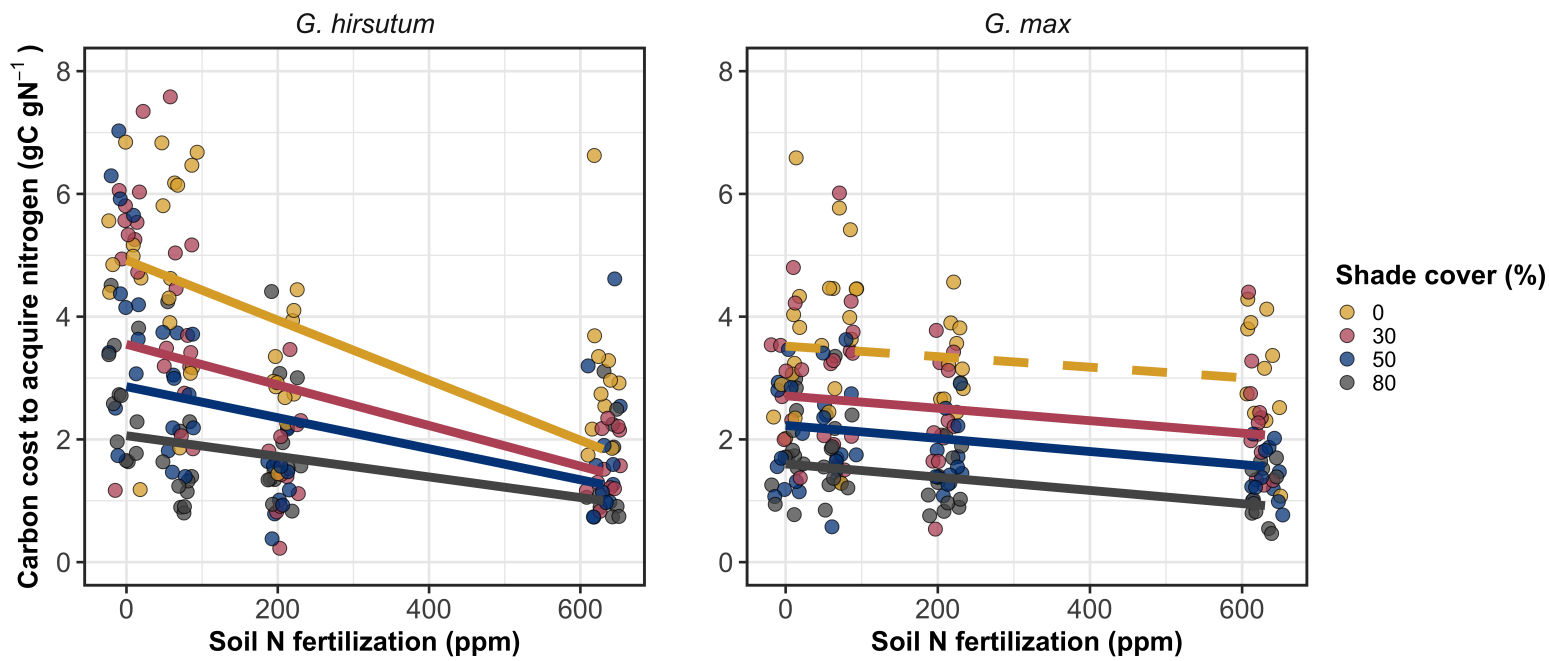


Figure 2.1. Relationships between soil nutrient fertilization and light availability on carbon costs to acquire nitrogen in *G. hirsutum* and *G. max*. Nitrogen fertilization treatments are represented on the x-axis. Shade cover treatments are represented through colored points and trendlines. Trendlines were created by back-transforming marginal mean slopes and intercepts from species-specific linear mixed-effects models. These values were calculated using the ‘emtrends’ and ‘emmeans’ functions in the ‘emmeans’ R package (Lenth, 2019). Yellow points and trendlines represent the 0% shade cover treatment, red points and trendlines represent the 30% shade cover treatment, blue points and trendlines represent the 50% shade cover treatment, and gray points and trendlines represent the 80% shade cover treatment. Solid trendlines indicate slopes that are significantly different from zero (Tukey: $p < 0.05$), while dashed trendlines indicate slopes that are not statistically different from zero.

357 2.3.2 *Whole plant nitrogen biomass*

358 Whole-plant nitrogen biomass in *G. hirsutum* was driven by an interaction
359 between light availability and nitrogen fertilization ($p = 0.001$; Table 2.1; Fig.
360 2.2). This interaction indicated a greater stimulation of whole-plant nitrogen
361 biomass by nitrogen fertilization as light levels increased (Table 2.1; Fig. 2.2).

362 Whole-plant nitrogen biomass in *G. max* increased with increasing light
363 availability ($p < 0.001$) and nitrogen fertilization ($p < 0.001$), with no interaction
364 between light availability and nitrogen fertilization ($p = 0.231$; Table 2.1; Fig.
365 2.2).

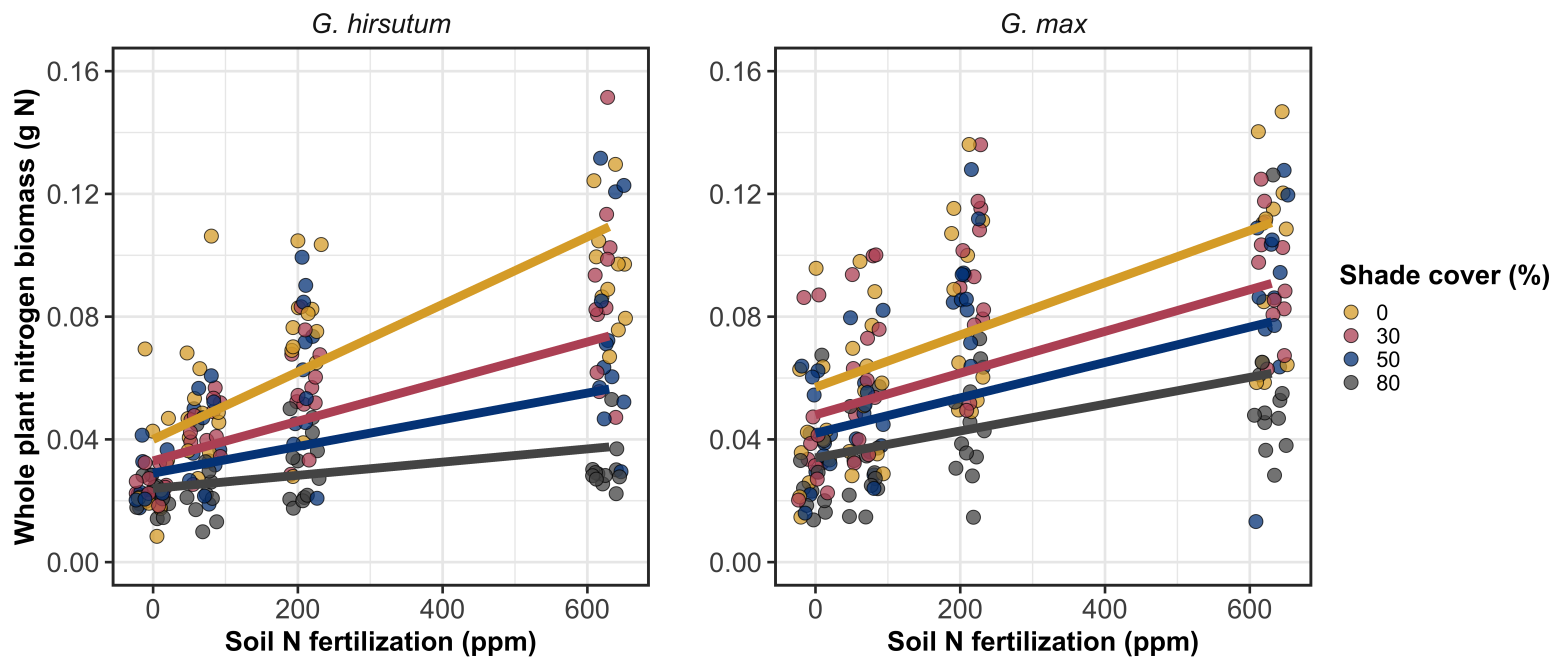


Figure 2.2. Relationships between soil nutrient fertilization and light availability on whole-plant nitrogen biomass in *G. hirsutum* and *G. max*. Whole-plant nitrogen biomass is the denominator of the carbon cost to acquire nitrogen calculation. Nitrogen fertilization treatments are represented on the x-axis. Shade cover treatments are represented through colored points and trendlines. Trendlines were created by back-transforming marginal mean slopes and intercepts from species-specific linear mixed-effects models. These values were calculated using the ‘emtrends’ and ‘emmeans’ functions in the ‘emmeans’ R package (Lenth 2019). Points are jittered for visibility. Colored points and trendlines are as explained in Fig. 2.1. Solid trendlines indicate slopes that are significantly different from zero (Tukey: $p < 0.05$), while dashed trendlines indicate slopes that are not statistically different from zero.

366 2.3.3 *Root carbon biomass*

367 Root carbon biomass in *G. hirsutum* significantly increased with increasing
368 light availability ($p < 0.001$; Table 2.1; Fig. 2.3) and marginally increased with
369 nitrogen fertilization ($p = 0.089$; Table 2.1; Fig. 2.3). There was also a marginal
370 interaction between light availability and nitrogen fertilization ($p = 0.076$; Table
371 2.1), driven by an increase in the positive response of root carbon biomass to
372 increasing nitrogen fertilization as light availability increased. This resulted in
373 significantly positive trends between root carbon biomass and nitrogen fertilization
374 in the two highest light treatments (Tukey: $p < 0.05$ in both cases; Table 2.3;
375 Fig. 2.3) and no effect of nitrogen fertilization in the two lowest light treatments
376 (Tukey: $p > 0.05$ in both cases; Table 2.3; Fig. 2.3).

377 There was an interaction between light availability and nitrogen fertiliza-
378 tion on root carbon biomass in *G. max* ($p = 0.001$; Table 2.1; Fig. 2.3). Post-hoc
379 analyses indicated that the positive effects of nitrogen fertilization on *G. max* root
380 carbon biomass increased with increasing light availability (Table 2.3; Fig. 2.3).
381 There were also positive individual effects of increasing nitrogen fertilization ($p <$
382 0.001) and light availability ($p < 0.001$) on *G. max* root carbon biomass (Table
383 2.1; Fig. 2.3).

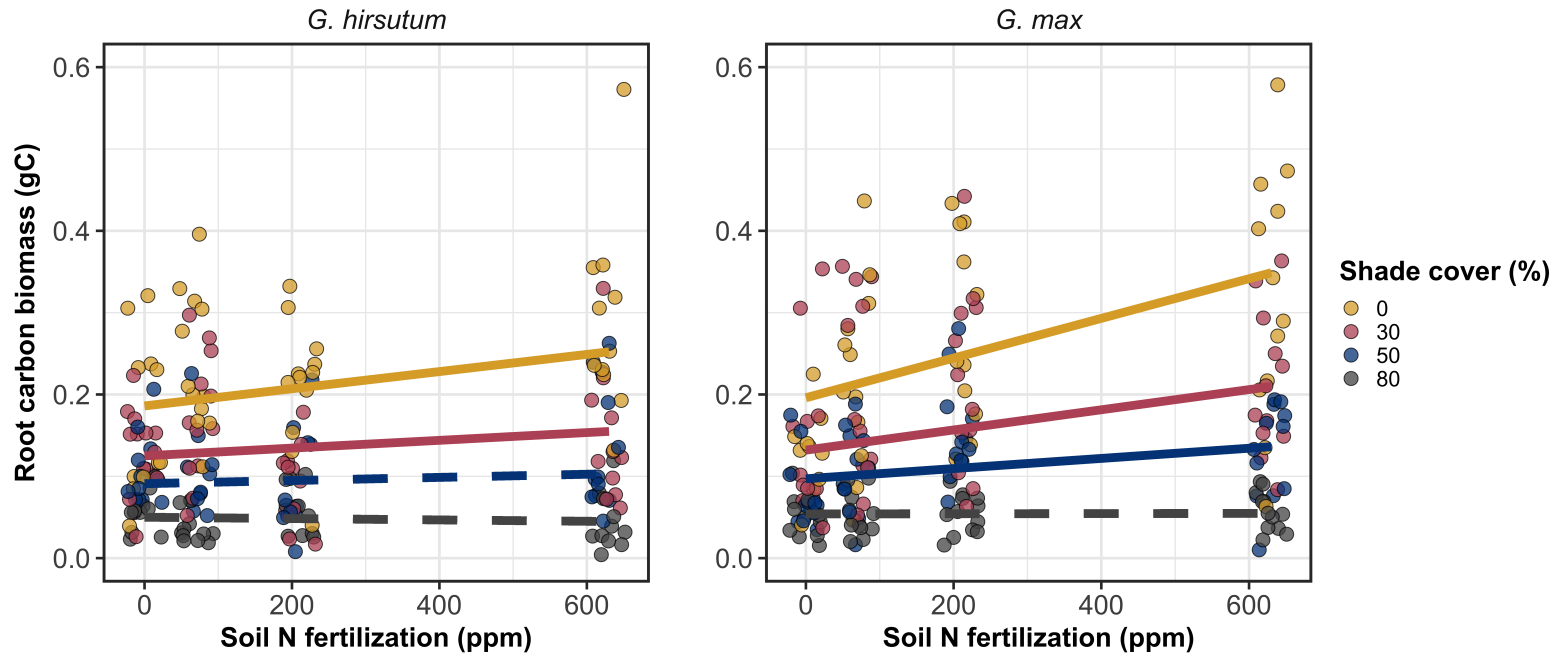


Figure 2.3. Relationships between soil nutrient fertilization and light availability on root carbon biomass in *G. hirsutum* and *G. max*. Root carbon biomass is the numerator of the carbon cost to acquire nitrogen calculation. Nitrogen fertilization treatments are represented on the x-axis. Shade cover treatments are represented through colored points and trendlines. Trendlines were created by back-transforming marginal mean slopes and intercepts from species-specific linear mixed-effects models. These values were calculated using the ‘emtrends’ and ‘emmmeans’ functions in the ‘emmeans’ R package (Lenth 2019). Points are jittered for visibility. Colored points and trendlines are as explained in Fig. 2.1.

Yellow points and trendlines represent the 0% shade cover treatment, blue points and trendlines represent the 30% shade cover treatment, green points and trendlines represent the 50% shade cover treatment, and purple points and trendlines represent the 80% shade cover treatment. Solid trendlines indicate slopes that are significantly different from zero (Tukey: $p < 0.05$), while dashed trendlines indicate slopes that are not statistically different from zero.

384 2.3.4 *Root nodule biomass*

385 Root nodule biomass in *G. max* increased with increasing light availability
386 ($p < 0.001$; Table 2.2; Fig. 2.4A) and decreased with increasing nitrogen fertiliza-
387 tion ($p < 0.001$; Table 2.2; Fig. 2.4A). There was no interaction between nitrogen
388 fertilization and light availability ($p = 0.133$; Table 2.2; Fig. 2.4A). The ratio of
389 root nodule biomass to root biomass did not change in response to light avail-
390 ability ($p = 0.481$; Table 2.2; Fig. 2.4B) but decreased with increasing nitrogen
391 fertilization ($p < 0.001$; Table 2.2; Fig. 2.4B). There was no interaction between
392 nitrogen fertilization and light availability on the ratio of root nodule biomass to
393 root biomass ($p = 0.621$; Table 2.2; Fig. 2.4B).

Table 2.2. Analysis of variance results exploring effects of light availability, nitrogen fertilization, and their interactions on *G. max* root nodule biomass and the ratio of root nodule biomass to root biomass*

	Nodule biomass			Nodule biomass: root biomass			<i>p</i>
	df	Coefficient	χ^2	<i>p</i>	Coefficient	χ^2	
(Intercept)		0.302	-	-	0.448	-	-
Light (L)	1	-1.81E-03	72.964	<0.001	-8.76E-05	0.496	0.481
Nitrogen (N)	1	-2.83E-04	115.377	<0.001	-5.09E-04	156.476	<0.001
L*N	1	1.14E-06	2.226	0.133	-7.30E-07	0.244	0.621

394 *Significance determined using Wald's χ^2 tests ($\alpha = 0.05$). *P*-values less than 0.05 are in bold. Negative coefficients
 395 for light treatments indicate a positive effect of increasing light availability on all response variables, as light avail-
 396 ability is treated as percent shade cover in all linear mixed-effects models. Root nodule biomass and nodule biomass:
 397 root biomass models were only constructed for *G. max* because *G. hirsutum* was not inoculated with *B. japonicum*
 398 and is not capable of forming root nodules.

Table 2.3. Slopes of the regression line describing the relationship between each dependent variable and nitrogen fertilization at each light level*

Shade cover	Carbon cost to acquire nitrogen	Whole plant N biomass	Belowground C biomass	Root nodule biomass	Nodule biomass: root biomass
<i>G. hirsutum</i>					
0%	-1.34E-03^a	1.83E-03^a	1.15E-04^b	-	-
30%	-1.22E-03^a	1.43E-03^a	1.17E-04^b	-	-
50%	-1.14E-03^a	1.17E-03^a	3.12E-05 ^b	-	-
80%	-1.02E-03^a	7.66E-04^a	-1.89E-06 ^b	-	-
<i>G. max</i>					
0%	-2.35E-04 ^b	1.55E-05^b	2.51E-04^b	-2.83E-04^b	-5.09E-04^b
30%	-3.22E-04^b	1.35E-05^b	1.57E-04^b	-2.49E-04^b	-5.31E-04^b
50%	-3.80E-04^b	1.23E-05^b	9.37E-05^b	-2.26E-04^b	-5.45E-04^b
80%	-4.66E-04^b	1.04E-05^b	-9.95E-07 ^b	-1.92E-04^b	-5.67E-04^b

25

399 *Slopes represent estimated marginal mean slopes from linear mixed-effects models described in the Methods. Slopes
 400 were calculated using the ‘emmeans’ R package (Lenth 2019). Superscripts indicate slopes fit to natural-log (^a) or
 401 square root (^b) transformed data. Slopes statistically different from zero (Tukey: $p < 0.05$) are indicated in bold.
 402 Marginally significant slopes (Tukey: $0.05 < p < 0.1$) are italicized.

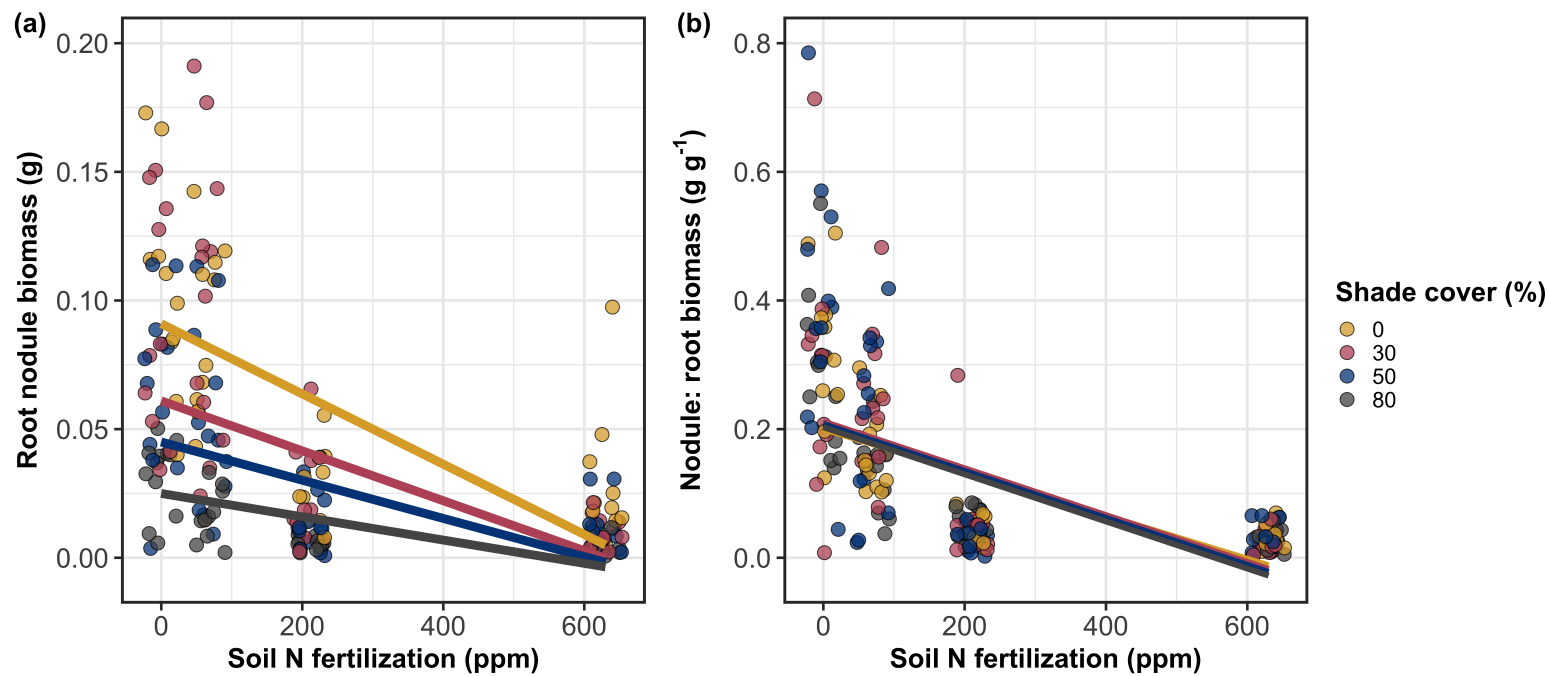


Figure 2.4. Effects of shade cover and nitrogen fertilization on root nodule biomass (A) and the ratio of root nodule biomass to root biomass (B) in *G. max*. Nitrogen fertilization treatments are represented on the x-axis. Shade cover treatments are represented through colored points and trendlines. Trendlines were created by back-transforming marginal mean slopes and intercepts from species-specific linear mixed-effects models. These values were calculated using the ‘emtrends’ and ‘emmeans’ functions in the ‘emmeans’ R package (Lenth 2019). Points are jittered for visibility. Yellow points and trendlines represent the 0% shade cover treatment, blue points and trendlines represent the 30% shade cover treatment, green points and trendlines represent the 50% shade cover treatment, and purple points and trendlines represent the 80% shade cover treatment. Solid trendlines indicate slopes that are significantly different from zero (Tukey: $p < 0.05$), while dashed trendlines indicate slopes that are not statistically different from zero.

403 2.4 Discussion

404 In this chapter, I determined the effects of light availability and soil ni-
405 trogen fertilization on root mass carbon costs to acquire nitrogen in *G. hirsutum*
406 and *G. max*. In support of my hypotheses, I found that carbon costs to acquire
407 nitrogen generally increased with increasing light availability and decreased with
408 increasing soil nitrogen fertilization in both species. These findings suggest that
409 carbon costs to acquire nitrogen are determined by factors that influence plant
410 nitrogen demand and soil nitrogen availability. In contrast to my second hypothe-
411 sis, root nodulation data suggested that *G. max* and *G. hirsutum* achieved similar
412 directional carbon cost responses to nitrogen fertilization despite a likely shift in
413 *G. max* allocation from nodulation to root biomass along the nitrogen fertilization
414 gradient (Fig. 2.4B).

415 2.4.1 *Carbon costs to acquire nitrogen increase with light availability and*
416 *decrease with fertilization*

417 Both *G. max* and *G. hirsutum* experienced an increase in carbon costs to
418 acquire nitrogen due to increasing light availability. These patterns were driven by
419 a larger increase in root carbon biomass than whole-plant nitrogen biomass. In-
420 creases in root carbon biomass due to factors that increase plant nitrogen demand
421 are a commonly observed pattern, as carbon allocated belowground provides sub-
422 strate needed to produce and maintain structures that satisfy aboveground plant
423 nitrogen demand (Nadelhoffer and Raich 1992; Giardina et al. 2005; Raich et al.
424 2014). Findings suggest that plants allocate relatively more carbon for acquiring
425 nitrogen when demand increases over short temporal scales, which may cause a

426 temporary state of diminishing return due to asynchrony between belowground
427 carbon and whole-plant nitrogen responses to plant nitrogen demand (Kulmatiski
428 et al. 2017; Noyce et al. 2019). These responses might be attributed to a temporal
429 lag associated with producing structures that enhance nitrogen acquisition. For
430 example, fine roots (Matamala and Schlesinger 2000; Norby et al. 2004; Arndal
431 et al. 2018) and root nodules (Parvin et al. 2020) take time to build and first
432 require the construction of coarse roots. Thus, full nitrogen returns from these
433 investments may not occur immediately (Kayler et al. 2010; Kayler et al. 2017),
434 and may vary by species acquisition strategy. I speculate that increases in ni-
435 trogen acquisition from a given carbon investment may occur beyond the 5-week
436 scope of this experiment. A similar study conducted over a longer temporal scale
437 would address this.

438 Increasing soil nitrogen fertilization generally decreased carbon costs to
439 acquire nitrogen in both species. These patterns were driven by a larger increase
440 in whole-plant nitrogen biomass than root carbon biomass. In *G. hirsutum*, re-
441 ductions in carbon costs to acquire nitrogen may have been due to an increase in
442 per-root nitrogen uptake, allowing individuals to maximize the amount of nitro-
443 gen acquired from a belowground carbon investment. Interestingly, increased soil
444 nitrogen fertilization increased whole-plant nitrogen biomass in *G. max* despite
445 reductions in root nodule biomass that likely reduced the nitrogen-fixing capac-
446 ity of *G. max* (Andersen et al. 2005; Muñoz et al. 2016). While reductions in
447 root nodulation due to increased soil nitrogen availability are commonly observed
448 (Gibson and Harper 1985; Fujikake et al. 2003), root nodulation responses were
449 observed in tandem with increased root carbon biomass, implying that *G. max*

450 shifted relative carbon allocation from nitrogen fixation to soil nitrogen acquisition
451 (Markham and Zekveld 2007; Dovrat et al. 2020). This was likely because
452 there was a reduction in the carbon cost advantage of acquiring fixed nitrogen
453 relative to soil nitrogen, and suggests that species capable of associating with
454 symbiotic nitrogen-fixing bacteria shift their relative nitrogen acquisition path-
455 way to optimize nitrogen uptake (Rastetter et al. 2001). Future studies should
456 further investigate these patterns with a larger quantity of phylogenetically re-
457 lated species, or different varieties of a single species that differ in their ability to
458 form associations with symbiotic nitrogen-fixing bacteria to more directly test the
459 impact of nitrogen fixation on the patterns observed in this study.

460 2.4.2 *Modeling implications*

461 Carbon costs to acquire nitrogen are subsumed in the general discussion of
462 economic analogies to plant resource uptake (Bloom et al. 1985; Rastetter et al.
463 2001; Vitousek et al. 2002; Phillips et al. 2013; Terrer et al. 2018; Henneron et al.
464 2020). Despite this, terrestrial biosphere models rarely include costs of nitrogen
465 acquisition within their framework for predicting plant nitrogen uptake. There
466 is currently one plant resource uptake model, FUN, that quantitatively predicts
467 carbon costs to acquire nitrogen within a framework for predicting plant nitrogen
468 uptake for different nitrogen acquisition strategies (Fisher et al. 2010; Brzostek
469 et al. 2014). Iterations of FUN are currently coupled to two terrestrial biosphere
470 models: the Community Land Model 5.0 and the Joint UK Land Environment
471 Simulator (Shi et al. 2016; Lawrence et al. 2019; Clark et al. 2011). Recent work
472 suggests that coupling FUN to CLM 5.0 caused a large overprediction of plant

473 nitrogen uptake associated with nitrogen fixation (Davies-Barnard et al. 2020)
474 compared to other terrestrial biosphere model products. Thus, empirical data
475 from manipulative experiments that explicitly quantify carbon costs to acquire
476 nitrogen in species capable of associating with nitrogen-fixing bacteria across dif-
477 ferent environmental contexts is an important step toward identifying potential
478 biases in models such as FUN.

479 My findings broadly support the FUN formulation of carbon costs to ac-
480 quire nitrogen in response to soil nitrogen availability. FUN calculates carbon
481 costs to acquire nitrogen based on the sum of carbon costs to acquire nitrogen
482 via nitrogen fixation, mycorrhizal active uptake, non-mycorrhizal active uptake,
483 and retranslocation (Fisher et al. 2010; Brzostek et al. 2014). Carbon costs to
484 acquire nitrogen via mycorrhizal or non-mycorrhizal active uptake pathways are
485 derived as a function of nitrogen availability, root biomass, and two parameterized
486 values based on nitrogen acquisition strategy (Brzostek et al. 2014). Due to this,
487 FUN simulates a net decrease in carbon costs to acquire nitrogen with increasing
488 nitrogen availability for mycorrhizal and non-mycorrhizal active uptake pathways,
489 assuming constant root biomass. This was a pattern I observed in *G. hirsutum*
490 regardless of light availability. In contrast, FUN would not simulate a net change
491 in carbon costs to acquire nitrogen via nitrogen fixation due to nitrogen avail-
492 ability. This is because carbon costs to acquire nitrogen via nitrogen fixation are
493 derived from a well established function of soil temperature, which is independent
494 of soil nitrogen availability (Houlton et al. 2008; Fisher et al. 2010). I observed
495 a net reduction in carbon costs to acquire nitrogen in *G. max*, except when in-
496 dividuals were grown under 0% shade cover (Fig. 2.1). While a net reduction of

497 carbon costs in response to nitrogen fertilization runs counter to nitrogen fixa-
498 tion carbon costs simulated by FUN, these patterns were likely because *G. max*
499 individuals switched their primary mode of nitrogen acquisition from symbiotic
500 nitrogen fixation to a non-symbiotic active uptake pathway (Fig. 2.4B).

501 2.4.3 *Study limitations*

502 It should be noted that the metric used in this study to determine carbon
503 costs to acquire nitrogen has several limitations. Most notably, this metric uses
504 root carbon biomass as a proxy for estimating the amount of carbon spent on
505 nitrogen acquisition. While it is true that most carbon allocated belowground has
506 at least an indirect structural role in acquiring soil resources, it remains unclear
507 whether this assumption holds true for species that acquire nitrogen via symbi-
508 otic nitrogen fixation. I also cannot quantify carbon lost through root exudates
509 or root turnover, which may increase due to factors that increase plant nitrogen
510 demand (Tingey et al. 2000; Phillips et al. 2011), and can increase the magni-
511 tude of available nitrogen from soil organic matter through priming effects on soil
512 microbial communities (Uselman et al. 2000; Bengtson et al. 2012). It is also not
513 clear whether these assumptions hold under all environmental conditions, such
514 as those that shift belowground carbon allocation toward a different mode of ni-
515 trogen acquisition (Taylor and Menge 2018; Friel and Friesen 2019) or between
516 species with different acquisition strategies. In this study, increasing soil nitrogen
517 fertilization increased carbon investment to roots relative to carbon transferred
518 to root nodules (Fig. 2.4B). By assuming that carbon allocated to root carbon
519 was proportional to carbon allocated to root nodules across all treatment com-

520 binations, these observed responses to soil nitrogen fertilization were likely to be
521 overestimated in *G. max*. I encourage future research to quantify these carbon
522 fates independently.

523 Researchers conducting pot experiments must carefully choose pot volume
524 to minimize the likelihood of growth limitations induced by pot volume (Poorter
525 et al. 2012). Poorter et al. (2012) indicate that researchers are likely to avoid
526 growth limitations associated with pot volume if measurements are collected when
527 the plant biomass:pot volume ratio is less than 1 g L⁻¹. In this experiment, all
528 treatment combinations in both species had biomass:pot volume ratios less than
529 1 g L⁻¹ except for *G. max* and *G. hirsutum* that were grown under 0% shade
530 cover and had received 630 ppm N. Specifically, *G. max* and *G. hirsutum* had
531 average respective biomass:pot volume ratios of 1.24±0.07 g L⁻¹ and 1.34±0.13 g
532 L⁻¹, when grown under 0% shade cover and received 630 ppm N (Supplementary
533 Tables S2, S3; Supplementary Fig. S1). If growth in this treatment combination
534 was limited by pot volume, then individuals may have had larger carbon costs
535 to acquire nitrogen than would be expected if they were grown in larger pots.
536 This pot volume induced growth limitation could cause a reduction in per-root
537 nitrogen uptake associated with more densely packed roots, which could reduce
538 the positive effect of nitrogen fertilization on whole-plant nitrogen biomass relative
539 to root carbon biomass (Poorter et al. 2012).

540 Growth limitation associated with pot volume provides a possible explana-
541 tion for the marginally insignificant effect of increasing nitrogen fertilization on *G.*
542 *max* carbon costs to acquire nitrogen when grown under 0% shade cover (Table
543 2.3; Fig. 2.1). This is because the regression line describing the relationship be-

544 tween carbon costs to acquire nitrogen and nitrogen fertilization in *G. max* grown
545 under 0% shade cover would have flattened if growth limitation had caused larger
546 than expected carbon costs to acquire nitrogen in the 0% shade cover, 630 ppm
547 N treatment combination. This may have been exacerbated by the fact that *G.*
548 *max* likely shifted relative carbon allocation from nitrogen fixation to soil nitrogen
549 acquisition, which could have increased the negative effect of more densely packed
550 roots on nitrogen uptake. These patterns could have also occurred in *G. hirsutum*
551 grown under 0% shade cover; however, there was no change in the effect of nitro-
552 gen fertilization on *G. hirsutum* carbon costs to acquire nitrogen grown under 0%
553 shade cover relative to other shade cover treatments. Regardless, the possibility
554 of growth limitation due to pot volume suggests that effects of increasing nitro-
555 gen fertilization on carbon costs to acquire nitrogen in both species grown under
556 0% shade cover could have been underestimated. Follow-up studies using a simi-
557 lar experimental design with a larger pot volume would be necessary in order to
558 determine whether these patterns were impacted by pot volume-induced growth
559 limitation.

560 2.4.4 *Conclusions*

561 In conclusion, this chapter provides empirical evidence that carbon costs to
562 acquire nitrogen are influenced by light availability and soil nitrogen fertilization
563 in a species capable of acquiring nitrogen via symbiotic nitrogen fixation and a
564 species not capable of forming such associations. We show that carbon costs to
565 acquire nitrogen generally increase with increasing light availability and decrease
566 with increasing nitrogen fertilization. This chapter provides important empirical

567 data needed to evaluate the formulation of carbon costs to acquire nitrogen in
568 terrestrial biosphere models, particularly carbon costs to acquire nitrogen that
569 are associated with symbiotic nitrogen fixation. My findings broadly support the
570 general formulation of these carbon costs in the FUN biogeochemical model in
571 response to shifts in nitrogen availability. However, there is a need for future
572 studies to explicitly quantify carbon costs to acquire nitrogen under different en-
573 vironmental contexts, over longer temporal scales, and using larger selections of
574 phylogenetically related species. In addition, I suggest that future studies mini-
575 mize the limitations associated with the metric used here by explicitly measuring
576 belowground carbon fates independently.

577

Chapter 3

578 Soil nitrogen availability modifies leaf nitrogen economies in mature
579 temperate deciduous forests: a direct test of photosynthetic least-cost
580 theory

581 3.1 Introduction

582 Photosynthesis represents the largest carbon flux between the atmosphere
583 and land surface (IPCC 2021), and plays a central role in biogeochemical cycling
584 at multiple spatial and temporal scales (Vitousek and Howarth 1991; LeBauer and
585 Treseder 2008; Kaiser et al. 2015; Wieder et al. 2015). Therefore, carbon and
586 energy fluxes simulated by terrestrial biosphere models are sensitive to the formu-
587 lation of photosynthetic processes (Ziehn et al. 2011; Bonan et al. 2011; Booth
588 et al. 2012; Smith et al. 2016; Smith et al. 2017) and must be represented using
589 robust, empirically tested processes (Prentice et al. 2015; Wieder et al. 2019).
590 Current formulations of photosynthesis vary across terrestrial biosphere models
591 (Smith and Dukes 2013; Rogers et al. 2017), which causes variation in modeled
592 ecosystem processes (Knorr 2000; Knorr and Heimann 2001; Bonan et al. 2011;
593 Friedlingstein et al. 2014) and casts uncertainty on the ability of these models to
594 accurately predict terrestrial ecosystem responses and feedbacks to global change
595 (Zaehle et al. 2005; Schaefer et al. 2012; Davies-Barnard et al. 2020).

596 Terrestrial biosphere models commonly represent C₃ photosynthesis th-
597 rough variants of the Farquhar et al. (1980) biochemical model (Smith and Dukes
598 2013; Rogers 2014; Rogers et al. 2017). This well-tested photosynthesis model
599 estimates leaf-level carbon assimilation, or photosynthetic capacity, as a function
600 of the maximum rate of Ribulose-1,5-bisphosphate carboxylase-oxygenase (Ru-

601 bisco) carboxylation (V_{cmax}) and the maximum rate of Ribulose-1,5-bisphosphate
602 (RuBP) regeneration (J_{max}) (Farquhar et al. 1980). Many terrestrial biosphere
603 models predict these model inputs based on plant functional group specific linear
604 relationships between leaf nutrient content and V_{cmax} (Smith and Dukes 2013;
605 Rogers 2014; Rogers et al. 2017) under the tenet that a large fraction of leaf
606 nutrients, and nitrogen (N) in particular, are partitioned toward building and
607 maintaining enzymes that support photosynthetic capacity, such as Rubisco (Brix
608 1971; Gulmon and Chu 1981; Evans 1989; Kattge et al. 2009; Walker et al. 2014).
609 Terrestrial biosphere models also predict leaf nutrient content from soil nutrient
610 availability based on the assumption that increasing soil nutrients generally in-
611 creases leaf nutrients (Firn et al. 2019; Li et al. 2020; Liang et al. 2020) which, in
612 the case of N, generally corresponds with an increase in photosynthetic processes
613 (Li et al. 2020; Liang et al. 2020).

614 Recent work calls the generality of relationships between soil nutrient avail-
615 ability, leaf nutrient content, and photosynthetic capacity into question, suggest-
616 ing instead that leaf nutrients and photosynthetic capacity are better predicted as
617 an integrated product of aboveground climate, leaf traits, and soil nutrient avail-
618 ability, rather than soil nutrient availability alone (Dong et al. 2017; Dong et al.
619 2020; Dong et al. 2022; Firn et al. 2019; Smith et al. 2019; Peng et al. 2021).
620 It has been reasoned that this result is because plants allocate added nutrients to
621 growth and storage rather than alterations in leaf chemistry (Smith et al. 2019),
622 perhaps as a result of nutrient limitation of primary productivity (LeBauer and
623 Treseder 2008; Fay et al. 2015). Additionally, recent work suggests that relation-
624 ships between leaf nutrient content and photosynthesis vary across environments,

625 and that the proportion of leaf nutrient content allocated to photosynthetic tis-
626 sue varies over space and time with plant acclimation and adaptation responses
627 to light availability, vapor pressure deficit, soil pH, soil nutrient availability, and
628 environmental factors that influence leaf mass per area (Pons and Pearcy 1994;
629 Niinemets and Tenhunen 1997; Evans and Poorter 2001; Hikosaka and Shigeno
630 2009; Ghimire et al. 2017; Onoda et al. 2017; Luo et al. 2021). The use of linear
631 relationships between leaf nutrient content and Vcmax to predict photosynthetic
632 capacity, as commonly used in terrestrial biosphere models (Rogers 2014), is not
633 capable of detecting such responses.

634 Photosynthetic least-cost theory provides an alternative framework for un-
635 derstanding relationships between soil nutrient availability, leaf nutrient content,
636 and photosynthetic capacity (Harrison et al. 2021). Leveraging a two-input mi-
637 croeconomics approach (Wright et al. 2003), the theory posits that plants accli-
638 mate to a given environment by optimizing leaf photosynthesis rates at the lowest
639 summed cost of using nutrients and water (Prentice et al. 2014; Wang et al. 2017;
640 Smith et al. 2019; Paillassa et al. 2020). Across resource availability gradients,
641 the theory predicts that optimal photosynthetic rates can be achieved by trading
642 less efficient use of a resource that is less costly to acquire (or more abundant)
643 for more efficient use of a resource more costly to acquire (or less abundant). For
644 example, an increase in soil nutrient availability should reduce the cost of acquir-
645 ing and using nutrients (Bae et al. 2015; Eastman et al. 2021; Perkowski et al.
646 2021), which could increase leaf nutrient investments in photosynthetic proteins to
647 allow similar photosynthetic rates to be achieved with higher nutrient use (lower
648 nutrient use efficiency) but lower water use (greater water use efficiency). The

649 theory suggests similar tradeoffs in response to increasing soil pH (Paillassa et al.
650 2020), specifically, that increasing soil pH should reduce the cost of acquiring soil
651 nutrients due to an increase in plant-available nutrient concentration (Paillassa
652 et al. 2020; Dong et al. 2022). The theory is also capable of reconciling dynamic
653 leaf nutrient-photosynthesis relationships at global scales (Luo et al. 2021).

654 Patterns expected from photosynthetic least-cost theory have recently re-
655 ceived empirical support both in global environmental gradient (Smith et al.
656 2019; Paillassa et al. 2020; Luo et al. 2021; Querejeta et al. 2022; Wester-
657 band et al. 2023) and local manipulative invasion (Bialic-Murphy et al. 2021)
658 studies. However, nutrient addition experiments that directly examine nutrient-
659 water use tradeoffs expected from the theory are rare (Guerrieri et al. 2011), and
660 only global gradient studies testing the theory have considered soil pH in their
661 analyses. As a result, there is a need to use nutrient addition and soil pH manu-
662 lation experiments to test mechanisms driving responses predicted by the theory.
663 Such experiments would also be useful to detect whether patterns expected from
664 theory translate to finer spatial scales.

665 In this study, we measured leaf responses to soil N availability in five decid-
666 uous tree species growing in the upper canopy of mature closed canopy temperate
667 forests in the northeastern United States. Soil N availability and pH were manipu-
668 lated through an N-by-pH field manipulation experiment with treatments applied
669 since 2011, eight years prior to measurement. Two different soil N treatments
670 were applied to increase N availability with opposing effects on soil pH. An addi-
671 tional N-free acidifying treatment was expected to decrease soil pH. I hypothesized
672 that increased soil N availability would enable plants to increase nutrient uptake

673 and create more photosynthetic enzymes per leaf, allowing similar photosynthetic
674 rates achieved with lower leaf C_i:C_a and increased leaf N content allocated to
675 photosynthetic leaf tissue. I expected that this response would be driven by a
676 reduction in the cost of acquiring N, which would cause trees to sacrifice efficient
677 N use to enable more efficient use of other limiting resources (i.e., water). Finally,
678 I hypothesized similar leaf responses to increasing soil pH.

679 3.2 Methods

680 3.2.1 *Study site description*

681 We conducted this study in summer 2019 at three stands located within
682 a 20-km radius of Ithaca, NY, USA (42.444 °N, 76.502 °W). All stands contain
683 mature, closed-canopy forests dominated by deciduous tree species. Stands con-
684 tained abundant sugar maple (*Acer saccharum* Marshall), American beech (*Fagus*
685 *grandifolia* Ehrh.), and white ash (*Fraxinus americana* L.), accounting for 43%,
686 15%, and 17% of the total aboveground biomass across the three stands, respec-
687 tively, with less frequent red maple (*Acer rubrum* L.; 9% of total aboveground
688 biomass) and red oak occurrences (*Quercus rubra* L.; 10% of total aboveground
689 biomass). Soils at each site were broadly classified as a channery silt loam Incep-
690 tisols using the USDA NRCS Web Soil Survey data product (Soil Survey Staff
691 2022). Between 2006 and 2020, study sites averaged 972 mm of precipitation per
692 year and had an average temperature of 7.9 °C per a weather station located near
693 the Cornell University campus (42.449 °N, 76.449 °W) part of the NOAA NCEI
694 Global Historical Climatology Network (Menne et al. 2012).

695 3.2.2 *Experimental design*

696 Four 40 m x 40 m plots were set up at each site in 2009, each with an
697 additional 10 m buffer along plot perimeters (60 m x 60 m total). The plots
698 were set up as a nitrogen-by-pH field manipulation experiment, with one each of
699 four treatments at each site. Two nitrogen treatments were applied, both at 50
700 kg N ha⁻¹ yr⁻¹, as either sodium nitrate (NaNO₃) to raise soil pH, or ammonium
701 sulfate ((NH₄)₂SO₄) to acidify; an elemental sulfur treatment was selected to acid-
702 ify without N, applied at the same rate of S addition (57 kg S ha⁻¹ yr⁻¹); and
703 control plots received no additions. All amendments were added in pelletized form
704 using hand-held fertilizer spreaders to both the main plots and buffers. Amend-
705 ments were divided into three equal doses distributed across the growing season
706 from 2011-2017 and added as a single dose from 2018 onward. During 2019, plots
707 were fertilized during the week of May 20.

708 3.2.3 *Leaf gas exchange and trait measurements*

709 We sampled one leaf each from 6 to 10 individuals per plot between June
710 25 and July 12, 2019 for gas exchange measurements (Table S1). Leaves were
711 collected from deciduous broadleaf trees represented across all sites and plots
712 and were replicated in efforts to mimic the species abundance of each plot at
713 each site. We also attempted to collect leaves from the upper canopy to reduce
714 differential shading effects on leaf physiology. Leaves were accessed by pulling
715 down small branches using an arborist's slingshot and weighted beanbag attached
716 to a throw line. Branches were immediately recut under deionized water and
717 remained submerged to reduce stomatal closure and avoid xylem embolism (as in

718 Smith & Dukes, 2018) until gas exchange data were collected.

719 Randomly selected leaves with little to no visible external damage were
720 attached to a Li-COR LI-6800 (Li-COR Bioscience, Lincoln, Nebraska, USA)
721 portable photosynthesis machine to measure net photosynthesis (A_{net} ; $\mu\text{mol m}^{-2}$
722 s^{-1}), stomatal conductance (g_{sw} ; $\text{mol m}^{-2} \text{s}^{-1}$), and intercellular CO_2 concentra-
723 tion (C_i ; $\mu\text{mol mol}^{-1}$) at different reference CO_2 concentrations (C_a ; $\mu\text{mol mol}^{-1}$)
724 concentrations (i.e., an A_{net}/C_i curve) under saturating light conditions (2,000
725 $\mu\text{mol m}^{-2} \text{s}^{-1}$). Reference CO_2 concentrations followed the sequence: 400, 300,
726 200, 100, 50, 400, 400, 600, 800, 1000, 1200, 1500, and 2000 $\mu\text{mol mol}^{-1} \text{CO}_2$. Leaf
727 temperatures were not controlled in the cuvette and ranged from 21.8 °C to 31.7
728 °C (mean±SD: 27.2 ± 2.2 °C). A linear and second order log-polynomial nonlinear
729 regression suggested no effect of temperature on stomatal conductance measured
730 at 400 $\mu\text{mol mol}^{-1} \text{CO}_2$ or net photosynthesis measured at $\mu\text{mol mol}^{-1} \text{CO}_2$ (Ta-
731 ble S2-3; Fig. S1). All A_{net}/C_i curves were generated within one hour of branch
732 severance.

733 Leaf morphological and chemical traits were collected on the same leaf used
734 to generate each A_{net}/C_i curve. Images of each leaf were taken using a flat-bed
735 scanner to determine fresh leaf area using the ‘LeafArea’ R package (Katabuchi
736 2015), which automates leaf area calculations using ImageJ software (Schneider
737 et al. 2012). Each leaf was dried at 65°C for at least 48 hours, weighed, and
738 ground using a Retsch MM200 ball mill grinder (Verder Scientific, Inc., Newtown,
739 PA, USA) until homogenized. Leaf mass per area (M_{area} , g m^{-2}) was calculated
740 as the ratio of dry leaf biomass to fresh leaf area. Using a subsample of ground and
741 homogenized leaf biomass, leaf N content (N_{mass} ; gN g^{-1}) and leaf $\delta^{13}\text{C}$ (‰, rela-

742 tive to VPDB) were measured at the Cornell Stable Isotope Lab with an elemental
743 analyzer (NC 2500, CE Instruments, Wigan, UK) interfaced to an isotope ratio
744 mass spectrometer (Delta V Isotope Ratio Mass Spectrometer, ThermoFisher Sci-
745 entific, Waltham, MA, USA). Leaf N content per unit leaf area (N_{area} ; gN m⁻²)
746 was calculated by multiplying N_{mass} by M_{area} .

747 We used leaf $\delta^{13}\text{C}$ values to estimate χ (unitless), which is an isotope-
748 derived estimate of the leaf $C_i:C_a$ ratio. While intercellular and atmospheric CO₂
749 concentrations were directly measured during each A_{net}/C_i curve, deriving χ from
750 $\delta^{13}\text{C}$ provides a more integrative estimate of the $C_i:C_a$ over an individual leaf's
751 lifespan. We derived χ following the approach of Farquhar et al. (1989) described
752 in Cernusak et al. (2013):

$$\chi = \frac{\Delta^{13}\text{C} - a}{b - a} \quad (3.1)$$

753 where $\Delta^{13}\text{C}$ represents the relative difference between leaf $\delta^{13}\text{C}$ (‰) and air $\delta^{13}\text{C}$
754 (‰), and is calculated from the following equation:

$$\Delta^{13}\text{C} = \frac{\delta^{13}\text{C}_{\text{air}} - \delta^{13}\text{C}_{\text{leaf}}}{1 + \delta^{13}\text{C}_{\text{leaf}}} \quad (3.2)$$

755 where $\delta^{13}\text{C}_{\text{air}}$ is assumed to be -8‰ (Keeling et al. 1979; Farquhar et al. 1989), a
756 represents the fractionation between ¹²C and ¹³C due to diffusion in air, assumed
757 to be 4.4‰, and b represents the fractionation caused by Rubisco carboxylation,
758 assumed to be 27‰ (Farquhar et al. 1989).

759 3.2.4 A_{net}/C_i curve-fitting and parameter estimation

760 We fit A_{net}/C_i curves of each individual using the ‘fitaci’ function in the
761 ‘plantecophys’ R package (Duursma 2015). This function estimates the maxi-
762 mum rate of Rubisco carboxylation (V_{cmax} ; $\mu\text{mol m}^{-2} \text{s}^{-1}$) and maximum rate
763 of electron transport for RuBP regeneration (J_{max} ; $\mu\text{mol m}^{-2} \text{s}^{-1}$) based on the
764 Farquhar, von Caemmerer, and Berry biochemical model of C₃ photosynthesis
765 (Farquhar et al. 1980). For each curve fit, we included triose phosphate uti-
766 lization (TPU) limitation to avoid underestimating J_{max} (Gregory et al. 2021).
767 Curves were visually examined to confirm the likely presence of TPU limitation.

768 We determined Michaelis-Menten coefficients for Rubisco affinity to CO₂
769 (K_c ; $\mu\text{mol mol}^{-1}$) and O₂ (K_o ; $\mu\text{mol mol}^{-1}$), and the CO₂ compensation point
770 (Γ^* ; $\mu\text{mol mol}^{-1}$) using leaf temperature and equations described in Medlyn et al.
771 (2002) and derived in Bernacchi et al. (2001). Specifically, K_c and K_o were
772 calculated as:

$$K_c = 404.9 * \exp^{\frac{79430(T_k - 298)}{298RT_k}} \quad (3.3)$$

773 and

$$K_o = 278.4 * \exp^{\frac{36380(T_k - 298)}{298RT_k}} \quad (3.4)$$

774 while Γ^* was calculated as:

$$\Gamma^* = 42.75 * \exp^{\frac{37830(T_k - 298)}{298RT_k}} \quad (3.5)$$

775 In all three equations, T_k is the leaf temperature (in Kelvin) during each A_{net}/C_i

776 curve and R is the universal gas constant ($8.314 \text{ J mol}^{-1} \text{ K}^{-1}$).

777 We standardized V_{cmax} and J_{max} estimates to 25°C using a modified Ar-

778 rhenius equation (Kattge and Knorr 2007):

$$k_{25} = \frac{k_{\text{obs}}}{e^{\frac{H_a(T_{\text{obs}} - T_{\text{ref}})}{T_{\text{ref}}RT_{\text{obs}}}} * \frac{1+e^{\frac{T_{\text{ref}}\Delta S - H_d}{T_{\text{obs}}}}}{1+e^{\frac{T_{\text{obs}}\Delta S - H_d}{T_{\text{obs}}}}}} \quad (3.6)$$

779 k_{25} represents the standardized V_{cmax} or J_{max} rate at 25°C , k_{obs} represents

780 the V_{cmax} or J_{max} estimate at the average leaf temperature measured inside the

781 cuvette during the A_{net}/C_i curve. H_a is the activation energy of V_{cmax} ($71,513$

782 J mol^{-1}) Kattge and Knorr (2007) or J_{max} ($49,884 \text{ J mol}^{-1}$) (Kattge and Knorr

783 2007). H_d represents the deactivation energy of both V_{cmax} and J_{max} ($200,000 \text{ J}$

784 mol^{-1}) (Medlyn et al. 2002), and R represents the universal gas constant (8.314

785 $\text{J mol}^{-1} \text{ K}^{-1}$). T_{ref} represents the standardized temperature of 298.15 K (25°C)

786 and T_{obs} represents the mean leaf temperature (in K) during each A_{net}/C_i curve.

787 ΔS is an entropy term that (Kattge and Knorr 2007) derived as a linear relation-

788 ship with average growing season temperature (T_g ; $^\circ\text{C}$), where:

$$\Delta S_{v_{\text{cmax}}} = -1.07 T_g + 668.39 \quad (3.7)$$

789 and

$$\Delta S_{j_{\text{max}}} = -0.75 T_g + 659.70 \quad (3.8)$$

790 We estimated T_g in Equations 3.7 and 3.8 based on mean daily (24-hour) air
791 temperature of the 30 days leading up to the day of each sample collection using
792 the same weather station reported in the site description. We then used V_{cmax25}
793 and J_{max25} estimates to calculate the ratio of J_{max25} to V_{cmax25} ($J_{max25}:V_{cmax25}$;
794 unitless).

795 3.2.5 *Proportion of leaf nitrogen allocated to photosynthesis and structure*

796 We used equations from Niinemets and Tenhunen (1997) to estimate the
797 proportion of leaf N content allocated to Rubisco and bioenergetics. The propor-
798 tion of leaf N allocated to Rubisco (ρ_{rub} ; gN gN $^{-1}$) was calculated as a function
799 of V_{cmax25} and N_{area} :

$$\rho_{rubisco} = \frac{V_{cmax25} N_r}{V_{cr} N_{area}} \quad (3.9)$$

800 where N_r is the amount of nitrogen in Rubisco, set to 0.16 gN (gN in Rubisco) $^{-1}$
801 and V_{cr} is the maximum rate of RuBP carboxylation per unit Rubisco protein,
802 set to 20.5 μ mol CO $_2$ (g Rubisco) $^{-1}$. The proportion of leaf nitrogen allocated to
803 bioenergetics (ρ_{bioe} ; gN gN $^{-1}$) was similarly calculated as a function of J_{max25} and
804 N_{area} :

$$\rho_{bioe} = \frac{J_{max25} N_b}{J_{mc} N_{area}} \quad (3.10)$$

805 where N_b is the amount of nitrogen in cytochrome f, set to 0.12407 gN (μ mol
806 cytochrome f) $^{-1}$ assuming a constant 1: 1: 1.2 cytochrome f: ferredoxin NADP
807 reductase: coupling factor molar ratio (Evans and Seemann 1989; Niinemets and

808 Tenhunen 1997), and J_{mc} is the capacity of electron transport per cytochrome f,
809 set to $156 \mu\text{mol electron} (\mu\text{mol cytochrome f})^{-1}\text{s}^{-1}$.

810 We estimated the proportion of leaf N content allocated to photosynthetic
811 tissue (ρ_{photo} ; gN gN^{-1}) as the sum of ρ_{rub} and ρ_{bioe} . This calculation is an un-
812 derestimate of the proportion of leaf N allocated to photosynthetic tissue because
813 it does not include N allocated to light harvesting proteins. This leaf N pool was
814 not included because we did not perform chlorophyll extractions on focal leaves.
815 However, the proportion of leaf N content allocated to light harvesting proteins
816 tends to be small relative to ρ_{rub} and ρ_{bioe} , and may scale with changes in ρ_{rub}
817 and ρ_{bioe} (Niinemets and Tenhunen 1997).

818 Finally, we estimated the proportion of leaf N content allocated to struc-
819 tural tissue (ρ_{str} ; gN gN^{-1}) using an empirical equation from Onoda et al. (2017):

$$N_{cw} = 0.000355 * M_{area}^{1.39} \quad (3.11)$$

820 where N_{cw} is the leaf N content allocated to cell walls (gN m^{-2}). ρ_{str} was estimated
821 by dividing N_{cw} by N_{area} .

822 3.2.6 *Tradeoffs between nitrogen and water use*

823 Photosynthetic nitrogen use efficiency (PNUE; $\mu\text{mol CO}_2 \text{ mol}^{-1} \text{ N s}^{-1}$)
824 was calculated by dividing A_{net} by N_{area} , first converting N_{area} to mol N m^{-2}
825 using the molar mass of N (14 g mol^{-1}). We used χ as an indicator of water
826 use efficiency, which exploratory analyses suggest had similar responses to soil N
827 availability and pH as intrinsic water use efficiency measured from gas exchange

828 (A_{net}/g_s). Tradeoffs between nitrogen and water use were determined by cal-
829 culating the ratio of N_{area} to χ ($N_{\text{area}}:\chi$; g N m⁻²) and V_{cmax25} to χ ($V_{\text{cmax25}}:\chi$;
830 $\mu\text{mol m}^{-2} \text{s}^{-1}$). This approach is similar to tradeoff calculations in which nitrogen-
831 water use tradeoffs are measured as the ratio of N_{area} or V_{cmax25} to g_s (Paillassa
832 et al. 2020; Bialic-Murphy et al. 2021). In this study, we quantify these re-
833 lationships using χ in lieu of g_s because g_s rapidly changes with environmental
834 conditions and therefore may have been altered by recent tree branch severance
835 and/or placement in the cuvette.

836 3.2.7 *Soil nitrogen availability and pH*

837 To characterize soil N availability at the time of our leaf gas exchange
838 measurements, we used mixed bed resin bags to quantify mobile ammonium-N
839 and nitrate-N concentrations in each plot. Lycra mesh bags were filled with 5 g
840 of Dowex® Marathon MR-3 hydrogen and hydroxide form resin (MilliporeSigma,
841 Burlington, MA USA) and sealed with a zip tie. Each bag was activated by
842 soaking in 0.5 M HCl for 20 minutes, then in 2 M NaCl until pH of the saline
843 solution stabilized, as described in Allison et al. (2008). Five resin bags were
844 inserted about 10 cm below the soil surface at each plot on June 25, 2019: one
845 near each of the four plot corners and one near the plot center. All resin bags
846 were collected 24 days later on July 19, 2019 and were frozen until extracted.

847 Prior to anion and cation extraction, each resin bag was rinsed with ul-
848 trapure water (MilliQ IQ 7000; Millipore Sigma, Burlington, MA) to remove any
849 surface soil residues. Anions and cations were extracted from surface-cleaned resin
850 bags by individually soaking and shaking each bag in 100 mL of a 0.1 M HCl/2.0

851 M NaCl matrix for one hour. Using a microplate reader (Biotek Synergy H1;
852 Biotek Instruments, Winooski, VT USA), nitrate-N concentrations were quanti-
853 fied spectrophotometrically at 540 nm with the end product of a single reagent
854 vanadium (III) chloride reaction (Doane and Horwáth 2003), and ammonium-N
855 concentrations quantified at 650 nm with the end product of a modified phenol-
856 hypochlorite reaction (Weatherburn 1967; Rhine et al. 1998). Both the single
857 reagent vanadium (III) chloride and modified phenol-hypochlorite methodologies
858 have been well established for determining nitrate-N and ammonium-N concen-
859 trations in resin bag extracts (Arnone 1997; Allison et al. 2008). We used a
860 series of negative and positive controls throughout each well plate to verify the
861 accuracy and precision of our measurements, assaying each resin bag extract and
862 control in triplicate. Soil N availability was estimated as the sum of the nitrate-N
863 and ammonium-N concentration in each resin bag, normalized per g of resin and
864 duration in the field ($\mu\text{g N g}^{-1} \text{ resin d}^{-1}$), then subsequently averaged across all
865 resin bags in a plot for a plot-level mean.

866 Soil pH was measured on 0-10 cm mineral soil samples collected prior to
867 fertilization in 2019. Near each of the four plot corners, three 5.5 cm diameter soil
868 cores were collected after first removing the forest floor where present. Each set
869 of three cores was placed in a plastic bag, and later composited by hand mixing
870 and sieved to 4mm. Soil pH was determined for a 1:2 soil:water slurry (10 g field-
871 moist soil to 20 mL DI water) of each sample using an Accumet AB15 pH meter
872 with flushable junction probe (Fisher Scientific; Hampton, NH, USA), and was
873 estimated at the plot level as the mean soil pH within each plot.

874 3.2.8 *Statistical analyses*

875 We built two separate series of linear mixed-effects models to explore effects
876 of soil N availability, soil pH, species, and leaf N content on leaf physiological
877 traits. In the first series of linear mixed-effects models, we explored the effect
878 of soil N availability, soil pH, and species on leaf N content, leaf photosynthesis,
879 stomatal conductance, and nitrogen-water use tradeoffs. Models included plot-
880 level soil N availability and plot-level soil pH as continuous fixed effects, species
881 as a categorical fixed effect, and site as a categorical random intercept term.
882 Interaction terms between fixed effects were not included due to the small number
883 of experimental plots. We built a series of separate models with this independent
884 variable structure to quantify individual effects of soil N availability, soil pH,
885 and species on N_{area} , M_{area} , N_{mass} , A_{net} , V_{cmax25} , J_{max25} , $J_{\text{max25}}:V_{\text{cmax25}}$, ρ_{rubisco} ,
886 $\rho_{\text{bioenergetics}}$, ρ_{photo} , $\rho_{\text{structure}}$, χ , PNUE, $N_{\text{area}}:\chi$, and $V_{\text{cmax25}}:\chi$.

887 A second series of linear mixed-effects models were built to investigate
888 relationships between leaf N content and photosynthetic parameters. Statistical
889 models included N_{area} as a single continuous fixed effect with species and site des-
890 ignated as individual random intercept terms. We used this independent variable
891 structure to quantify individual effects of leaf N content on A_{net} , V_{cmax25} , J_{max25} ,
892 $J_{\text{max25}}:V_{\text{cmax25}}$, and χ .

893 For all linear mixed-effects models, we used Shapiro-Wilk tests of normal-
894 ity to determine whether linear mixed-effects models satisfied residual normality
895 assumptions. If residual normality assumptions were not met, then models were
896 fit using dependent variables that were natural log transformed. If residual nor-
897 mality assumptions were still not met (Shapiro-Wilk: $p < 0.05$), then models were

898 fit using dependent variables that were square root transformed. All residual nor-
899 mality assumptions for both sets of models that did not originally satisfy residual
900 normality assumptions were met with either a natural log or square root data
901 transformation (Shapiro-Wilk: $p > 0.05$ in all cases).

902 In the first series of models, models for N_{area} , M_{area} , N_{mass} , V_{cmax25} , J_{max25} ,
903 χ , $N_{\text{area}}:\chi$, and $V_{\text{cmax25}}:\chi$, ρ_{rubisco} , $\rho_{\text{bioenergetics}}$, ρ_{photo} , $\rho_{\text{structure}}$ satisfied residual
904 normality assumptions without data transformations (Shapiro-Wilk: $p > 0.05$ in
905 all cases). The model for $J_{\text{max25}}:V_{\text{cmax25}}$ satisfied residual normality assumptions
906 with a natural log data transformation, while models for A_{net} and PNUE each
907 satisfied residual normality assumptions with square root data transformations.
908 In the second series of models, models for V_{cmax25} , J_{max25} , χ , and $V_{\text{cmax25}}:\chi$ satisfied
909 residual normality assumptions without data transformations (Shapiro-Wilk: p
910 > 0.05 in all cases). The model for $J_{\text{max25}}:V_{\text{cmax25}}$ required a natural log data
911 transformation and the model for A_{net} required a square root data transformation
912 (Shapiro-Wilk: $p > 0.05$ in both cases).

913 In all models, we used the ‘lmer’ function in the ‘lme4’ R package (Bates
914 et al. 2015) to fit each model and the ‘Anova’ function in the ‘car’ R package (Fox
915 and Weisberg 2019) to calculate Type II Wald’s χ^2 and determine the significance
916 level ($\alpha = 0.05$) of each fixed effect coefficient. Finally, we used the ‘emmeans’
917 R package (Lenth, 2019) to conduct post-hoc comparisons using Tukey’s tests,
918 where degrees of freedom were approximated using the Kenward-Roger approach
919 (Kenward and Roger 1997). All analyses and plots were conducted in R version
920 4.1.1 (R Core Team 2021). All figure regression lines and associated 95% confi-
921 dence interval error bars were plotted using predictions generated across the soil

922 nitrogen availability gradient using the ‘emmeans’ R package (Lenth 2019).

923 3.3 Results

924 3.3.1 *Leaf N content*

925 Increasing soil N availability generally increased N_{area} (Table 3.1; Fig.
926 3.1a). This pattern was driven by an increase in N_{mass} (Table 3.1; Fig. 3.1c)
927 and a marginal increase in M_{area} (Table 3.1; Fig. 3.1e) with increasing soil N
928 availability. There was no effect of soil pH on N_{area} , N_{mass} , or M_{area} (Table 3.1);
929 however, we did observe strong differences in N_{area} (Fig. 3.1b), N_{mass} (Fig. 3.1d),
930 and M_{area} (Fig. 3.1e) between species (Table 3.1).

Table 3.1. Effects of soil N availability, soil pH, and species on leaf N content per unit leaf area (N_{area}), leaf N content per unit leaf mass (N_{mass}), and leaf mass per unit leaf area (M_{area})

	N_{area}			N_{mass}			M_{area}			
	df	Coefficient	χ^2	p	Coefficient	χ^2	p	Coefficient	χ^2	p
Intercept	-	9.03E-01	-	-	1.68E+00	-	-	4.60E+01	-	-
Soil N	1	1.68E-02	11.990	0.001	1.25E-02	6.902	0.009	4.87E-01	4.143	0.042
Soil pH	1	9.28E-02	0.836	0.361	8.08E-02	0.663	0.415	4.05E+00	0.653	0.419
Species	4	-	72.128	<0.001	-	35.074	<0.001	-	29.869	<0.001

931 *Significance determined using Type II Wald χ^2 tests ($\alpha = 0.05$). P-values < 0.05 are in bold.

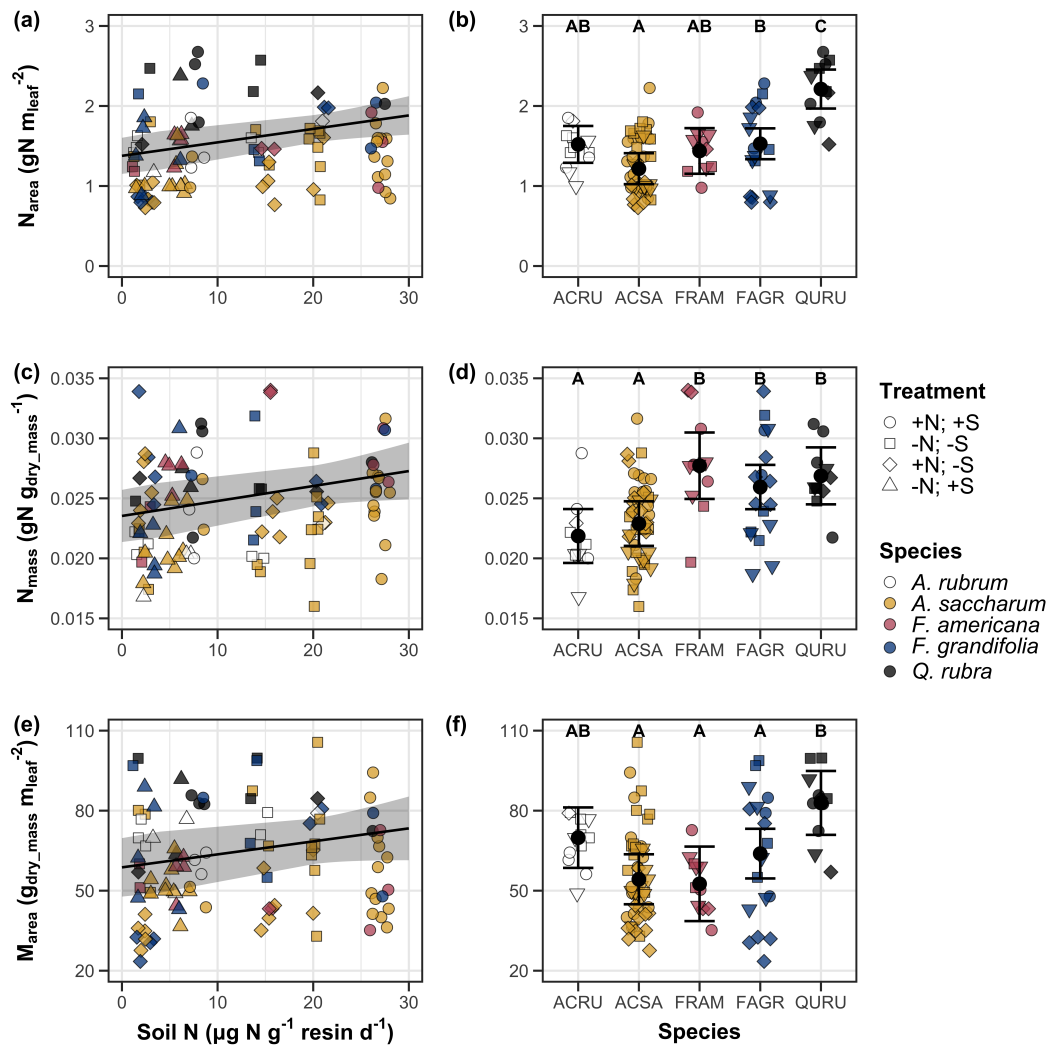


Figure 3.1. Effects of soil N availability and species on leaf N content per unit leaf area (a-b), leaf nitrogen content per unit leaf biomass (c-d), and leaf mass per leaf area (e-f). Soil N availability is represented on the x-axis in the left column of panels, while species is represented on the x-axis in the right column of panels. Tree species are represented as colored points and treatment plots are represented as shaped points, jittered for visibility. Species are abbreviated in the right column of panels through their assigned NRCS PLANTS Database symbol (USDA NRCS 2022), grouped along the x-axis per common mycorrhizal association, where the first three species commonly associate with arbuscular mycorrhizae (ACRU, ASCA, FAGR) and the second two species with ectomycorrhizae (FAGR, QURU). Trendlines are only included when the regression slope is statistically different from zero ($p < 0.05$).

932 3.3.2 *Net photosynthesis and leaf biochemistry*

933 Increasing soil N availability generally had no effect on A_{net} , V_{cmax25} , J_{max25} ,
934 or $J_{\text{max25}}:V_{\text{cmax25}}$ (Table 3.2, Figs. 3.2a, 3.2d, 3.2g). We also observed strong
935 species effects on all measured leaf photosynthetic traits (Table 3.2; Figs. 3.2b,
936 3.2e, 3.2h). Increasing soil pH had a marginal negative effect on A_{net} , but had no
937 effect on V_{cmax25} , J_{max25} , or $J_{\text{max25}}:V_{\text{cmax25}}$ (Table 3.2). There was a weak positive
938 effect of increasing N_{area} on A_{net} (Fig. 3.2c), but quite strong positive effects of
939 increasing N_{area} on V_{cmax25} and J_{max25} (Table 3.2; Fig. 3.2f and 3.2i).

Table 3.2. Effects of soil N availability, soil pH, species, and N_{area} on leaf biochemistry

	A_{net}			V_{cmax25}			J_{max25}			
	df	Coefficient	χ^2	p	Coefficient	χ^2	p	Coefficient	χ^2	p
(Intercept)	-	3.29E+00 ^b	-	-	6.38E+01	-	-	1.12E+02	-	-
Soil N	1	-1.23E-03 ^b	1.798	0.180	-3.84E-01	1.745	0.187	-6.70E-01	2.172	0.141
Soil pH	1	-3.09E-01 ^b	3.312	0.069	-4.91E+00	0.655	0.418	-8.18E+00	0.742	0.389
Species	4	-	11.838	0.019	-	31.748	<0.001	-	27.291	<0.001
(N_{area} int.)	-	6.59E-01 ^b	-	-	1.45E-01	-	-	2.86E+01	-	-
N_{area}	4	3.13E-01 ^b	4.790	0.029	2.43E+01	22.616	<0.001	4.04E+01	28.259	<0.001

	$J_{\text{max25}}:V_{\text{cmax25}}$			
	df	Coefficient	χ^2	p
(Intercept)	-	6.59E-01 ^a	-	-
Soil N	1	7.04E-04 ^a	0.088	0.767
Soil pH	1	-7.84E-03 ^a	0.025	0.874
Species	4	-	12.745	0.013
(N_{area} int.)	-	6.69E-01 ^a	-	-
N_{area}	4	-4.69E-02 ^a	1.142	0.285

940 *Significance determined using Type II Wald χ^2 tests ($\alpha = 0.05$). P-values < 0.05 are in bold, while p-values between
 941 0.05 and 0.1 are italicized. Superscript letters indicate model coefficients fit to natural-log (^a) or square-root (^b)
 942 transformed data. Relationships between N_{area} and each response variable were fit using the second series of bivariate
 943 mixed-effects models, so model coefficients and results are independent of model coefficients and results reported
 944 for relationships between soil N, soil pH, and species for each response variable. Key: A_{net} – light saturated net
 945 photosynthesis rate; V_{cmax25} – maximum rate of Rubisco carboxylation at 25°C; J_{max25} – maximum rate of electron
 946 transport for RuBP regeneration at 25°C, $J_{\text{max25}}:V_{\text{cmax25}}$ – the ratio of J_{max25} to V_{cmax25} .

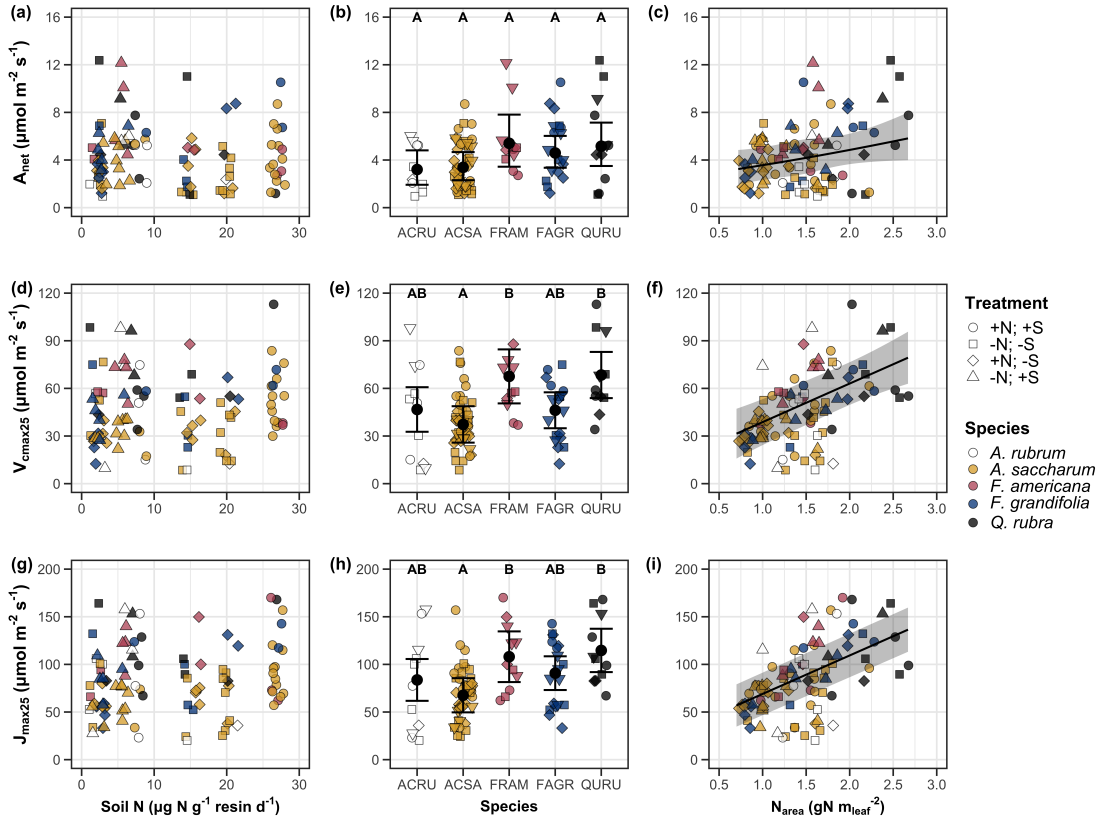


Figure 3.2. Effects of soil N availability (left column of panels), species (middle column of panels), and leaf N content per unit leaf area (right column of panels) on net photosynthesis (a-c), maximum Rubisco carboxylation rate (d-f), and maximum RuBP regeneration rate (g-i). Soil N availability is represented on the x-axis in the left column of panels, species is represented on the x-axis in the middle column of panels, and leaf N content per unit leaf area is represented continuously on the x-axis in the right column of panels. Species abbreviations and position along the x-axis in the middle column of panels, colored points, shapes, and trendlines are as explained in Figure 3.1.

947 3.3.3 *Leaf N allocation*

948 Neither soil N availability nor soil pH affected the proportion of leaf N
949 allocated to Rubisco or bioenergetics (Table 3.3; Fig. 3.3a, Fig. 3.3c), nor was
950 there any subsequent effect on the proportion of leaf N allocated to photosynthesis
951 (Table 3.3; Fig. 3.3f). We also found no effect of soil N availability or soil pH on
952 the proportion of leaf N allocated to structure (Table 3.3; Fig 3.3g). Species varied
953 in the proportion of leaf N allocated to Rubisco, photosynthesis, and structure (Fig
954 3.3b, Fig. 3.3d, Fig 3.3h), with no detectable species effect on the proportion of
955 leaf N allocated to bioenergetics (Table 3.3).

Table 3.3. Effects of soil N availability, soil pH, and species on the proportion of leaf nitrogen content allocated to photosynthesis, Rubisco, bioenergetics, and structure

	ρ_{photo}			ρ_{rub}			ρ_{bioe}			
	df	Coefficient	χ^2	p	Coefficient	χ^2	p	Coefficient	χ^2	p
Intercept	-	4.93E-01	-	-	4.17E-01	-	-	7.64E-02	-	-
Soil N	1	-1.23E-03	0.521	0.470	-1.04E-03	0.501	0.479	-1.77E-04	0.557	0.455
Soil pH	1	-4.37E-02	1.581	0.209	-3.70E-02	1.511	0.219	-6.84E-03	1.941	0.164
Species	4	-	13.106	0.011	-	14.152	0.007	-	7.300	0.121

	ρ_{str}			
	df	Coefficient	χ^2	p
Intercept	-	9.77E-02	-	-
Soil N	1	-2.29E-04	1.165	0.280
Soil pH	1	-1.87E-03	0.179	0.672
Species	4	-	16.428	0.002

58

956 *Significance determined using Type II Wald χ^2 tests ($\alpha = 0.05$). P-values < 0.05 are in bold. Key: ρ_{photo} -
 957 proportion of leaf nitrogen content allocated to photosynthesis; ρ_{rub} - proportion of leaf nitrogen content allocated
 958 to Rubisco; ρ_{bioe} - proportion of leaf nitrogen content allocated to bioenergetics; ρ_{str} - proportion of leaf nitrogen
 959 content allocated to structure.

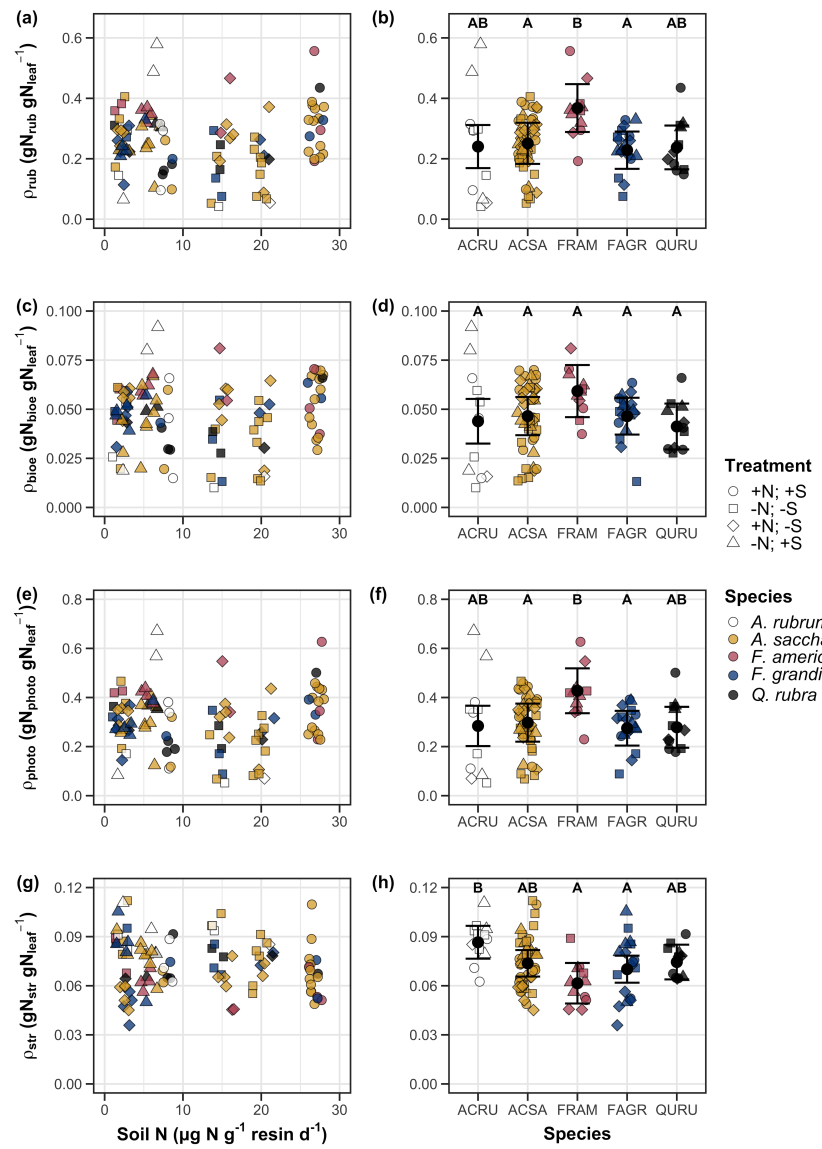


Figure 3.3. Effects of soil nitrogen availability and species on the proportion of leaf nitrogen content allocated to Rubisco (a-b), bioenergetics (c-d), photosynthesis (e-f), and structure (g-h). Soil nitrogen availability is represented on the x-axis in the left column of panels and species are represented on the x-axis in the right column of panels. Species abbreviations and position along the x-axis in the middle column of panels, colored points, shapes, trendlines, error bars, and compact lettering are as explained in Figure 3.1.

960 3.3.4 *Tradeoffs between nitrogen and water use*

961 Although soil N availability did not affect χ (Table 3.4; Fig. 3.4a), increasing
962 soil N availability decreased PNUE (Table 3.4; Fig. 3.4d) and increased the
963 ratio of $N_{\text{area}}:\chi$ (Table 3.4; Fig. 3.4f). Specifically, this response yielded a 26%
964 reduction in PNUE and 37% stimulation in $N_{\text{area}}:\chi$ across the soil nitrogen avail-
965 ability gradient. There was no apparent effect of soil N availability on $V_{\text{cmax25}}:\chi$
966 (Table 3.4; Fig. 3.4h). Increasing soil pH had a weak marginal negative effect
967 on PNUE, but did not influence χ , $N_{\text{area}}:\chi$, or $V_{\text{cmax25}}:\chi$ (Table 3.4). We also
968 observed differences in χ (Fig. 3.4b), PNUE (Fig. 3.4e), $N_{\text{area}}:\chi$ (Fig. 3.4g), and
969 $V_{\text{cmax25}}:\chi$ (Fig. 3.4i) between species (Table 3.4). Finally, increasing N_{area} had a
970 strong negative effect on χ (Table 3.4; Fig. 3.4c) and a strong positive effect on
971 $V_{\text{cmax25}}:\chi$ (Table 3.4; Fig. 3.4j).

Table 3.4. Effects of soil N availability, soil pH, species, and N_{area} on tradeoffs between nitrogen and water use

	χ	PNUE				$N_{\text{area}}:\chi$				
	df	Coefficient	χ^2	p	Coefficient	χ^2	p	Coefficient	χ^2	p
(Intercept)	-	8.12E-01	-	-	9.57E+00	-	-	9.19E-01	-	-
Soil N	1	-1.14E-03	1.698	0.193	-6.63E-02	6.396	0.011	2.60E-02	9.533	0.002
Soil pH	1	-1.91E-02	1.087	0.297	-9.25E-01	2.843	<i>0.092</i>	2.03E-01	1.321	0.250
Species	4	-	18.843	0.001	-	13.454	0.009	-	52.983	<0.001
$(N_{\text{area}} \text{ int.})$	-	8.93E-01	-	-	-	-	-	-	-	-
N_{area}	1	-1.11E-01	80.606	<0.001	-	-	-	-	-	-

	$V_{\text{cmax25}}:\chi$			
	df	Coefficient	χ^2	p
(Intercept)	-	7.20E+01	-	-
Soil N	1	3.99E-01	0.963	0.326
Soil pH	1	-3.12E+00	0.138	0.711
Species	4	-	31.450	<0.001
$(N_{\text{area}} \text{ int.})$	-	1.18E+01	-	-
N_{area}	4	3.87E+01	32.797	<0.001

*Significance determined using Type II Wald χ^2 tests ($\alpha = 0.05$). P-values < 0.05 are in bold, while p-values between 0.05 and 0.1 are italicized. Superscript letters indicate model coefficients fit to natural-log ^(a) or square-root ^(b) transformed data. Relationships between N_{area} and each response variable were fit using the second series of bivariate mixed-effects models, so model coefficients and results are independent of model coefficients and results reported for relationships between soil N, soil pH, and species for each response variable. Key: χ - isotope-derived estimate of the $C_i:C_a$; PNUE - photosynthetic N use efficiency, ratio of net photosynthesis to leaf N content per unit leaf area; $N_{\text{area}}:\chi$ - ratio of N_{area} to χ ; $V_{\text{cmax25}}:\chi$ - ratio of V_{cmax25} to χ .

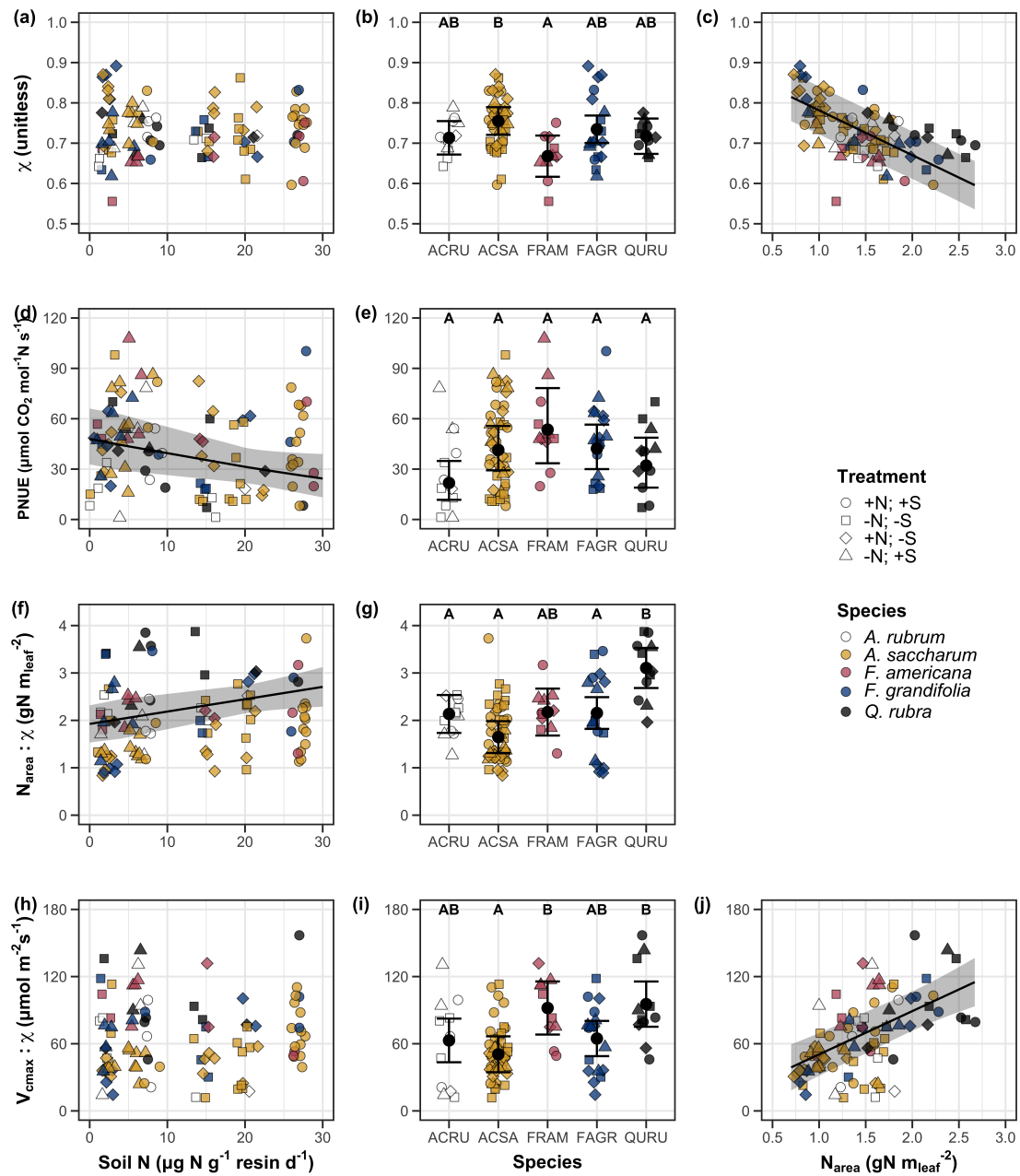


Figure 3.4. Effects of soil nitrogen availability and species on the proportion of leaf nitrogen content allocated to Rubisco (a-b), bioenergetics (c-d), photosynthesis (Rubisco + bioenergetics; e-f), and structure (g-h). Soil nitrogen availability is represented on the x-axis in the left column of panels and species are represented on the x-axis in the right column of panels. Species abbreviations and position along the x-axis in the middle column of panels, colored points, shapes, trendlines, error bars, and compact lettering are as explained in Figure 3.1.

979 3.4 Discussion

980 Photosynthetic least-cost theory provides an explanation for understand-
981 ing relationships between soil nutrient availability, leaf nutrient allocation, and
982 photosynthetic capacity. The theory suggests that plants acclimate to a given
983 environment by optimizing leaf photosynthesis rates at the lowest summed cost
984 of using nutrients and water Prentice et al. (2014), Wang et al. (2017), Smith
985 et al. (2019), Paillassa et al. (2020). The theory predicts that an increase in
986 soil nutrient availability should allow similar photosynthesis rates to be achieved
987 with increased leaf nutrient content and photosynthetic capacity (i.e., V_{cmax25} and
988 J_{max25}) at lower leaf $C_i:C_a$ (χ), resulting in an increase in water use efficiency,
989 decrease in nutrient use efficiency, and increase in both leaf nutrient content and
990 photosynthetic capacity per unit χ . The theory predicts similar leaf responses to
991 increasing soil pH under acidic conditions, presumably due to generally faster nu-
992 trient cycle dynamics and consequent reductions in the cost of acquiring nutrients
993 relative to water with increasing soil pH (Wang et al. 2017; Paillassa et al. 2020;
994 Dong et al. 2020).

995 Supporting the theory, we showed that increasing soil N availability was
996 associated with increased leaf N content (Fig 3.1a, 3.1c), a pattern that reduced
997 photosynthetic N use efficiency (Fig 3.4d) and increased leaf N content per unit
998 χ (Fig 3.4f). Increasing soil N coincided with slight, but non-significant decreases
999 in χ and increases in V_{cmax25} and J_{max25} ($p < 0.2$, Table 3.2). The positive trend
1000 between soil N availability and photosynthetic capacity was supported by the con-
1001 current strong increase in leaf N content with increasing soil N availability, which
1002 resulted in no change in the proportion of leaf N content allocated to photosynthe-

1003 sis across the soil N availability gradient. Additionally, leaf N content exhibited a
1004 strong negative correlation with χ , indicative of strong nitrogen-water use trade-
1005 offs at the leaf level. Responses tended to vary more due to soil N availability
1006 than soil pH. Overall, these findings are consistent with the nutrient-water use
1007 tradeoffs predicted from theory.

1008 3.4.1 *Soil nitrogen availability modifies tradeoffs between nitrogen and water use*

1009 In support of expected least-cost outcomes and past environmental gradient
1010 studies (Dong et al. 2017; Paillassa et al. 2020), we found that increasing soil N
1011 availability was associated with increased leaf N content. Soil N availability had
1012 smaller impacts on measures of net photosynthesis and χ , which led to reductions
1013 in PNUE and increases in leaf N content per unit χ , as expected from theory.
1014 Photosynthetic least-cost theory suggests that reductions in PNUE should be
1015 driven by an increase in the proportion of leaf N allocated to photosynthetic tissue,
1016 a pattern that should allow plants to achieve optimal photosynthetic rates with
1017 greater photosynthetic capacity to make better use of available light. Contrasting
1018 theory predictions, we found no effect of soil N availability on photosynthetic
1019 capacity. However, photosynthetic capacity did tend to increase with increasing
1020 soil N availability ($p < 0.20$; Table 3.2) resulting in no effect of soil N availability on
1021 the relative fraction of leaf N allocated to photosynthesis, Rubisco, or bioenergetics
1022 (Fig. 3.3). These lines of evidence support the idea that trees use additional N
1023 to support increased leaf N allocation toward photosynthetic tissue and enhance
1024 photosynthetic capacity (Wright et al. 2003).

1025 Soil N availability had a stronger effect on leaf N than photosynthetic ca-

1026 pacity. This pattern suggests that additional plant N uptake due to increased
1027 soil N availability was also being used to support non-photosynthetic N pools,
1028 possibly to structural tissue or stress-induced amino acid and polyamine synthe-
1029 sis (Minocha et al. 2000; Onoda et al. 2004; Bubier et al. 2011). While we
1030 found no change in the proportion of leaf N allocated to leaf structural tissue, the
1031 overall stimulation in leaf N content with increasing soil N availability suggests an
1032 increase in the net amount of N invested in leaf structural tissue along the N avail-
1033 ability gradient. Importantly, leaf N allocated to structure was calculated using
1034 an empirical relationship between M_{area} and the amount of leaf N allocated to cell
1035 walls (Onoda et al. 2017). As the generality of relationships between M_{area} and
1036 the amount of leaf N allocated to cell walls has been called into question (Harrison
1037 et al. 2009), future work should consider explicitly measuring N allocation to cell
1038 wall tissue and stress-induced amino acid synthesis to confirm these patterns.

1039 In opposition to patterns expected from least-cost theory, increasing soil
1040 N availability had no apparent effect on χ (Fig. 3.4a). Interestingly, despite
1041 the null effect of soil N availability on χ , we observed a strong negative effect of
1042 increasing N_{area} on χ (Fig. 3.4c), consistent with the nitrogen-water use tradeoffs
1043 expected from theory. The null response of χ to increasing soil N availability may
1044 have been due to a lack of water limitation in the system, given that the area
1045 received approximately 20% more precipitation (1167 mm) during the 12-month
1046 period leading up to our measurement period than normally expected (972 mm).
1047 However, droughts can and do occur in temperate forests of the northeastern
1048 United States (Sweet et al. 2017), so the observed increase in leaf N content
1049 with increasing soil N availability could be a strategy that allows trees to hedge

1050 bets against drier than normal growing seasons (Onoda et al. 2004; Onoda et al.
1051 2017; Hallik et al. 2009). As was suggested in Paillassa et al. (2020), and more
1052 recently by Querejeta et al. (2022), negative effects of soil N availability on χ may
1053 increase with increasing aridity. This strategy would be especially advantageous if
1054 it allows individuals growing in arid regions to maintain carbon assimilation rates
1055 with reduced water loss. Future work should attempt to quantify interactive roles
1056 of climate and soil nitrogen availability on nitrogen-water use tradeoffs, which
1057 could be done by leveraging coordinated and multifactor nutrient (Borer et al.
1058 2014) and water (Knapp et al. 2017) manipulation experiments across broad
1059 climatic gradients.

1060 3.4.2 *Soil pH did not modify tradeoffs between nitrogen and water usage*

1061 While the primary purpose of this study was to examine the role of soil N
1062 availability on nitrogen-water use tradeoffs, our experimental design manipulated
1063 both soil N and pH, providing an opportunity to isolate the roles of these variables.
1064 Previous correlational studies along environmental gradients identified soil pH as
1065 a particularly important factor that can modify tradeoffs between nutrient and
1066 water use (Smith et al. 2019; Paillassa et al. 2020; Westerband et al. 2023)
1067 and the proportion of leaf nitrogen allocated to photosynthesis (Luo et al. 2021).
1068 Such studies implied that these patterns may be driven by reductions in the cost of
1069 acquiring nutrients relative to water with increasing pH, which may be exacerbated
1070 in acidic soils.

1071 Consistent with theory (Wright et al. 2003; Prentice et al. 2014), our
1072 results indicate that increasing soil pH was negatively associated with PNUE.

1073 However, there was no effect of soil pH on leaf N content, χ , or leaf N content per
1074 unit χ , most likely because the experimental N additions increased soil N sup-
1075 ply while both increasing (sodium nitrate) and decreasing (ammonium sulfate)
1076 soil pH. These results suggest that soil pH did not play a major role in modify-
1077 ing expected photosynthetic least-cost theory patterns, contrasting findings from
1078 Paillassa et al. (2020) and other gradient studies that note positive effects of in-
1079 creasing soil pH on leaf N content, Rubisco carboxylation, and χ (Viet et al. 2013;
1080 Cornwell et al. 2018; Luo et al. 2021). Instead, null responses to soil pH show
1081 that leaf photosynthetic parameters depend more on soil N availability than pH
1082 per se, and that inferences from gradient studies might be confounding covariation
1083 between N availability and soil acidity.

1084 3.4.3 *Species identity explains a large amount of variation in leaf and whole*
1085 *plant traits*

1086 Species generally explained a larger amount of variation in measured leaf
1087 traits than soil N availability or soil pH. Interspecies variation is an important
1088 factor to consider when deducing mechanisms that drive photosynthetic least-
1089 cost theory, particularly for species that form distinct mycorrhizal associations or
1090 have different photosynthetic pathways, growth forms, or leaf habit (Espelta et al.
1091 2005; Adams et al. 2016; Bialic-Murphy et al. 2021; Scott and Smith 2022). The
1092 need to consider species may also be important when comparing nutrient-water
1093 use tradeoffs in early and late successional species, or in species with different
1094 resource economic strategies (Abrams and Mostoller 1995; Ellsworth and Reich
1095 1996; Wright et al. 2004; Reich 2014; Onoda et al. 2017; Ziegler et al. 2020).

1096 A strength of the study design and sampling effort is that it controls for
1097 many species differences that should modify nitrogen-water use tradeoffs expected
1098 from theory. All tree species measured in this study shared the leaf habit of decid-
1099 uous broadleaves, were growing in forests of similar successional stage, but differed
1100 in mycorrhizal association and consequent resource economic strategies. As stands
1101 tended to be dominated by trees that associate with arbuscular mycorrhizae (*Frax-*
1102 *inus* and both *Acer* species made up 70% of total aboveground biomass across
1103 stands), ecosystem biogeochemical cycle dynamics may be more closely aligned
1104 to the inorganic nutrient economy proposed in Phillips et al. (2013), which may
1105 promote stronger nitrogen-water use tradeoffs in tree species that associate with
1106 arbuscular mycorrhizae. This result was not observed here, as photosynthetic
1107 properties varied as much within as across the two mycorrhizal associations rep-
1108 resented. Given the high variability in measured photosynthetic traits within
1109 and across species, effects of mycorrhizal association likely require more intensive
1110 sampling efforts to detect than were possible here.

1111 3.4.4 *Implications for photosynthetic least-cost theory model development*

1112 In the field, soil nutrient availability is heterogeneous across time and space
1113 (Table S4). Unaccounted within-plot heterogeneity may have contributed to the
1114 low amount of variation explained by soil N availability in our statistical mod-
1115 els, as resin bags are a coarse surrogate for soil N availability. Despite this, we
1116 still observed evidence for nutrient-water use tradeoffs, suggesting that observed
1117 responses reported here may be an underestimate toward the net effect of soil
1118 N availability on these tradeoffs. While we urge caution in the interpretation of

1119 these results, they do provide a promising baseline for future studies investigating
1120 patterns expected from photosynthetic least-cost theory at finer spatiotemporal
1121 resolutions.

1122 The general stronger relationship between leaf N content and photosynthetic parameters versus between leaf N content and soil N availability suggests
1123 that leaf N content is more directly tied to photosynthesis than soil N availability. While this could be due to the high spatiotemporal heterogeneity of soil N
1124 availability, principles from photosynthetic least-cost theory suggest that leaf N
1125 content is the downstream product of leaf nutrient demand to build and maintain
1126 photosynthetic machinery, which is set by aboveground environmental conditions
1127 such as light availability, CO₂, temperature, or vapor pressure deficit (Smith
1128 et al. 2019; Paillassa et al. 2020; Peng et al. 2021; Westerband et al. 2023). The
1129 stronger relationship between leaf N and photosynthetic parameters paired with
1130 the strong negative relationship between leaf N and χ could indicate a relatively
1131 stronger effect of climate on leaf N-photosynthesis relationships than soil resource
1132 availability. However, the short distance between plots and across sites limited
1133 our ability to test this mechanism.

1136 Variation in soil pH affected least cost responses less than variations in
1137 soil N availability, in part because experimental treatments directly increased soil
1138 N and affected soil pH in opposite directions. While soil pH has been shown
1139 to drive nitrogen-water tradeoffs in global gradient analyses (Viet et al. 2013;
1140 Paillassa et al. 2020), these responses may be due to covariations between soil pH
1141 and nutrient cycling rather than a role of pH per se. The direct manipulations
1142 of soil pH and soil N availability in this study allowed us to partly disentangle

1143 these factors and show that variation in N availability matters more for least-cost
1144 tradeoffs than pH alone.

1145 3.4.5 *Conclusions*

1146 Increasing soil N availability generally increased leaf N content (both area-
1147 and mass-based), but did not significantly influence χ . This shift in leaf N led
1148 to a reduction in PNUE, and an increase in leaf N per unit χ with increasing
1149 soil N availability. Despite null effects of soil N availability on χ , we observed a
1150 strong negative relationship between leaf N content and χ . These results provide
1151 empirical support for the nutrient-water use tradeoffs expected from photosyn-
1152 thetic least-cost theory in response to soil nutrient availability, but suggest that
1153 all tenets of the theory may not hold in every environment. These results exper-
1154 imentially test previous work suggesting that leaf water-nitrogen economies vary
1155 across gradients of soil nutrient availability and pH, and show that variations in
1156 nutrient availability matter more for determining variation in leaf photosynthetic
1157 traits than soil pH.

1158

Chapter 4

1159 The relative cost of resource use for photosynthesis drives variance in
1160 leaf nitrogen content across a climate and soil resource availability
1161 gradient

1162 4.1 Introduction

1163 Terrestrial biosphere models, which comprise the land surface component of Earth
1164 system models, are sensitive to the formulation of photosynthetic processes (Knorr
1165 2000; Ziehn et al. 2011; Booth et al. 2012). This is because photosynthesis is the
1166 largest carbon flux between the atmosphere and terrestrial biosphere, and is con-
1167 strained by ecosystem carbon and nutrient cycles (Hungate et al. 2003; LeBauer
1168 and Treseder 2008; IPCC 2021; Fay et al. 2015). Many terrestrial biosphere mod-
1169 els formulate photosynthesis by parameterizing photosynthetic capacity within
1170 plant functional groups through empirical linear relationships between area-based
1171 leaf nitrogen content (N_{area}) and the maximum carboxylation rate of Ribulose-
1172 1,5-bisphosphate carboxylase/oxygenase (Kattge et al. 2009; Rogers 2014; Rogers
1173 et al. 2017). Models are also beginning to include connected carbon-nitrogen cy-
1174 cles (Wieder et al. 2015; Shi et al. 2016; Davies-Barnard et al. 2020; Braghieri
1175 et al. 2022), which allows leaf photosynthesis to be predicted directly through
1176 changes in N_{area} and indirectly through changes in soil nitrogen availability (e.g.,
1177 LPJ-GUESS, Smith et al., 2014; CLM5.0, Lawrence et al., 2019). Despite recent
1178 model developments, open questions remain regarding the generality of ecologi-
1179 cal relationships between soil nitrogen availability, leaf nitrogen content, and leaf
1180 photosynthesis across edaphic and climatic gradients.

1181 Empirical support for positive relationships between soil nitrogen avail-

ability and N_{area} is abundant (Firn et al. 2019; Liang et al. 2020), and is a result often attributed to the high nitrogen cost of building and maintaining Rubisco (Evans 1989; Evans and Seemann 1989; Onoda et al. 2004; Onoda et al. 2017; Dong et al. 2020). Such patterns imply that positive relationships between soil nitrogen availability and N_{area} should cause an increase in leaf photosynthesis and photosynthetic capacity by increasing the maximum rate of Rubisco carboxylation through increased investments to Rubisco construction and maintenance. This integrated N_{area} -photosynthesis response to soil nitrogen availability has been observed both in manipulative experiments and across environmental gradients (Field and Mooney 1986; Evans 1989; Walker et al. 2014; Li et al. 2020), and is thought to be driven by ecosystem nitrogen limitation, which limits its primary productivity globally (LeBauer and Treseder 2008; Fay et al. 2015). However, this response is not consistently observed, as recent studies note variable N_{area} -photosynthesis relationships across soil nitrogen availability gradients (Liang et al. 2020; Luo et al. 2021) and that aboveground growing conditions (e.g., light availability, temperature, vapor pressure deficit) or species identity traits (e.g., photosynthetic pathway, nitrogen acquisition strategy) may be more important for explaining variance in N_{area} and photosynthetic capacity across environmental gradients (Adams et al. 2016; Dong et al. 2017; Dong et al. 2020; Dong et al. 2022; Smith et al. 2019; Peng et al. 2021; Westerband et al. 2023).

One hypothesized mechanism to explain variance in N_{area} across environmental gradients has been proposed via photosynthetic least-cost theory (Wright et al. 2003; Prentice et al. 2014; Paillassa et al. 2020; Harrison et al. 2021). The theory predicts that plants acclimate to environments by optimizing photo-

1206 synthetic assimilation rates at the lowest summed cost of nitrogen and water use
1207 (Wright et al. 2003; Prentice et al. 2014). In a given environment, the theory
1208 proposes that nitrogen and water use can be substituted for each other to main-
1209 tain the lowest summed cost to satisfy leaf resource demand, such that optimal
1210 photosynthetic rates are achieved with less efficient use of the more abundant
1211 and less costly resource to acquire in exchange for more efficient use of the less
1212 abundant and more costly resource to acquire.

1213 Photosynthetic least-cost theory predicts that, all else equal, an increase
1214 in soil nitrogen availability should decrease the cost of acquiring and using nitro-
1215 gen relative to water (β), resulting in optimal photosynthetic rates achieved with
1216 greater N_{area} at lower stomatal conductance and lower leaf $C_i:C_a$ (Wright et al.
1217 2003; Prentice et al. 2014). Alternatively, an increase in soil moisture should
1218 reduce costs of water acquisition and use, increasing β , stomatal conductance,
1219 and leaf $C_i:C_a$, resulting in optimal photosynthetic rates achieved with decreased
1220 N_{area} . The theory also predicts variability in stomatal conductance and N_{area} in
1221 response to climatic factors, suggesting that the optimal response to increased va-
1222 por pressure deficit (VPD) should be a reduction in stomatal conductance and leaf
1223 $C_i:C_a$ that is counterbalanced by an increase in N_{area} to support the higher pho-
1224 tosynthetic capacity needed to maintain high assimilation at lower conductance
1225 (Grossiord et al. 2020; Dong et al. 2020; Westerband et al. 2023).

1226 Leaf nitrogen allocation responses to changing climates or soil resource
1227 availability may also depend on their mode of nutrient acquisition or photo-
1228 synthetic pathway. For example, species that form associations with symbiotic
1229 nitrogen-fixing bacteria (referred as “N-fixing species” from this point forward)

1230 should, in theory, have access to a less finite nitrogen supply, which may result in
1231 lower β values than species not capable of forming such associations (referred as
1232 “non-fixing species” from this point forward). This result was previously shown
1233 in a greenhouse experiment, where a leguminous species generally had lower costs
1234 of nitrogen acquisition compared to a non-leguminous species, although these dif-
1235 ferences were generally stronger under increased nitrogen limitation (Fig. 2.1)
1236 (Perkowski et al. 2021). Lower β values could be a possible explanation for
1237 why N-fixing species commonly have higher leaf nitrogen content than non-fixing
1238 species (Adams et al. 2016; Dong et al. 2017).

1239 Similarly, leaf nitrogen allocation patterns across environmental gradients
1240 may be dependent on photosynthetic pathway. General lower leaf $C_i:C_a$ values in
1241 C_4 species suggests that C_4 species should have lower β values than C_3 species, a
1242 pattern that could be the result of increased costs associated with water acquisition
1243 and use or reduced costs associated with nutrient acquisition and use relative to
1244 C_3 species. No study to date has directly quantified leaf $C_i:C_a$ in C_4 species aside
1245 from the dataset used to initially parameterize an optimality model for C_4 species
1246 (Scott and Smith 2022).

1247 While photosynthetic least-cost theory provides a unified hypothesis for
1248 understanding effects of climate and soil resource availability on N_{area} , empiri-
1249 cal tests of the theory are sparse. Increasing soil nitrogen availability has been
1250 previously shown to decrease the cost of acquiring nutrients (Bae et al. 2015; Lu
1251 et al. 2022; Eastman et al. 2021), which can induce predictable nutrient-water use
1252 tradeoffs expected from the theory across broad environmental gradients (Paillassa
1253 et al. 2020; Querejeta et al. 2022; Westerband et al. 2023) and in manipulation

1254 experiments (Bialic-Murphy et al. 2021). Additionally, increasing VPD has been
1255 shown to have a positive effect on N_{area} (Dong et al. 2017; Dong et al. 2020; Firn
1256 et al. 2019). However, studies have been restricted to exploring these patterns
1257 with C₃ species and, while previous studies have shown that variance in N_{area}
1258 across environmental gradients is driven by strong negative relationships with leaf
1259 C_i:C_a (Fig 3.4c)(Dong et al. 2017; Paillassa et al. 2020; Westerband et al. 2023),
1260 no study to date has explicitly investigated effects of soil resource availability or
1261 plant functional group on N_{area} using β as a direct predictor of leaf C_i:C_a. Addi-
1262 tionally, as N_{area} can be broken down into structural (leaf mass per area; M_{area} ;
1263 g m⁻²) and metabolic (mass-based leaf nitrogen content; N_{mass} ; gN g⁻¹) compo-
1264 nents (Dong et al. 2017), no study has investigated which component of N_{area}
1265 drives the hypothesized response of N_{area} to leaf C_i:C_a, which would be useful for
1266 detecting whether changes in N_{area} due to leaf C_i:C_a are driven by changes in leaf
1267 morphology or stoichiometry.

1268 Here, I measured N_{area} , N_{mass} , M_{area} , leaf δ¹³C-derived estimates of leaf
1269 C_i:C_a, and leaf δ¹³C-derived estimates of β in 520 individuals spanning 57 species
1270 scattered across 24 grassland sites in Texas, USA (Table S1). Texas contains a
1271 diverse climatic gradient, indicated by 2006-2020 mean annual precipitation totals
1272 ranging from 204 to 1803 mm and 2006-2020 mean annual temperature ranging
1273 from 11.8° to 24.6°C. Variability in soil nitrogen availability and soil moisture was
1274 expected across sites, owing to differences in soil texture and aboveground climate
1275 that would drive differential rates of water retention and nitrogen transformations
1276 to plant-available substrate. I leveraged the expected climatic and soil resource
1277 variability across sites to test the following hypotheses:

- 1278 1. Soil nitrogen availability will decrease β through a reduction in costs of
1279 nitrogen acquisition and use, while soil moisture will increase β through a
1280 reduction in costs of water acquisition and use. We expected that N-fixing
1281 species would have lower β values due to their ability to minimize costs
1282 of nitrogen acquisition under low nitrogen availability and that C₄ species
1283 would have lower β values due to increased costs of water acquisition and
1284 use or reduced costs of nitrogen acquisition and use.
- 1285 2. leaf C_i:C_a will be positively related to β , a pattern that will result in a neg-
1286 ative indirect effect of increasing soil nitrogen availability, positive indirect
1287 effect of increasing soil moisture on leaf C_i:C_a, and lower leaf C_i:C_a in both
1288 N-fixing species and C₄ species. We also expected that leaf C_i:C_a would be
1289 negatively related to VPD, as increasing atmospheric dryness should cause
1290 plants to close stomata to minimize water loss.
- 1291 3. N_{area} will be negatively related to leaf C_i:C_a. This response will result in
1292 an indirect positive effect of increasing soil nitrogen availability, a negative
1293 effect of increasing soil moisture on N_{area} , and generally larger N_{area} values in
1294 both N-fixing species. We expected these patterns to be mediated through
1295 a positive relationship between β and leaf C_i:C_a. While theory predicts that
1296 negative relationships between N_{area} and leaf C_i:C_a should yield generally
1297 larger N_{area} in C₄ species, we expected that C₄ species would have lower N_{area}
1298 due to generally greater nitrogen use efficiency in C₄ species than C₃ species.
1299 Additionally, VPD was expected to increase N_{area} , a pattern that would be
1300 directly mediated through the reduction in leaf C_i:C_a with increasing VPD.

1301 4.2 Methods

1302 4.2.1 *Site descriptions and sampling methodology*

1303 I collected leaf and soil samples from 24 open grassland sites across central and
1304 eastern Texas in summer 2020 and summer 2021 (Fig. 4.1). Twelve sites were vis-
1305 ited between June and July 2020 and 14 sites (11 unique from 2020) were visited
1306 between May and June 2021 (Table 1). I explicitly chose sites that maximized
1307 variability in precipitation and edaphic variability between sites while minimizing
1308 temperature variability across the environmental gradient (Table 1). No site with
1309 personally communicated or anecdotal evidence of grazing or disturbance (e.g.,
1310 mowing, feral hog activity, etc.) were used. I collected leaf material from three
1311 individuals each of the five most abundant species at random locations at each
1312 site, only selecting species that were broadly classified as graminoid or forb/herb
1313 growth habits per the USDA PLANTS database (USDA NRCS 2022). All col-
1314 lected leaves were fully expanded with no visible herbivory or other external dam-
1315 age and also free from shading by nearby shrubs or trees. Five soil samples were
1316 collected from 0-15cm below the soil surface at each site near the leaf collection
1317 sample locations. Soil samples were later mixed together by hand to create one
1318 composite soil sample per site.

1319 4.2.2 *Leaf trait measurements*

1320 Images of each leaf were taken immediately following each site visit using a flat-
1321 bed scanner. Fresh leaf area was determined from each image using the 'LeafArea'
1322 R package (Katabuchi 2015), which automates leaf area calculations using ImageJ
1323 software (Schneider et al. 2012). Each leaf was dried at 65°C for at least 48 hours

1324 to a constant mass, weighed, and manually ground in a mortar and pestle until
1325 homogenized. Leaf mass per area (M_{area} ; g m⁻²) was calculated as the ratio of
1326 dry leaf biomass to fresh leaf area. Subsamples of dried and homogenized leaf
1327 tissue were used to measure leaf nitrogen content (N_{mass} ; gN g⁻¹) through ele-
1328 mental combustion analysis (Costech-4010, Costech Instruments, Valencia, CA).
1329 Leaf nitrogen content per unit leaf area (N_{area} ; gN m⁻²) was then calculated as
1330 the product of N_{mass} and M_{area} .

1331 Subsamples of dried and homogenized leaf tissue were sent to the University
1332 of California-Davis Stable Isotope Facility to determine leaf $\delta^{13}\text{C}$. Leaf $\delta^{13}\text{C}$ values
1333 were determined using an elemental analyzer (PDZ Europa ANCA-GSL; Sercon
1334 Ltd., Chestshire, UK) interfaced to an isotope ratio mass spectrometer (PDZ
1335 Europa 20-20 Isotope Ratio Mass Spectrometer, Sercon Ltd., Chestshire, UK).
1336 I used leaf $\delta^{13}\text{C}$ values (‰; relative to Vienna Pee Dee Belemnite international
1337 reference standard) to estimate the ratio of intercellular (C_i) to extracellular (C_a)
1338 CO₂ ratio (leaf $C_i:C_a$; unitless) following the approach of Farquhar et al. (1989)
1339 described in Cernusak et al. (2013). Specifically, I derived leaf C_i:C_a as:

$$\text{Leaf } \frac{C_i}{C_a} = \frac{\Delta^{13}\text{C} - a}{b - a} \quad (4.1)$$

1340 where $\Delta^{13}\text{C}$ represents the relative difference between leaf $\delta^{13}\text{C}$ (‰) and air $\delta^{13}\text{C}$
1341 (‰), and is calculated as:

$$\Delta^{13}\text{C} = \frac{\delta^{13}\text{C}_{\text{air}} - \delta^{13}\text{C}_{\text{leaf}}}{1 + \delta^{13}\text{C}_{\text{leaf}}} \quad (4.2)$$

1342 $\delta^{13}\text{C}_{\text{air}}$, traditionally assumed to be -8‰ (Keeling et al. 1979; Farquhar et al.

1343 1989), was calculated as a function of calendar year t using an empirical equation
1344 derived in Feng (1999):

$$\delta^{13}C_{air} = -6.429 - 0.006e^{0.0217(t-1740)} \quad (4.3)$$

1345 This calculation resulted in $\delta^{13}C_{air}$ values for 2020 and 2021 as -9.04 and -9.09,
1346 respectively. a represents the fractionation between ^{12}C and ^{13}C due to diffusion
1347 in air, assumed to be 4.4‰, and b represents the fractionation caused by Rubisco
1348 carboxylation, assumed to be 27‰ (Farquhar et al. 1989). For C_4 species, b in
1349 Eqn. 4.1 was set to 6.3‰, and was derived from:

$$b = c + (d \cdot \phi) \quad (4.4)$$

1350 Where c was set to -5.7‰ and d was set to 30‰ (Farquhar et al. 1989). ϕ , which
1351 is the bundle sheath leakiness term, was set to 0.4. All leaf $C_i:C_a$ values less than
1352 0.2 and greater than 1.0 were assumed to be incorrect and removed.

1353 I derived the unit cost of resource use (β) using leaf leaf $C_i:C_a$ and site
1354 climate data with equations first described in Prentice et al. (2014) and simplified
1355 in Lavergne et al. (2020):

$$\beta = 1.6\eta^* D \frac{\chi - (\frac{\Gamma^*}{C_a})^2}{(1 - \chi)^2(K_m + \Gamma^*)} \quad (4.5)$$

1356 where η^* is the viscosity of water relative to 25°C, calculated using elevation and
1357 mean air temperature of the seven days leading up to each site visit following
1358 equations in Huber et al. (2009). D represents vapor pressure deficit (Pa), set

1359 to the mean vapor pressure deficit of the seven days leading up to each site visit,
1360 C_a represents atmospheric CO₂ concentration, arbitrarily set to 420 $\mu\text{mol mol}^{-1}$
1361 CO². K_m (Pa) is the Michaelis-Menten coefficient for Rubisco affinity to CO₂ and
1362 O₂, calculated as:

$$K_m = K_c \cdot \left(1 + \frac{O_i}{K_o}\right) \quad (4.6)$$

1363 where K_c (Pa) and K_o (Pa) are the Michaelis-Menten coefficients for Rubisco
1364 affinity to CO₂ and O₂, respectively, and O_i is the intercellular O₂ concentration.
1365 Γ^* (Pa) is the CO₂ compensation point in the absence of dark respiration. K_c , K_o ,
1366 and Γ^* were determined using equations described in Medlyn et al. (2002) and
1367 derived in Bernacchi et al. (2001), invoking an elevation correction for atmospheric
1368 pressure as explained in Stocker et al. (2020).

Table 4.1. Site locality information, sampling year(s), 2006-2020 mean annual precipitation (MAP; mm), mean annual temperature (MAT; °C), and water holding capacity (WHC; mm)*

Site	Latitude	Longitude	Sampling year	MAP	MAT	WHC
Edwards_2019_17	29.95	-100.36	2020	563.5	19.0	224.7
Uvalde_2020_02	29.59	-100.09	2020, 2021	648.5	19.5	224.7
Menard_2020_01	30.91	-99.59	2020	641.9	18.3	220.2
Kerr_2020_03	30.06	-99.34	2021	672.4	18.3	237.5
Bandera_2020_03	29.85	-99.30	2021	789.4	18.8	235.1
Sansaba_2020_01	31.29	-98.62	2020	733.0	18.8	234.3
Comal_2020_21	29.79	-98.43	2020	878.5	19.9	220.7
Blanco_2019_16	29.99	-98.43	2020	833.0	19.2	222.2
Bexar_2019_13	29.24	-98.43	2020	759.3	21.5	206.0
Burnet_2020_14	30.84	-98.34	2021	763.3	19.5	217.8
Comal_2020_19	30.01	-98.32	2021	845.0	19.3	220.4
Hays_2020_54	29.96	-98.17	2021	861.3	20.0	225.6
Burnet_2020_12	30.82	-98.06	2021	815.1	19.4	245.3
Williamson_2019_09	30.71	-97.86	2020	867.7	19.7	270.2
Williamson_2019_10	30.54	-97.77	2020	819.5	19.9	239.8
Bell_2021_08	31.06	-97.55	2021	937.3	19.6	232.3
Fayette_2021_12	29.86	-97.21	2021	985.7	20.4	165.6
Fayette_2019_04	30.09	-96.78	2020	1017.4	20.6	226.9
Fayette_2020_09	29.86	-96.71	2021	1002.7	20.8	187.6
Washington_2020_08	30.28	-96.41	2021	1077.4	20.4	203.9
Austin_2020_03	29.78	-96.24	2021	1108.7	20.6	253.0
Brazos_2020_16	30.93	-96.23	2021	1078.0	20.1	202.2
Brazos_2020_18	30.52	-96.21	2020, 2021	1099.4	20.4	233.5
Harris_2020_03	29.88	-95.31	2020, 2021	1492.0	21.6	265.6

1369 *Rows are arranged by longitude to visualize precipitation variability across sites

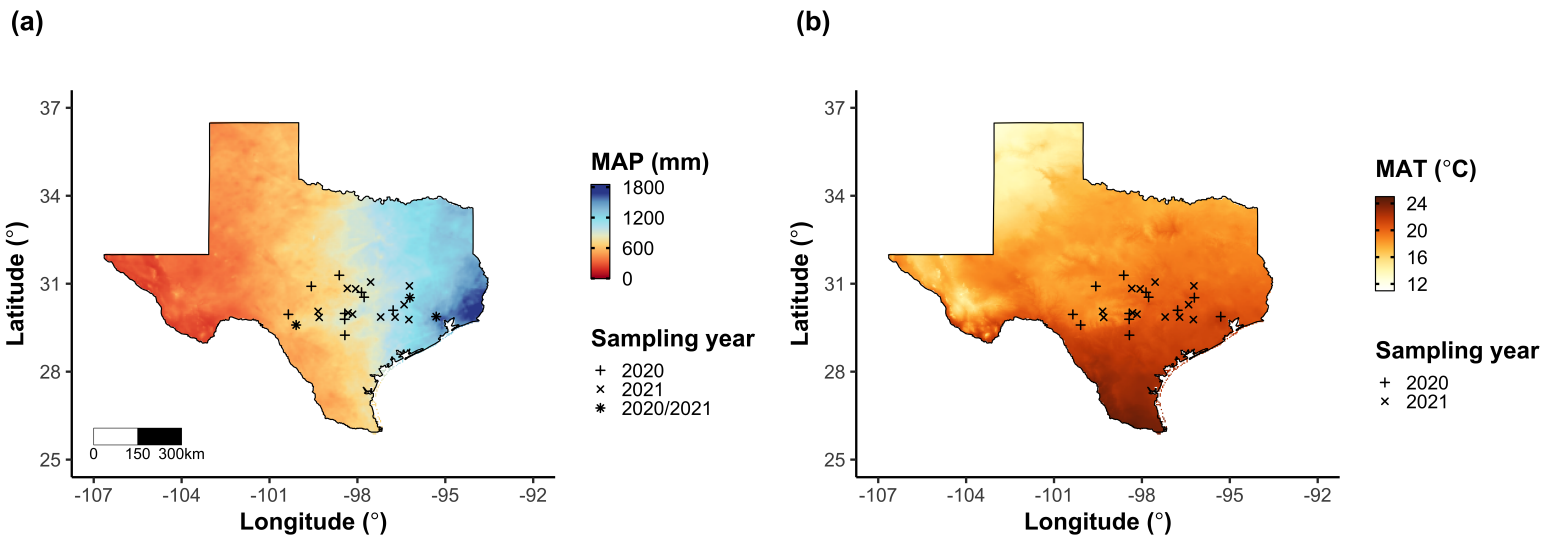


Figure 4.1. Maps that detail site locations along 2006-2020 mean annual precipitation (a) and mean annual temperature (b) gradients in Texas, USA. Precipitation and temperature data were plotted at a 4-km grid resolution and are masked to include only grid cells that occur in the Texas state boundary in the United States. In both panels, open circles refer to sites visited in 2020, open triangles to sites visited in 2021, and closed circles to sites visited in 2020 and 2021. The scale bar in panel A also applies to panel B.

1370 4.2.3 *Site climate data*

1371 I used the Parameter-elevation Regressions on Independent Slopes Model (PRISM)
1372 (Daly et al. 2008)climate product to access gridded daily temperature and precip-
1373 itation data for the coterminous United States at a 4-km grid resolution between
1374 January 1, 2006 and July 31, 2021 (PRISM Climate Group, Oregon State Uni-
1375 versity, <https://prism.oregonstate.edu>, data created 4 Feb 2014, accessed 24 Mar
1376 2022). Daily mean air temperature, mean VPD, and total precipitation data were
1377 extracted from the grid cell that contained the latitude and longitude of each
1378 property using the ‘extract’ function in the ‘terra’ R package (Hijmans 2022).
1379 PRISM data were used in lieu of local weather station data because several rural
1380 sites did not have a local weather station present within a 20-km radius of the site.
1381 Daily site climate data were used to estimate mean annual precipitation and mean
1382 annual temperature for each site between 2006 and 2020 (Table 1). I calculated
1383 total precipitation and mean daily VPD for the prior 1, 2, 3, 4, 5, 6, 7, 8, 9, 10,
1384 15, 20, 25, 30, 60, and 90 days leading up to each site visit.

1385 4.2.4 *Site edaphic characteristics*

1386 Subsamples of composited soil samples were sent to the Texas A & M Soil, Water
1387 and Forage Laboratory to quantify soil nitrate concentration (NO₃-N; ppm). Soil
1388 NO₃-N was determined by extracting composite soil samples in 1 M KCl, mea-
1389 suring absorbance values of extracts at 520 nm using the end product of a NO₃-N
1390 to NO₂-N cadmium reduction reaction (Kachurina et al. 2000). Soil texture data
1391 from 0-15cm below the soil surface were accessed using the SoilGrids2.0 data prod-
1392 uct (Poggio et al. 2021) through the ‘fetchSoilGrids’ function in the ‘soilDB’ R

1393 package (Beaudette et al. 2022). I used SoilGrids2.0 to access soil texture data
1394 in lieu of analyses using the collected composite soil sample due to a lack of soil
1395 material from some sites after sending samples for soil NO₃-N.

1396 Soil moisture was not measured in the field, but was estimated using
1397 the ‘Simple Process-Led Algorithms for Simulating Habitats’ model (‘SPLASH’)
1398 (Davis et al. 2017). This model, derived from the STASH model (Cramer and
1399 Prentice 1988), spins up a bucket model using Priestley-Taylor equations (Priest-
1400 ley and Taylor 1972) to calculate daily soil moisture (W_n ; mm) as a function
1401 of the previous day’s soil moisture (W_{n-1} ; mm), daily precipitation (P_n ; mm),
1402 condensation (C_n ; mm), actual evapotranspiration (E_n^a ; mm), and runoff (RO;
1403 mm):

$$W_n = W_{n-1} + P_n + C_n - E_n^a - RO \quad (4.7)$$

1404 Models were spun up by equilibrating the previous day’s soil moisture using
1405 successive model iterations with daily mean air temperature, daily precipitation
1406 total, the number of daily sunlight hours, and latitude as model inputs (Davis et al.
1407 2017). Daily sunlight hours were estimated for each day at each site using the
1408 ‘getSunlightTimes’ function in the ‘suncalc’ R package, which estimated sunrise
1409 and sunset times of each property using date and site coordinates (Thieurmel and
1410 Elmarhraoui 2019). Water holding capacity (mm), or bucket size, was estimated
1411 as a function of soil texture using pedotransfer equations explained in Saxton and
1412 Rawls (2006), as done in Stocker et al. (2020) and Bloomfield et al. (2023). A
1413 summary of these equations is included in the Supplemental Information.

1414 Daily soil moisture outputs from the SPLASH model for each site were
1415 used to calculate mean daily soil moisture for the prior 1, 2, 3, 4, 5, 6, 7, 8, 9,
1416 10, 15, 20, 25, 30, 60, and 90 days leading up to each site visit. Mean daily
1417 soil moisture values were then expressed as a fraction of water holding capacity
1418 to normalize across sites with different bucket depths, as done in Stocker et al.
1419 (2018).

1420 4.2.5 *Plant functional group assignments*

1421 Plant functional group was assigned to each species and used as the primary
1422 descriptor of species identity. Specifically, I assigned plant functional groups
1423 based on photosynthetic pathway (C_3 , C_4) and ability to form associations with
1424 symbiotic nitrogen-fixing bacteria. The ability to form associations with symbi-
1425 otic nitrogen-fixing bacteria was assigned based on whether species were in the
1426 *Fabaceae* family, and photosynthetic pathway of each species was determined from
1427 past literature and confirmed through leaf $\delta^{13}\text{C}$ values. We chose these plant func-
1428 tional groups based on *a priori* hypotheses regarding the functional role of nitrogen
1429 fixation and photosynthetic pathway on the sensitivity of plant nitrogen uptake
1430 and leaf nitrogen allocation to soil nutrient availability and aboveground growing
1431 conditions. These plant functional group classifications resulted in three distinct
1432 plant functional groups within our dataset: C_3 legumes ($n = 53$), C_3 non-legumes
1433 ($n = 350$), and C_4 non-legumes ($n = 117$).

1434 4.2.6 *Data analysis*

1435 All analyses and plotting were conducted in R version 4.1.1 (R Core Team 2021).

1436 I constructed a series of separate linear mixed-effects models to investigate en-

1437 vironmental drivers of β , leaf $C_i:C_a$, N_{area} , N_{mass} , and M_{area} , followed by a path

1438 analysis using a piecewise structural equation model to investigate direct and

1439 indirect effects of climate and soil resource availability on N_{area} .

1440 To explore environmental drivers of β , I built a linear mixed-effects model

1441 that included soil moisture, soil nitrogen availability, and plant functional group

1442 as fixed effect coefficients. Species were designated as a random intercept term.

1443 Interaction coefficients between all possible combinations of the three fixed effect

1444 coefficients were also included. β was natural log transformed to linearize data.

1445 I used an information-theoretic model selection approach to determine whether

1446 90-, 60-, 30-, 20-, 15-, 10-, 9-, 8-, 7-, 6-, 5-, 4-, 3-, 2-, or 1-day mean daily soil

1447 moisture conferred the best model fit for β . To do this, I constructed 16 separate

1448 linear mixed-effects models where log-transformed β was included as the response

1449 variable and each soil moisture time step was separately included as a single

1450 continuous fixed effect. Species were included as a random intercept term for all

1451 models. I used corrected Akaike Information Criterion (AICc) to select the soil

1452 moisture timescale that conferred the best model fit, indicated by the model with

1453 the lowest AICc score (Table S2; Fig. S2).

1454 To explore environmental drivers of leaf $C_i:C_a$, I constructed a second linear

1455 mixed effects model that included VPD, soil moisture, soil nitrogen availability,

1456 and plant functional group as fixed effect coefficients. Two-way interactions be-

1457 tween plant functional group and VPD, soil nitrogen availability, or soil moisture

1458 were also included as fixed effect coefficients, in addition to a three-way interaction
1459 between soil moisture, soil nitrogen availability, and plant functional group.
1460 Species were included as a random intercept term. I used an information-theoretic
1461 model selection approach to determine whether 90-, 60-, 30-, 20-, 15-, 10-, 9-, 8-,
1462 7-, 6-, 5-, 4-, 3-, 2-, or 1-day mean daily VPD conferred the best model fit for leaf
1463 $C_i:C_a$ using the same approach explained above for the soil moisture effect on β .
1464 The soil moisture timescale was set to the same timescale that conferred the best
1465 fit for β .

1466 To explore environmental drivers of N_{area} , N_{mass} , and M_{area} , I constructed
1467 three separate linear mixed effects model that each included leaf $C_i:C_a$, soil ni-
1468 trogen availability, soil moisture, and plant functional group as fixed effect coef-
1469 ficients. Two-way interactions between plant functional group and β , leaf $C_i:C_a$,
1470 soil nitrogen availability, or soil moisture were included as additional fixed effect
1471 coefficients, in addition to a three-way interaction between soil nitrogen availabil-
1472 ity, soil moisture, and plant functional group. Species were included as a random
1473 intercept term, with the soil moisture timescale set to the same timescale that
1474 conferred the best fit for β .

1475 In all linear mixed-effects models explained above, including those to select
1476 relevant timescales, I used the 'lmer' function in the 'lme4' R package (Bates et al.
1477 2015) to fit each model and the 'Anova' function in the 'car' R package (Fox and
1478 Weisberg 2019) to calculate Type II Wald's χ^2 and determine the significance
1479 level ($\alpha = 0.05$) of each fixed effect coefficient. I used the 'emmeans' R package
1480 (Lenth 2019) to conduct post-hoc comparisons using Tukey's tests, where degrees
1481 of freedom were approximated using the Kenward-Roger approach (Kenward and

1482 Roger 1997). Trendlines and error ribbons for all plots were drawn using a series
1483 of ‘emmeans’ outputs across the range in plotted x-axis values.

1484 Finally, I conducted a path analysis using a piecewise structural equa-
1485 tion model to examine direct and indirect pathways that determined variance in
1486 N_{area} . Seven separate linear mixed effects models were loaded into the piecewise
1487 structural equation model. Models were constructed per our *a priori* hypotheses
1488 following patterns expected from photosynthetic least-cost theory. The first model
1489 regressed N_{area} against leaf $C_i:C_a$, N_{mass} , and M_{area} . The second model regressed
1490 M_{area} against leaf $C_i:C_a$. The third model regressed N_{mass} against leaf $C_i:C_a$ and
1491 M_{area} (Dong et al. 2017; Dong et al. 2020). The fourth model regressed leaf
1492 $C_i:C_a$ against β and VPD. The fifth model regressed β against soil nitrogen avail-
1493 ability, soil moisture, ability to associate with symbiotic nitrogen-fixing bacteria,
1494 and photosynthetic pathway. The sixth model regressed soil nitrogen availability
1495 against soil moisture, while the seventh model regressed VPD against soil mois-
1496 ture (Novick et al. 2016; Sulman et al. 2016). All models included the relevant
1497 timescale selected in the individual linear mixed effect models explained above
1498 (2-day soil moisture, 4-day vapor pressure deficit). Models also included species
1499 as a random intercept term, were built using the ‘lme’ function in the ‘nlme’
1500 R package (Pinheiro and Bates 2022), and subsequently loaded into the piece-
1501 wise structural equation model using the ‘psem’ function in the ‘piecewiseSEM’
1502 R package (Lefcheck 2016).

1503 4.3 Results

1504 4.3.1 *Cost to acquire nitrogen relative to water (β)*

1505 Model selection indicated that 2-day soil moisture was the timescale that con-
1506 fered the best model fit for β (AICc = 1227.83; Table S2; Fig. S1). Increasing
1507 soil nitrogen availability generally decreased β ($p < 0.001$; Table 4.2), a pattern
1508 driven by a negative effect of increasing soil nitrogen availability on β in C₃ non-
1509 legumes (Tukey: $p < 0.001$) and C₃ legumes (Tukey: $p = 0.004$; Fig. 4.2a). C₄
1510 nonlegumes also demonstrated a negative trend in the effect of increasing soil ni-
1511 trogen availability on β , but this pattern was not significantly different from zero
1512 (Tukey: $p = 0.307$; Fig. 4.2a). There was no apparent effect of soil moisture on
1513 β ($p = 0.264$; Table 4.2; Fig. 4.2b). A functional group effect ($p < 0.001$; Table
1514 4.2) indicated that C₄ nonlegumes generally had lower β values than both C₃
1515 legumes and C₃ non-legumes when averaged across soil moisture and soil nitrogen
1516 availability values (Tukey: $p < 0.001$ in both cases), while average β values in C₃
1517 legumes did not differ from C₃ nonlegumes (Tukey: $p = 0.691$).

Table 4.2. Effects of soil moisture, soil nitrogen availability, and plant functional group on β

	df	Coefficient	χ^2	p
Intercept	-	3.20E+00	-	-
Soil moisture (SM_2)	1	2.19E-01	1.244	0.265
Soil N (N)	1	-1.70E-02	26.823	<0.001
PFT	2	-	199.617	<0.001
SM_2*N	1	1.77E-03	0.438	0.508
SM_2*PFT	2	-	2.038	0.361
$N*PFT$	2	-	7.668	0.022
$SM_2*N*PFT$	2	-	0.127	0.939

1518 *Significance determined using Type II Wald χ^2 tests ($\alpha = 0.05$). P-values < 0.05

1519 are in bold. Model coefficients are expressed on the natural-log scale and are only

1520 included for continuous fixed effects. Key: df = degrees of freedom, χ^2 = Wald

1521 Type II chi-square test statistic

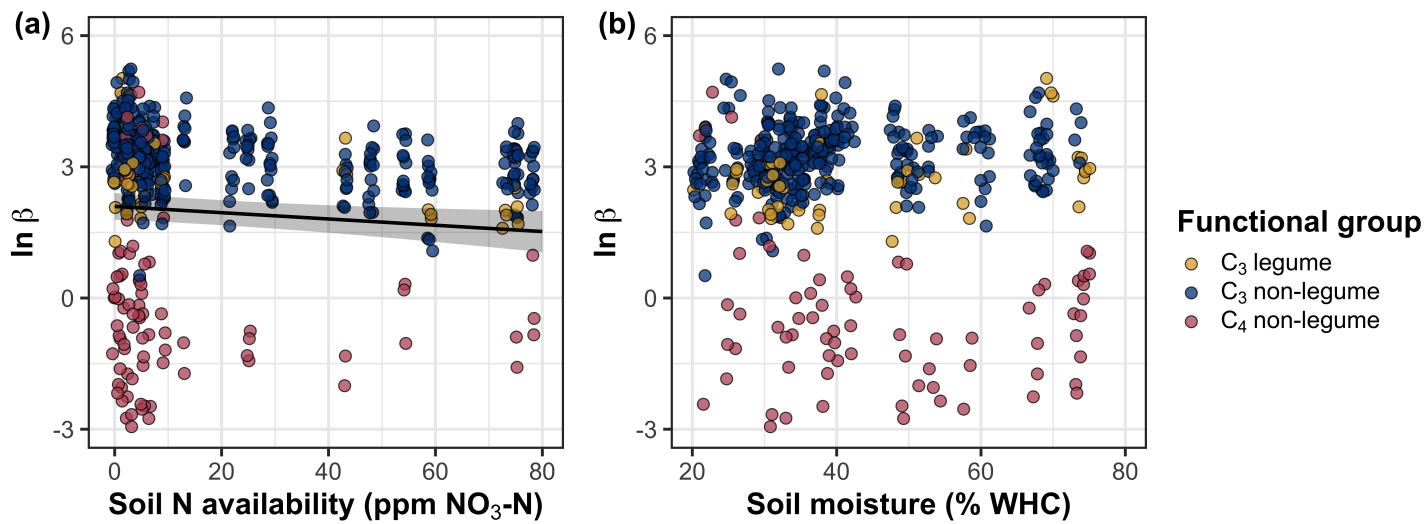


Figure 4.2. Effects of soil nitrogen availability (a) and soil moisture (b) on the unit cost ratio β . In (b), soil moisture is represented as a percent of site water holding capacity. Yellow shading and trendlines indicate C_3 legumes, blue shading and trendlines indicate C_3 non-legumes, and red shading and trendlines indicate C_4 non-legumes. Points are jittered for visibility. Variably colored trendlines are only included if there is an interaction between the x-axis and plant functional group, where solid trendlines indicate slopes that are different from zero ($p < 0.05$) and dashed trendlines indicate slopes that are not different from zero ($p > 0.05$). Error ribbons represent the upper and lower 95% confidence intervals of each fitted trendline.

1522 4.3.2 *Leaf C_i:C_a*

1523 Model selection indicated that 4-day daily VPD was the timescale that conferred

1524 the best model fit for leaf C_i:C_a (AICc = -883.97; Table S1; Fig. S2).

1525 Variance in leaf C_i:C_a was driven by a series of two-way interactions be-

1526 tween functional group and VPD ($p = 0.006$; Table 3), soil moisture ($p = 0.033$,

1527 Table 3.3), and soil nitrogen availability ($p = 0.022$; Table 3). The interaction be-

1528 tween 4-day VPD and functional group revealed that the general negative effect of

1529 increasing VPD ($p < 0.001$; Table 3) was driven by a negative effect of increasing

1530 VPD on leaf C_i:C_a in C₃ nonlegumes (Tukey: $p < 0.001$) and marginal negative

1531 effect in C₃ legumes (Tukey: $p = 0.074$) paired with a positive trending, but in-

1532 significant effect of increasing VPD in C₄ nonlegumes (Tukey: $p = 0.130$; Fig. 3a).

1533 The interaction between 2-day soil moisture and functional group indicated that

1534 the general negative effect of increasing soil moisture on leaf C_i:C_a was driven by a

1535 positive effect of increasing soil moisture on leaf C_i:C_a in C₄ nonlegumes (Tukey:

1536 $p = 0.009$) despite a positive trending but insignificant effect of increasing soil

1537 moisture on leaf C_i:C_a in C₃ legumes (Tukey: $p = 0.116$) and a null effect of

1538 soil moisture on leaf C_i:C_a in C₃ nonlegumes (Tukey: $p = 0.693$; Fig. 3c). The

1539 interaction between soil nitrogen availability and plant functional group revealed

1540 a weak negative effect of increasing soil nitrogen availability on leaf C_i:C_a in C₃

1541 legumes (Tukey: $p = 0.045$), with no apparent effect in C₃ nonlegumes (Tukey:

1542 $p = 0.706$) or C₄ nonlegumes (Tukey: $p = 0.757$). Finally, an individual effect

1543 of functional group ($p < 0.001$; Table 3) revealed that C₄ nonlegumes generally

1544 had lower leaf C_i:C_a than C₃ legumes and C₃ nonlegumes (Tukey: $p < 0.001$ in

1545 both cases), with no apparent difference between C₃ legumes and C₃ nonlegumes

1546 (Tukey: $p = 0.831$).

Table 4.3. Effects of soil moisture, soil nitrogen availability, and plant functional group on χ^*

	df	Coefficient	χ^2	p
Intercept	-	9.33E-01	-	-
Vapor pressure deficit (VPD_4)	1	-1.78E-01	20.792	<0.001
Soil moisture (SM_2)	1	4.53E-02	1.972	0.160
Soil N (N)	1	-1.30E-03	0.168	0.682
PFT	2	-	172.624	<0.001
SM_2^*N	1	7.40E-04	0.849	0.357
VPD_4^*PFT	2	-	10.241	0.006
SM_2^*PFT	2	-	6.806	0.033
N^*PFT	2	-	7.602	0.022
$SM_2^*N^*PFT$	2	-	0.732	0.694

1547 *Significance determined using Type II Wald χ^2 tests ($\alpha = 0.05$). *P*-values less
1548 than 0.05 are in bold and *p*-values where $0.05 < p < 0.1$ are italicized. Leaf C_i:C_a
1549 was not transformed prior to model fitting, so model coefficients are reported
1550 on the response scale. Model coefficients are only included for continuous fixed
1551 effects.

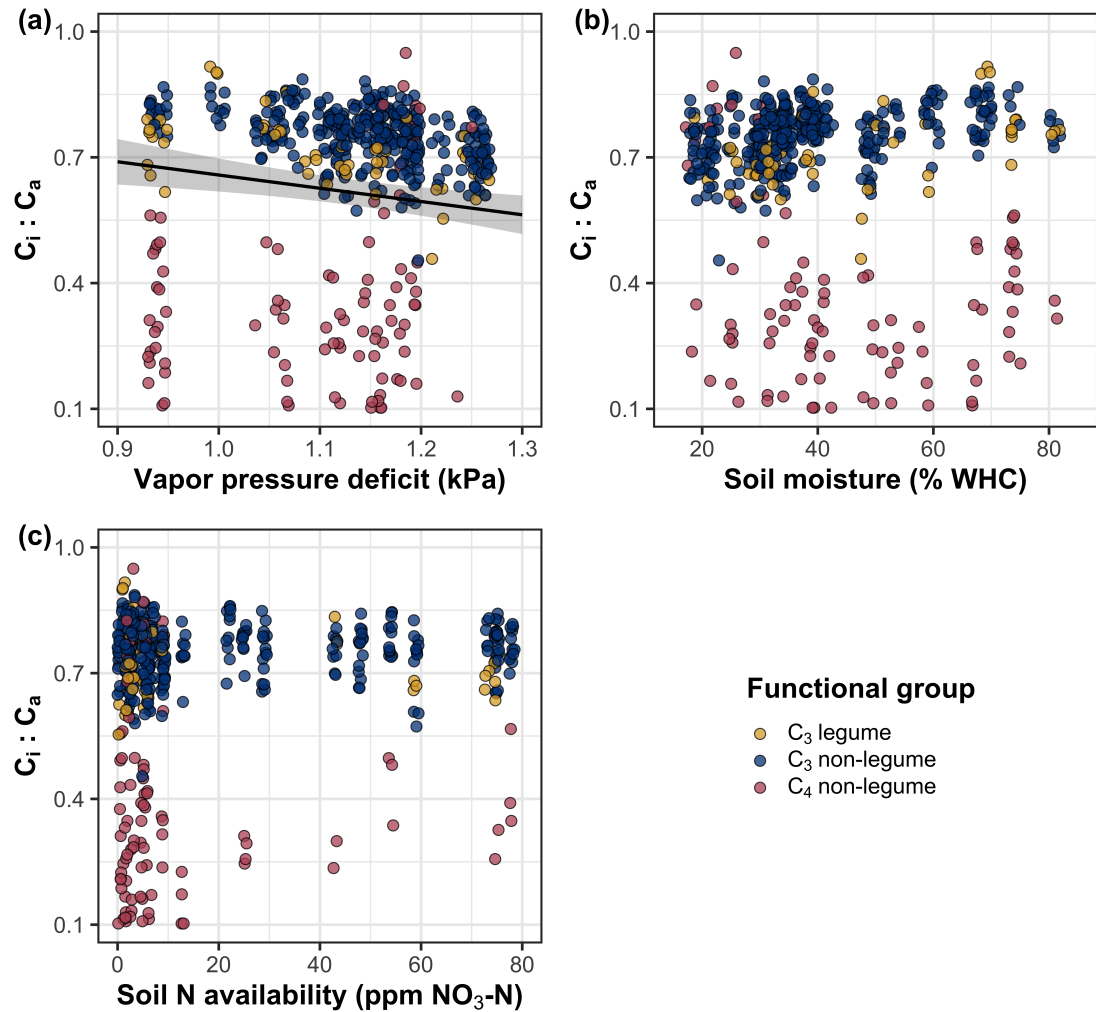


Figure 4.3. Effects of 4-day mean vapor pressure deficit (a), 2-day soil moisture (per water holding capacity; b), and soil nitrogen availability (c) on leaf $C_i:C_a$. Shading and trendlines are as explained in Figure 2. Points are jittered for visibility. Variably colored trendlines are only included if there is an interaction between the x-axis and plant functional group, where solid trendlines indicate slopes that are different from zero ($p < 0.05$) and dashed trendlines indicate slopes that are not different from zero ($p >= 0.05$). Error ribbons represent the upper and lower 95% confidence intervals of each fitted trendline.

1552 4.3.3 *Leaf nitrogen content*

1553 An interaction between leaf C_i:C_a and plant functional group ($p < 0.001$; Table
1554 4) revealed that the general negative effect of increasing leaf C_i:C_a on N_{area} ($p <$
1555 0.001; Table 4) was driven by a negative effect of increasing leaf C_i:C_a on N_{area} in
1556 C₃ nonlegumes (Tukey: $p < 0.001$) and C₃ legumes (Tukey: $p = 0.002$) despite a
1557 null effect of leaf C_i:C_a on N_{area} in C₄ nonlegumes (Tukey: $p = 0.795$; Fig. 4a). An
1558 interaction between soil nitrogen availability and soil moisture ($p = 0.028$; Table
1559 4) indicated that the marginal positive effect of increasing soil nitrogen availability
1560 on N_{area} ($p = 0.091$; Table 4) decreased with increasing soil moisture, despite no
1561 apparent individual effect of soil moisture on N_{area} ($p = 0.692$; Table 4). Finally,
1562 a plant functional group effect ($p < 0.001$; Table 4) indicated that C₄ nonlegumes
1563 had lower N_{area} values on average compared to C₃ legumes (Tukey: $p < 0.001$)
1564 and C₃ nonlegumes (Tukey: $p = 0.001$), while C₃ legumes had lower average N_{area}
1565 values compared to C₃ nonlegumes (Tukey: $p = 0.012$).

1566 A marginal interaction between leaf C_i:C_a and plant functional group (p
1567 $= 0.088$; Table 4) revealed that, despite no apparent general effect of leaf C_i:C_a
1568 on N_{mass} ($p = 0.273$; Table 4), increasing leaf C_i:C_a decreased N_{mass} in C₃ non-
1569 legumes (Tukey: $p = 0.021$), but this effect was not apparent in C₄ nonlegumes
1570 (Tukey: $p = 0.693$) or C₃ legumes (Tukey: $p = 0.477$). An interaction between
1571 soil nitrogen availability and soil moisture ($p < 0.001$; Table 4) indicated that the
1572 general positive effect of increasing soil nitrogen availability on N_{mass} ($p < 0.001$;
1573 Table 4) generally decreased with increasing soil moisture, despite an apparent
1574 general positive effect of increasing soil moisture on N_{mass} ($p < 0.001$; Table 4).
1575 This interaction indicated that the positive effect of increasing soil nitrogen avail-

1576 ability on N_{mass} was only apparent when soil moisture was less than 70% the
1577 maximum water holding capacity (Tukey: $p < 0.05$ in all cases) despite a positive
1578 effect of increasing soil moisture on N_{mass} ($p < 0.001$; Table 4). Finally, a plant
1579 functional group effect ($p < 0.001$; Table 4) indicated that C₄ nonlegumes had
1580 lower N_{mass} values on average compared to C₃ legumes (Tukey: $p = 0.002$) and
1581 C₃ nonlegumes (Tukey: $p = 0.019$), while N_{mass} did not differ between C₃ legumes
1582 and C₃ nonlegumes (Tukey: $p = 0.149$).

1583 An interaction between leaf C_i:C_a and functional group ($p = 0.005$; Table
1584 4) indicated that the general negative effect of increasing leaf C_i:C_a on M_{area} ($p <$
1585 0.001; Table 4; Fig. 4c) was driven by a negative effect of increasing leaf C_i:C_a on
1586 M_{area} in C₃ legumes and C₃ nonlegumes (Tukey: $p < 0.001$ in both cases) despite a
1587 nonsignificant effect of increasing leaf C_i:C_a on M_{area} in C₄ nonlegumes (Tukey: p
1588 = 0.724). An interaction between soil nitrogen and soil moisture ($p < 0.001$; Table
1589 4) indicated that the general negative effect of increasing soil nitrogen availability
1590 on M_{area} ($p < 0.001$; Table 4) decreased with increasing soil moisture, despite an
1591 apparent general negative effect of increasing soil moisture on M_{area} ($p = 0.002$;
1592 Table 4). Specifically, the negative effect of increasing soil nitrogen availability on
1593 M_{area} was only apparent when soil moisture was less than 65% the maximum water
1594 holding capacity (Tukey: $p < 0.05$ in all cases). An additional interaction between
1595 soil nitrogen availability and functional group ($p = 0.034$; Table 4) indicated that
1596 the general negative effect of increasing soil nitrogen availability on M_{area} was
1597 driven by decreases in C₃ nonlegumes (Tukey: $p < 0.001$) and C₄ nonlegumes
1598 (Tukey: $p = 0.003$), with no apparent effect of soil nitrogen availability on M_{area}
1599 in C₃ legumes (Tukey: $p = 0.997$).

Table 4.4. Effects of soil nitrogen fertilization, inoculation, and CO₂ treatments on N_{area} , N_{mass} , and M_{area}

		N_{area}			N_{mass}			M_{area}		
	df	Coefficient	χ^2	p	Coefficient	χ^2	p	Coefficient	χ^2	p
(Intercept)	-	2.78E+00	-	-	4.42E-01	-	-	6.97E+00	-	-
χ	1	-2.53E+00	15.771	<0.001	4.56E-01	1.201	0.273	-3.10E+00	20.620	<0.001
Soil N (N)	1	1.08E-02	2.855	<i>0.091</i>	1.37E-02	54.531	<0.001	-2.87E-03	29.759	<0.001
Soil moisture (SM ₂)	1	3.61E-01	0.157	0.692	5.04E-01	16.255	<0.001	-1.26E-01	9.282	0.002
PFT	1	-	60.641	<0.001	-	21.539	<0.001	-	11.520	0.003
SM ₂ *N	1	-1.09E-02	4.779	0.029	-1.76E-02	41.784	<0.001	6.35E-03	14.111	<0.001
χ^*PFT	1	-	15.188	<0.001	-	4.864	<i>0.088</i>	-	17.032	0.025
N*PFT	1	-	2.289	<i>0.318</i>	-	0.914	0.633	-	6.760	0.034
SM ₂ *PFT	1	-	0.978	0.613	-	0.128	0.938	-	2.121	0.346
SM ₂ *N*PFT	1	-	1.289	0.525	-	2.180	0.336	-	0.629	0.730

9
1600 *Significance determined using Type II Wald χ^2 tests ($\alpha = 0.05$). P -values less than 0.05 are in bold and p -values
1601 where $0.05 < p < 0.1$ are italicized. Coefficients are reported on the natural-log scale and are only included for
1602 continuous fixed effects.

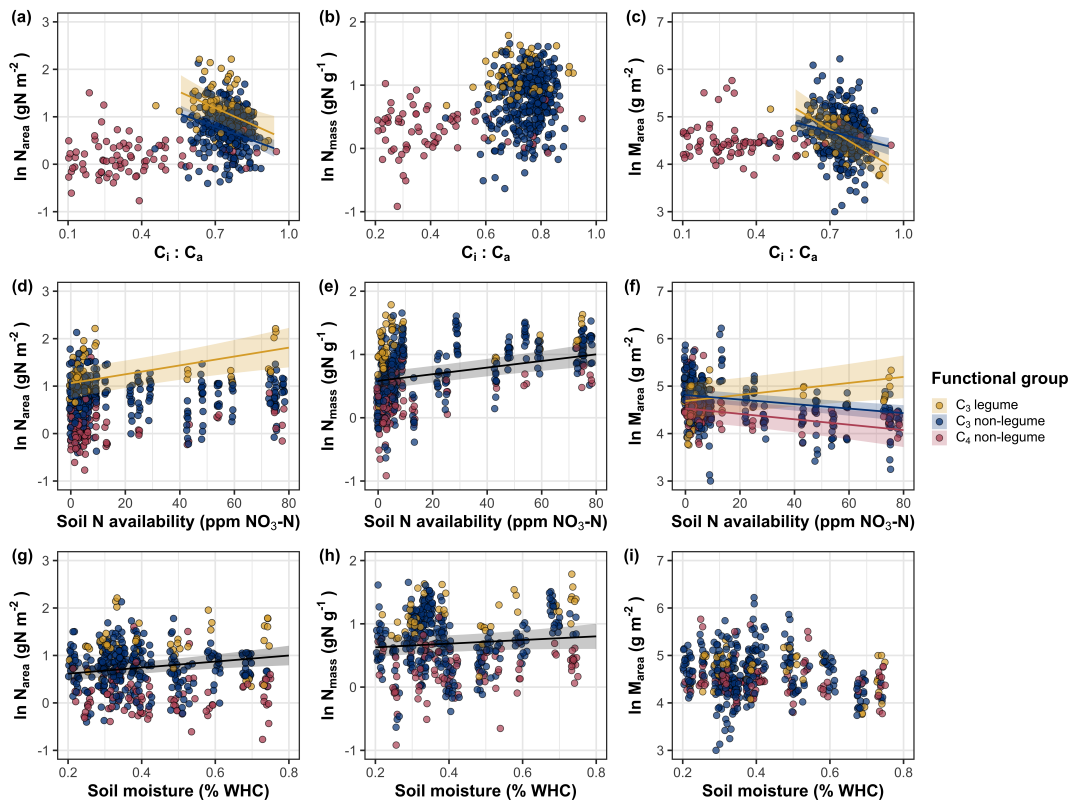


Figure 4.4. Effects of leaf $C_i : C_a$ (a-c), soil nitrogen availability (d-f), and soil moisture (g-i) on leaf nitrogen content per unit leaf area (a, d, g), leaf nitrogen content per unit leaf biomass (b, e, h), and leaf mass per area (c, f, i). A solid black trendline indicates the bivariate relationship between the fixed effect the x-axis and response variable on the y-axis and is only included when there is no interaction between the x-axis and plant functional group.

1603 4.3.4 *Structural equation model*

1604 The piecewise structural equation model explained 90%, 54%, 80%, 92%, and 41%
1605 of variance in N_{area} , N_{mass} , M_{area} , leaf $C_i:C_a$, and β , respectively (Table 5; Fig.
1606 5). Variance in N_{area} was driven by a negative effect of increasing leaf $C_i:C_a$ ($p <$
1607 0.001; Table 5) paired with positive effects of increasing N_{mass} and M_{area} ($p < 0.001$
1608 in both cases; Table 5; Fig. 5). Model results indicated that the negative effect of
1609 leaf $C_i:C_a$ on N_{area} was driven by a strong reduction in M_{area} with increasing leaf
1610 $C_i:C_a$ ($p < 0.001$; Table 5) paired with no change in leaf $C_i:C_a$ due to N_{mass} ($p =$
1611 0.150; Table 5). However, there was a strong negative effect of increasing M_{area} on
1612 N_{mass} ($p < 0.001$; Table 5; Fig. 5). Leaf $C_i:C_a$ generally increased with increasing
1613 β ($p < 0.001$; Table 5) and decreased with increasing VPD ($p < 0.001$; Table 5;
1614 Fig. 5). Variance in β was driven by a negative effect of increasing soil nitrogen
1615 availability ($p < 0.001$; Table 5) and was generally higher in C₃ species ($p <$
1616 0.001; Table 5; Fig. 5). However, β did not change with soil moisture ($p = 0.332$;
1617 Table 5) or with ability to acquire nitrogen via symbiotic nitrogen fixation ($p =$
1618 0.546; Table 5). Finally, soil nitrogen availability was positively associated with
1619 increasing soil moisture ($p < 0.001$; Table 5; Fig. 5), while VPD was negatively
1620 associated with increasing soil moisture ($p < 0.001$; Table 5; Fig. 5).

Table 4.5. Structural equation model results investigating direct effects of climatic and soil resource availability on N_{area} , N_{mass} , M_{area} , leaf $C_i:C_a$, and β

Predictor	Coefficient	<i>p</i>
$N_{\text{area}} (R^2_c) = 0.90$		
Leaf $C_i:C_a$	-0.140	<0.001
M_{area}	0.807	<0.001
N_{mass}	0.795	<0.001
$N_{\text{mass}} (R^2_c) = 0.54$		
χ	0.097	<0.001
$M_{\text{area}} (R^2_c) = 0.80$		
Leaf $C_i:C_a$	-0.372	0.150
M_{area}	-0.303	<0.001
Leaf $C_i:C_a (R^2_c) = 0.92$		
β	0.261	<0.001
VPD_4	-0.122	<0.001
$\beta (R^2_c) = 0.41$		
Soil N	-0.201	<0.001
SM_2	-0.048	0.332
Photo. pathway	0.490	<0.001
N-fixing ability	-0.053	0.546
Soil N (R^2_c) = 0.39		
SM_2	0.410	<0.001

1621 *Reported coefficients are standardized across the structural equation model. *P*-
1622 values less than 0.05 are noted in bold. Positive coefficients for photosynthetic
1623 pathway indicate generally larger values in C₃ species, while positive coefficients
1624 for N-fixing ability indicate generally larger values in N-fixing species. Key:
1625 N_{area} =leaf nitrogen content per unit leaf area, M_{area} =leaf mass per unit leaf dry
1626 biomass, N_{mass} =leaf nitrogen content per unit leaf dry biomass, β =cost of acquiring
1627 nitrogen relative to water, χ =isotope-derived estimate of the leaf Ci:Ca ratio,
1628 VPD_4 = 4-day mean vapor pressure deficit, SM_2 =2-day mean soil moisture, R^2_c
1629 = conditional R² value

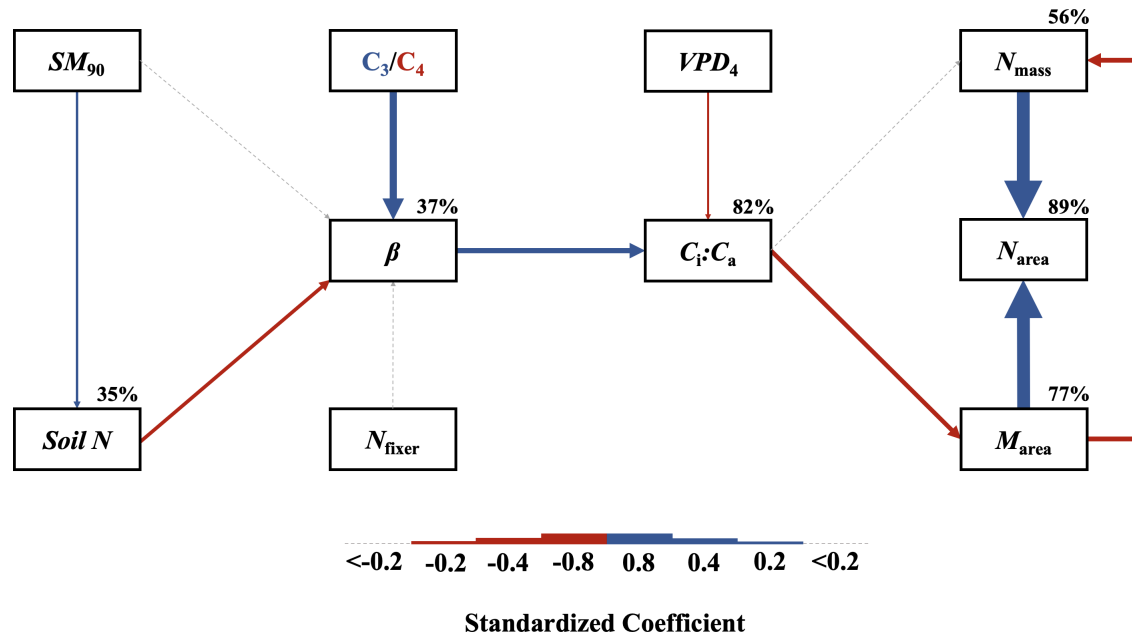


Figure 4.5. Structural equation model results exploring direct and indirect drivers of N_{area} . Boxes indicate measured edaphic factors, climatic factors, and leaf traits. Percentages above boxes indicate conditional R^2 values of each respective leaf trait. Solid arrows indicate bivariate relationships where $p < 0.05$, while dashed arrows indicate bivariate relationships where $p > 0.05$. Positive model coefficients are indicated through blue arrows, while negative model coefficients are indicated through red arrows. Arrow thickness scales with the standardized model coefficient of each bivariate relationship. A positive coefficient for photosynthetic pathway indicates generally larger values in C_3 species, while a positive coefficient for N_{fixer} indicates generally larger values in N-fixing species. Standardized model coefficients and associated p -values are reported in Table 5.

1630 4.4 Discussion

1631 In this study, we quantified direct and indirect effects of soil resource availability,
1632 climate, leaf $C_i:C_a$, and β on N_{area} and components of N_{area} (N_{mass} and M_{area}) in
1633 520 individuals spanning across a soil resource availability and climate gradient
1634 in Texas, USA. We found consistent support for patterns expected from photo-
1635 synthetic least-cost theory, a result driven by a strong direct negative relationship
1636 between the relative costs to acquire nitrogen versus water (β) on N_{area} as me-
1637 diated through changes in the leaf $C_i:C_a$ ratio. In further support of patterns
1638 expected from theory, increasing soil nitrogen availability had a strong negative
1639 effect on β , resulting in an indirect stimulation in N_{area} . Increasing VPD also
1640 indirectly increased N_{area} through a direct negative effect of increasing VPD on
1641 leaf $C_i:C_a$. Interestingly, a strong positive association between soil moisture and
1642 N_{area} was driven by positive covariance between soil moisture and soil nitrogen
1643 availability and was not associated with a direct effect of soil moisture on β .
1644 Overall, results provide strong and consistent support for patterns expected from
1645 photosynthetic least-cost theory, showing that both soil resource availability and
1646 climate drive variance in N_{area} through changes in leaf $C_i:C_a$.

1647 4.4.1 *Negative effects of leaf $C_i:C_a$ on N_{area} are driven by reductions in M_{area} ,*
1648 *not N_{mass}*

1649 A strong negative effect of increasing leaf $C_i:C_a$ on N_{area} was detected in both
1650 the linear mixed effect and piecewise structural equation models. The negative
1651 response of N_{area} to increasing leaf $C_i:C_a$ is consistent with previous environmental
1652 gradient (Dong et al. 2017; Querejeta et al. 2022) and manipulation experiments

1653 (Perkowski et al. n.d.), showing strong support for the nitrogen-water use tradeoffs
1654 expected from photosynthetic least cost theory (Wright et al. 2003; Prentice et al.
1655 2014). Negative effects of increasing leaf $C_i:C_a$ on N_{area} were driven by a strong
1656 negative effect of increasing $C_i:C_a$ on M_{area} , with no apparent effect of leaf $C_i:C_a$
1657 on N_{mass} , suggesting that changes in N_{area} were driven by changes in leaf structure
1658 and not leaf chemistry. Interestingly, increasing M_{area} was negatively associated
1659 with N_{mass} , indicating that an increase in N_{mass} was associated with larger, thinner
1660 leaves (i.e. lower M_{area}). These results are consistent with patterns reported
1661 from previous studies indicating that variance in N_{area} is driven by changes in
1662 M_{area} across environmental gradients, and that part of this response is due to
1663 negative covariance between M_{area} and N_{mass} associated with tradeoffs between
1664 leaf longevity and leaf productivity (Wright et al. 2004; Dong et al. 2017; Dong
1665 et al. 2022; Querejeta et al. 2022; Wang et al. 2023).

1666 The negative relationship between leaf $C_i:C_a$ and M_{area} could be also re-
1667 sponse that allows leaves to maximize productivity in shorter-lived leaves. Trade-
1668 offs between leaf longevity and leaf productivity are commonly observed and are
1669 included in a continuum of coordinated leaf traits that position individuals along
1670 a fast- or slow-growing leaf economics spectrum (Wright et al. 2003; Onoda et al.
1671 2004; Onoda et al. 2017; Reich 2014; Wang et al. 2023). Negative relationships
1672 between $C_i:C_a$ and M_{area} indicate that increased stomatal conductance and re-
1673 duced water use efficiency were associated with thinner, larger leaves (i.e., lower
1674 M_{area}). These patterns, combined with the negative relationship between M_{area}
1675 and N_{mass} mentioned above, likely allowed individuals to maximize light intercep-
1676 tion and productivity by exploiting high light environments, though this may come

1677 at the expense of increased water loss and decreased water-use efficiency. This
1678 strategy may be especially advantageous for fast-growing species in open canopy
1679 systems. In this study, C₃ legumes and C₃ nonlegumes dominated the dataset
1680 (78% of total sampling effort), of which 22% (17% of total sampling effort) were
1681 classified as annual species with short growing seasons. We observed no effect of
1682 leaf C_i:C_a on N_{area} or M_{area} in C₄ nonlegumes, which made up 22% of the sampling
1683 effort and were generally classified as warm season graminoid species with slower
1684 growth rates and longer growing seasons. These patterns indicate that stronger
1685 tradeoffs between nitrogen and water use may be more apparent in fast-growing
1686 species with high demand for building and maintaining productive leaf tissues.

1687 4.4.2 *Soil nitrogen availability increases N_{area} through changes in the cost to
1688 acquire nitrogen*

1689 The null effect of soil nitrogen availability on N_{area} was driven by positive
1690 and negative respective effects of increasing soil nitrogen availability on N_{mass} and
1691 M_{area} that were equal in magnitude. The null response of N_{area} to soil nitrogen
1692 availability occurred alongside a negative effect of increasing soil nitrogen availabil-
1693 ity on β , which, paired with the negative relationship between leaf C_i:C_a and N_{area},
1694 suggests a general positive effect of increasing soil nitrogen availability on N_{area},
1695 but only when mediated through changes in β . This result is consistent with our
1696 hypotheses and patterns expected from photosynthetic least-cost theory. These
1697 results suggest that positive direct effects of increasing soil nitrogen availability
1698 on N_{area} are not ubiquitous across environmental gradients. Instead, as predicted
1699 by our hypotheses and patterns expected from theory, positive responses of N_{area}

1700 to increasing soil nitrogen availability are a deterministic acclimation response to
1701 shifts in climate-related demand to build and maintain photosynthetic enzymes,
1702 which allows plants to optimize photosynthetic processes and resource use to a
1703 given environment (Paillassa et al. 2020; Peng et al. 2021; Dong et al. 2022;
1704 Westerband et al. 2023).

1705 4.4.3 *Soil moisture increases N_{area} by facilitating increases in soil nitrogen
1706 availability*

1707 Increasing soil moisture generally had no effect on N_{area} , a response that was as-
1708 sociated with a null effect of soil moisture on β . These results contrast patterns
1709 expected from theory, where increasing soil moisture is expected to indirectly de-
1710 crease N_{area} through an increase in β due to a reduction in costs associated with
1711 water acquisition and use (Wright et al. 2003; Prentice et al. 2014; Lavergne
1712 et al. 2020). Interestingly, structural equation model results revealed a strong
1713 positive association between soil moisture and soil nitrogen availability, indicat-
1714 ing an indirect positive effect of increasing soil moisture on N_{area} mediated by the
1715 negative effect of increasing soil nitrogen availability on β . In Texan grasslands,
1716 productivity and nutrient uptake are often co-limited by precipitation and nutrient
1717 availability (Yahdjian et al. 2011; Wang et al. 2017). Thus, increases in soil mois-
1718 ture may have facilitated more favorable and productive environments for soil
1719 microbial communities, thereby stimulating the accumulation of plant-available
1720 nitrogen substrate through increased ammonification or nitrification rates (Reich-
1721 man et al. 1966; Stark and Firestone 1995; Paul et al. 2003). Alternatively, soil
1722 moisture may have facilitated greater nitrogen mobility through soil solution. As
1723 discussed above, the positive indirect response of N_{area} to increasing soil nitrogen
1724 availability as mediated through reductions in β follow patterns expected from

1725 theory.

1726 4.4.4 *Indirect effects of climate on N_{area} are mediated through changes in leaf*
1727 *$C_i:C_a$ and β*

1728 In support of our hypothesis and patterns expected from theory, increasing VPD
1729 indirectly increased N_{area} , mediated through the negative effect of increasing VPD
1730 on leaf $C_i:C_a$. These responses are consistent with previous work noting strong
1731 reductions in stomatal conductance with increasing VPD (Oren et al. 1999; Novick
1732 et al. 2016; Sulman et al. 2016; Grossiord et al. 2020; López et al. 2021), a
1733 response that allows plants to minimize water loss as a result of high atmospheric
1734 water demand. Results also support findings from previous experiments across
1735 environmental gradients, where increasing VPD generally increases N_{area} at lower
1736 stomatal conductance across environmental gradients (Dong et al. 2017; Dong
1737 et al. 2022; Paillassa et al. 2020; Westerband et al. 2023).

1738 4.4.5 *Species identity traits modify effects of the environment on β , leaf $C_i:C_a$,*
1739 *and N_{area}*

1740 N-fixing species generally had higher N_{area} values on average compared to non-
1741 fixing species, a pattern driven by a stronger stimulation in N_{mass} in N-fixing
1742 species coupled with no change in M_{area} between species with different N-fixation
1743 ability. We found no evidence to suggest that N-fixing species had different β or
1744 leaf $C_i:C_a$ values compared to non-fixing species across the environmental gradient.
1745 These results follow patterns from previous environmental gradient experiments
1746 that investigate variance in leaf nitrogen allocation in N-fixing species (Adams
1747 et al. 2016; Dong et al. 2017; Dong et al. 2020), and that increases in N_{mass}
1748 and N_{area} in N-fixing species are not necessarily correlated to increases in water

1749 use efficiency or reductions in leaf $C_i:C_a$ (Adams et al. 2016). While our results
1750 are consistent with results from previous environmental gradient experiments,
1751 they do not necessarily support our hypothesis or patterns expected from theory,
1752 which predicts that stimulations in N_{area} by N-fixing species should be driven
1753 by a reduction in β relative to non-fixing species, and that this response should
1754 decrease stomatal conductance and leaf $C_i:C_a$.

1755 C_4 species generally had lower β , leaf $C_i:C_a$, and N_{area} than C_3 species.
1756 Reduced β and leaf $C_i:C_a$ values in C_4 species follow our hypothesis, a pattern
1757 that could be the result of either reduced costs of nitrogen acquisition and use or
1758 increased costs of water acquisition and use or both (Wright et al. 2003, Prentice
1759 et al. 2014). Results also indicate that β in C_4 nonlegumes was unresponsive to
1760 changes in soil nitrogen availability despite an apparent negative effect of increas-
1761 ing soil nitrogen availability on β in C_3 legumes and C_3 nonlegumes. Combined
1762 with a general null response of β to soil moisture regardless of plant functional
1763 group, these patterns imply that reduced β values in C_4 species may be the re-
1764 sult of lower costs of nitrogen acquisition and use relative to C_3 species. While
1765 lower β values in C_4 species provides a possible explanation for why C_4 species
1766 often have lower leaf $C_i:C_a$ and greater water use efficiency, theory predicts that
1767 this response should cause C_4 species to have greater N_{area} values compared to
1768 C_3 species, though C_4 species commonly exhibit lower N_{area} and higher nitrogen
1769 use efficiency than C_3 species (Schmitt and Edwards 1981; Sage and Pearcy 1987;
1770 Ghannoum et al. 2011). We speculate that lowered costs of nitrogen acquisition
1771 and use in C_4 species could be driven by more efficient Rubisco carboxylation effi-
1772 ciency in C_4 species associated with CO₂ concentrating mechanisms that eliminate

1773 photorespiration (Ghannoum et al. 2011), which could reduce or eliminate the
1774 need to sacrifice inefficient nitrogen use for efficient water use to achieve optimal
1775 photosynthesis rates.

1776 4.4.6 *Next steps for optimality model development*

1777 Optimality models for both C₃ and C₄ species have been developed using principles
1778 from photosynthetic least-cost theory (Prentice et al. 2014; Wang et al. 2017;
1779 Smith et al. 2019; Stocker et al. 2020; Scott and Smith 2022). In both C₃ and
1780 C₄ model variants, β values are held constant using global datasets of leaf $\delta^{13}\text{C}$
1781 (Wang et al. 2017; Cornwell et al. 2018). Specifically, the C₃ optimality model
1782 initially assumed a constant β value of 240 (Wang et al. 2017), later corrected to
1783 146 (Stocker et al. 2020), while the C₄ optimality model assumes a constant β
1784 value of 166 (Scott and Smith 2022). Our results, which build on findings from
1785 Paillassa et al. (2020), demonstrate high variability in calculated β values across
1786 environmental gradients. Specifically, β values in C₃ species ranged from 1.7 to
1787 188.0 (mean: 30.2; median: 23.1; standard deviation: 25.4), while ranged from 0.1
1788 to 110.6 in C₄ species (mean: 7.2; median: 0.7; standard deviation: 18.6). Mean
1789 β values in both C₃ and C₄ species were consistently lower than values currently
1790 implemented in optimality models, though this was likely the result of increased
1791 water limitation across our sites relative to global averages. Regardless, the high
1792 degree of β variability across this environmental gradient, together with findings
1793 from Lavergne et al. (2020) and Paillassa et al. (2020), suggests that the use of
1794 constant β values may contribute to erroneous errors when conducting optimality
1795 model simulations. We therefore build on suggestions from Wang et al. (2017),
1796 recommending future photosynthetic least-cost model developments to consider

1797 the use of dynamic β values.

1798 4.4.7 *Conclusions*

1799 To summarize, variability in N_{area} across an environmental gradient in Texan
1800 grasslands was driven by indirect effects of climate and soil resource availability
1801 mediated. Results from this experiment provide strong and consistent support
1802 for patterns expected from photosynthetic least-cost theory, demonstrating that
1803 negative relationships between $C_i:C_a$ and N_{area} unify expected effects of climatic
1804 and edaphic characteristics on N_{area} across environmental gradients. Our results
1805 also demonstrate a need to consider the dynamic nature of the relative cost of
1806 nitrogen versus water uptake (β) across environmental gradients in optimality
1807 models that leverage principles of photosynthetic least-cost theory.

1808

Chapter 5

1809 Optimal resource investment to photosynthetic capacity maximizes
1810 nutrient allocation to whole plant growth under elevated CO₂

1811 5.1 Introduction

1812 Terrestrial ecosystems are regulated by complex carbon and nitrogen cy-
1813 cles. As a result, terrestrial biosphere models, which are beginning to include
1814 coupled carbon and nitrogen cycles (Shi et al. 2016; Davies-Barnard et al. 2020;
1815 Braghiere et al. 2022), must accurately represent these cycles under different
1816 environmental scenarios to reliably simulate carbon and nitrogen atmosphere-
1817 biosphere fluxes (Hungate et al. 2003; Prentice et al. 2015). While the inclusion
1818 of coupled carbon and nitrogen cycles tends to reduce model uncertainty (Arora
1819 et al. 2020), large uncertainty in role of soil nitrogen availability and nitrogen ac-
1820 quisition strategy on leaf and whole plant acclimation responses to CO₂ remains
1821 (Smith and Dukes 2013; Terrer et al. 2018; Smith and Keenan 2020). This source
1822 of uncertainty likely contributes to the widespread divergence in future carbon
1823 and nitrogen flux simulations across terrestrial biosphere models (Friedlingstein
1824 et al. 2014; Zaehle et al. 2014; Meyerholt et al. 2020).

1825 Plants grown under elevated CO₂ generally have less leaf nitrogen content
1826 than those grown under ambient CO₂, a response that often corresponds with
1827 reductions in photosynthetic capacity and stomatal conductance at the leaf-level
1828 and biomass stimulation over time at the whole plant level (Curtis 1996; Drake
1829 et al. 1997; Ainsworth et al. 2002; Makino 2003; Morgan et al. 2004; Ainsworth
1830 and Long 2005; Ainsworth and Rogers 2007; Smith and Dukes 2013; Poorter et al.
1831 2022). As net primary productivity is generally limited by nitrogen availability

1832 (Vitousek and Howarth 1991; LeBauer and Treseder 2008; Fay et al. 2015), and
1833 soil nitrogen availability is often positively correlated with leaf nitrogen content
1834 and photosynthetic capacity (Field and Mooney 1986; Evans and Seemann 1989;
1835 Evans 1989; Walker et al. 2014; Firn et al. 2019; Liang et al. 2020), some
1836 have hypothesized that leaf and whole plant acclimation responses to CO₂ are
1837 constrained by soil nitrogen availability. The progressive nitrogen limitation hy-
1838 pothesis predicts that elevated CO₂ will increase plant nitrogen demand, which
1839 will increase plant nitrogen uptake and progressively deplete soil nitrogen if soil
1840 nitrogen supply does not exceed plant nitrogen demand (Luo et al. 2004). The
1841 hypothesis predicts that this response should result in strong acute stimulations in
1842 whole plant growth and primary productivity that diminish over time as nitrogen
1843 becomes more limiting. Assuming a positive relationship between soil nitrogen
1844 availability, leaf nitrogen content, and photosynthetic capacity, this hypothesis
1845 also implies that progressive reductions in soil nitrogen availability should be the
1846 mechanism that drives the downregulation in leaf nitrogen content and photosyn-
1847 thetic capacity under elevated CO₂. This hypothesis has received some support
1848 from free air CO₂ enrichment experiments (Reich et al. 2006; Norby et al. 2010),
1849 although is not consistently observed across experiments (Finzi et al. 2006; Moore
1850 et al. 2006; Liang et al. 2016).

1851 While possible that progressive nitrogen limitation may determine leaf and
1852 whole plant acclimation responses to CO₂, growing evidence indicates that leaf ni-
1853 trogen and photosynthetic capacity are more strongly determined through above-
1854 ground growing conditions than by soil resource availability (Dong et al. 2017;
1855 Dong et al. 2020; Dong et al. 2022; Smith et al. 2019; Smith and Keenan 2020;

1856 Paillassa et al. 2020; Peng et al. 2021; Querejeta et al. 2022; Westerband et al.
1857 2023), and satellite-derived chlorophyll fluorescence data indicate that increasing
1858 atmospheric CO₂ may decrease leaf and canopy demand for nitrogen (Dong et al.
1859 2022). Together, results from these studies suggest that the downregulation in
1860 leaf nitrogen content and photosynthetic capacity due to increasing CO₂ may not
1861 be as tightly linked to progressive nitrogen limitation as previously hypothesized.

1862 A unification of optimal coordination and photosynthetic least-cost the-
1863 ories predicts that leaves acclimate to elevated CO₂ by downregulating nitrogen
1864 allocation to Ribulose-1,5-bisphosphate (RuBP) carboxylase/oxygenase (Rubisco)
1865 to optimize resource use efficiencies at the leaf level, which allows for greater re-
1866 source allocation to whole plant growth (Drake et al. 1997; Wright et al. 2003;
1867 Prentice et al. 2014; Smith et al. 2019). The theory predicts that the downregu-
1868 lation in nitrogen allocation to Rubisco results in a stronger downregulation in the
1869 maximum rate of Rubisco carboxylation (V_{cmax}) than the maximum rate of RuBP
1870 regeneration (J_{max}), which maximizes photosynthetic efficiency by allowing net
1871 photosynthesis rates to be equally co-limited by Rubisco carboxylation and RuBP
1872 regeneration (Chen et al. 1993; Maire et al. 2012). This acclimation response
1873 allows plants to make more efficient use of available light while avoiding overin-
1874 vestment in Rubisco, which has high nitrogen and energetic costs of building and
1875 maintaining (Evans 1989; Evans and Clarke 2019). Instead, additional acquired
1876 resources not needed to optimize leaf photosynthesis are allocated to the mainte-
1877 nance of structures that support whole plant growth (e.g., total leaf area, whole
1878 plant biomass, etc.) or to allocation processes not related to leaf photosynthesis
1879 or growth, such as plant defense mechanisms or leaf structural tissue. Regardless,

1880 optimized resource allocation at the leaf level should allow for greater resource
1881 allocation to whole plant growth. The theory indicates that leaf acclimation re-
1882 sponses to CO₂ should be independent of changes in soil nitrogen availability.
1883 While this leaf acclimation response maximizes nitrogen allocation to structures
1884 that support whole plant growth, the theory suggests that the positive effect of
1885 elevated CO₂ on whole plant growth may be further stimulated by soil nitrogen
1886 availability through a reduction in the cost of acquiring nitrogen (Bae et al. 2015;
1887 Perkowski et al. 2021; Lu et al. 2022).

1888 Plants acquire nitrogen by allocating photosynthetically derived carbon be-
1889 lowground in exchange for nitrogen through different nitrogen acquisition strate-
1890 gies. These nitrogen acquisition strategies can include direct uptake pathways
1891 such as mass flow or diffusion (Barber 1962), symbioses with mycorrhizal fungi or
1892 symbiotic nitrogen-fixing bacteria (Vance and Heichel 1991; Marschner and Dell
1893 1994; Smith and Read 2008; Udvardi and Poole 2013), or through the release
1894 of root exudates that prime free-living soil microbial communities (Phillips et al.
1895 2011; Wen et al. 2022). Plants cannot acquire nitrogen without first allocating
1896 carbon belowground, which implies an inherent carbon cost to the plant for acquir-
1897 ing nitrogen regardless of nitrogen acquisition strategy. Carbon costs to acquire
1898 nitrogen often vary in species with different nitrogen acquisition strategies and
1899 are dependent on external environmental factors such as atmospheric CO₂, light
1900 availability, and soil nitrogen availability (Brzostek et al. 2014; Terrer et al. 2016;
1901 Terrer et al. 2018; Allen et al. 2020; Perkowski et al. 2021; Lu et al. 2022), which
1902 suggests that acquisition strategy may be an important factor in determining ef-
1903 fects of soil nitrogen availability on leaf and whole plant acclimation responses to

1904 elevated CO₂.

1905 A recent meta-analysis using data across 20 grassland and forest CO₂ en-
1906 richment experiments suggested that species which acquire nitrogen from sym-
1907 biotic nitrogen-fixing bacteria had reduced costs of nitrogen acquisition under
1908 elevated CO₂ (Terrer et al. 2018). Findings from this meta-analysis indicated
1909 that reductions in costs of nitrogen acquisition in species that form associations
1910 with symbiotic nitrogen-fixing bacteria under elevated CO₂ may drive stronger
1911 stimulations in whole plant growth and downregulations in V_{cmax} than species that
1912 associate with arbuscular mycorrhizal fungi (Smith and Keenan 2020), which gen-
1913 erally have higher costs of nitrogen acquisition under elevated CO₂ (Terrer et al.
1914 2018). However, plant investments in symbiotic nitrogen fixation generally de-
1915 cline with increasing nitrogen availability (Dovrat et al. 2018; Perkowski et al.
1916 2021), a response that has been previously inferred to be the result of a shift in
1917 the dominant mode of nitrogen acquisition to direct uptake pathways as costs of
1918 direct uptake decrease with increasing soil nitrogen availability (Rastetter et al.
1919 2001; Perkowski et al. 2021). Thus, effects of symbiotic nitrogen fixation on plant
1920 acclimation responses to CO₂ should decline with increasing soil nitrogen avail-
1921 ability, although manipulative experiments that directly test these patterns are
1922 rare.

1923 Here, I conducted a 7-week growth chamber experiment using *Glycine max*
1924 L. (Merr.) to examine the effects of soil nitrogen fertilization and inoculation with
1925 symbiotic nitrogen-fixing bacteria on leaf and whole plant acclimation responses
1926 to elevated CO₂. Following patterns expected from theory, I hypothesized that in-
1927 dividual leaves should acclimate to elevated CO₂ by more strongly downregulating

1928 V_{cmax} relative to J_{max} , allowing leaf photosynthesis to approach optimal coordination.
1929 I expected this response to correspond with a stronger downregulation in
1930 leaf nitrogen content than V_{cmax} and J_{max} , which would increase the fraction of
1931 leaf nitrogen content allocated to photosynthesis and photosynthetic nitrogen use
1932 efficiency. At the whole-plant level, I hypothesized that plants would acclimate
1933 to elevated CO₂ by stimulating whole plant growth and productivity, a response
1934 that would be driven by a strong positive response of total leaf area and above-
1935 ground biomass to elevated CO₂. I predicted that leaf acclimation responses to
1936 elevated CO₂ would be independent of soil nitrogen fertilization and inoculation
1937 with symbiotic nitrogen-fixing bacteria; however, I expected that increasing soil
1938 nitrogen fertilization would increase the positive effect of elevated CO₂ on mea-
1939 sures of whole plant growth due to a stronger reduction in the cost of acquiring
1940 nitrogen under elevated CO₂ with increasing fertilization. I also expected stronger
1941 stimulations in whole plant growth due to inoculation, but that this effect would
1942 only be apparent under low fertilization due to a reduction in root nodulation
1943 with increasing fertilization.

1944 5.2 Methods

1945 5.2.1 *Seed treatments and experimental design*

1946 *Glycine max* L. (Merr) seeds were planted in 144 6-liter surface sterilized
1947 pots (NS-600, Nursery Supplies, Orange, CA, USA) containing a steam-sterilized
1948 70:30 v:v mix of Sphagnum peat moss (Premier Horticulture, Quakertown, PA,
1949 USA) to sand (Pavestone, subsidiary of Quikrete Companies, Atlanta, GA, USA).
1950 Before planting, all *G. max* seeds were surface sterilized in 2% sodium hypochlorite

1951 for 3 minutes, followed by three separate 3-minute washes with ultrapure water
1952 (MilliQ 7000; MilliporeSigma, Burlington, MA USA). A subset of surface steril-
1953 ized seeds were inoculated with *Bradyrhizobium japonicum* (Verdesian N-Dure™
1954 Soybean, Cary, NC, USA) in a slurry following manufacturer recommendations
1955 (3.12 g inoculant and 241 g deionized water per 1 kg seed).

1956 Seventy-two pots were randomly planted with surface-sterilized seeds inoc-
1957 ulated with *B. japonicum*, while the remaining 72 pots were planted with surface-
1958 sterilized uninoculated seeds. Thirty-six pots within each inoculation treatment
1959 were randomly placed in one of two atmospheric CO₂ treatments (ambient and
1960 1000 μmol mol⁻¹ CO₂). Pots within each unique inoculation-by-CO₂ treatment
1961 combination randomly received one of nine soil nitrogen fertilization treatments
1962 equivalent to 0, 35, 70, 105, 140, 210, 280, 350, or 630 ppm N. Nitrogen fertil-
1963 ization treatments were created using a modified Hoagland solution (Hoagland
1964 and Arnon 1950) designed to keep concentrations of other macronutrients and
1965 micronutrients equivalent across treatments (Table S1). Pots received the same
1966 fertilization treatment throughout the entire duration experiment, which were ap-
1967 plied twice per week in 150 mL doses as topical agents to the soil surface through-
1968 out the duration of the experiment. This experimental design yielded a fully
1969 factorial experiment with four replicates per unique fertilization-by-inoculation-
1970 by-CO₂ combination.

1971 5.2.2 *Growth chamber conditions*

1972 Upon experiment initiation, pots were randomly placed in one of six Per-
1973 cival LED-41L2 growth chambers (Percival Scientific Inc., Perry, IA, USA) over

1974 two experimental iterations due to chamber space limitation. Two iterations were
1975 conducted such that one iteration included all elevated CO₂ pots and the second
1976 iteration included all ambient CO₂ pots. Average (\pm SD) CO₂ concentrations
1977 across chambers throughout the experiment were $439 \pm 5 \mu\text{mol mol}^{-1}$ for the
1978 ambient CO₂ treatment and $989 \pm 4 \mu\text{mol mol}^{-1}$ for the elevated CO₂ treatment.

1979 Daytime growing conditions were simulated using a 16-hour photoperiod,
1980 with incoming light radiation set to chamber maximum (mean \pm SD: 1240 ± 32
1981 $\mu\text{mol m}^{-2} \text{s}^{-1}$ across chambers), air temperature set to 25°C, and relative humid-
1982 ity set to 50%. The remaining 8 hours simulated nighttime growing conditions,
1983 with incoming light radiation set to 0 $\mu\text{mol m}^{-2} \text{s}^{-1}$, chamber temperature set
1984 to 17°C, and relative humidity set to 50%. Transitions between daytime and
1985 nighttime growing conditions were simulated by ramping incoming light radiation
1986 in 45-minute increments and temperature in 90-minute increments over a 3-hour
1987 period (Table S2).

1988 Including the two, 3-hour ramping periods, pots grew under average (\pm
1989 SD) daytime light intensity of $1049 \pm 27 \mu\text{mol m}^{-2} \text{s}^{-1}$. In the elevated CO₂
1990 iteration, pots grew under $24.0 \pm 0.2^\circ\text{C}$ during the day, $16.4 \pm 0.8^\circ\text{C}$ during the
1991 night, and $51.6 \pm 0.4\%$ relative humidity. In the ambient CO₂ iteration, pots grew
1992 under $23.9 \pm 0.2^\circ\text{C}$ during the day, $16.0 \pm 1.4^\circ\text{C}$ during the night, and $50.3 \pm 0.2\%$
1993 relative humidity. We accounted for climatic differences across the six chambers
1994 by shuffling the same group of pots daily throughout the growth chambers. This
1995 process was done by iteratively moving the group of pots on the top rack of a
1996 chamber to the bottom rack of the same chamber, while simultaneously moving
1997 the group of pots on the bottom rack of a chamber to the top rack of the adjacent

1998 chamber. I moved pots within and across chambers every day throughout the
1999 course of each experiment iteration.

2000 5.2.3 *Leaf gas exchange measurements*

2001 Gas exchange measurements were collected for all individuals on the sev-
2002 enth week of development. All gas exchange measurements were collected on
2003 the center leaf of the most recent fully expanded trifoliate leaf set. Specifi-
2004 cally, I measured net photosynthesis (A_{net} ; $\mu\text{mol m}^{-2} \text{s}^{-1}$), stomatal conductance
2005 (g_{sw} ; $\text{mol m}^{-2} \text{s}^{-1}$), and intercellular CO₂ (C_i ; $\mu\text{mol mol}^{-1}$) concentrations across
2006 a range of atmospheric CO₂ concentrations (i.e., an A_{net}/C_i curve) using the
2007 Dynamic Assimilation Technique™. The Dynamic Assimilation Technique™ has
2008 been shown to correspond well with traditional steady-state CO₂ response curves
2009 in *G. max* (Saathoff and Welles 2021). A_{net}/C_i curves were generated along a
2010 reference CO₂ ramp down from 420 $\mu\text{mol mol}^{-1}$ CO₂ to 20 $\mu\text{mol mol}^{-1}$ CO₂, fol-
2011 lowed by a ramp up from 420 $\mu\text{mol mol}^{-1}$ CO₂ to 1620 $\mu\text{mol mol}^{-1}$ CO₂ after
2012 a 90-second wait period at 420 $\mu\text{mol mol}^{-1}$ CO₂. The ramp rate for each curve
2013 was set to 200 $\mu\text{mol mol}^{-1} \text{min}^{-1}$, logging every five seconds, which generated 96
2014 data points per response curve. All A_{net}/C_i curves were generated after A_{net} and
2015 g_{sw} stabilized in a LI-6800 cuvette set to a 500 mol s^{-1} , 10,000 rpm mixing fan
2016 speed, 1.5 kPa vapor pressure deficit, 25°C leaf temperature, 2000 $\mu\text{mol m}^{-2} \text{s}^{-1}$
2017 incoming light radiation, and initial reference CO₂ set to 420 $\mu\text{mol mol}^{-1}$.

2018 With the same focal leaf used to generate A_{net}/C_i curves, I measured dark
2019 respiration (R_{d25} ; $\mu\text{mol m}^{-2} \text{s}^{-1}$) following at least a 30-minute period of darkness.
2020 Measurements were collected on a 5-second log interval for 60 seconds after stabi-

2021 lizing in a LI-6800 cuvette set to a 500 mol s^{-1} , 10,000 rpm mixing fan speed, 1.5
2022 kPa vapor pressure deficit, 25°C leaf temperature, and $420 \mu\text{mol mol}^{-1}$ reference
2023 CO₂ concentration (for both CO² concentrations), with incoming light radiation
2024 set to $0 \mu\text{mol m}^{-2} \text{ s}^{-1}$. A single dark respiration value was determined for each
2025 focal leaf by calculating the mean dark respiration value (i.e. the absolute value
2026 of A_{net} during the logging period) across the logging interval.

2027 5.2.4 *Leaf trait measurements*

2028 The focal leaf used to generate A_{net}/C_i curves and dark respiration was
2029 harvested immediately following gas exchange measurements. Images of each focal
2030 leaf were curated using a flat-bed scanner to determine wet leaf area using the
2031 'LeafArea' R package (Katabuchi 2015), which automates leaf area calculations
2032 using ImageJ software (Schneider et al. 2012). Each leaf was dried at 65°C for
2033 at least 48 hours, and subsequently weighed and ground until homogenized. Leaf
2034 mass per area (M_{area} ; g m⁻²) was calculated as the ratio of dry leaf biomass
2035 to fresh leaf area. Using subsamples of ground and homogenized leaf tissue, I
2036 measured leaf nitrogen content (N_{mass} ; gN g⁻¹) through elemental combustion
2037 analysis (Costech-4010, Costech, Inc., Valencia, CA, USA). Leaf nitrogen content
2038 per unit leaf area (N_{area} ; gN m⁻²) was calculated by multiplying N_{mass} and M_{area} .
2039 I extracted chlorophyll content from a second leaf in the same trifoliolate
2040 leaf set as the focal leaf used to generate A_{net}/C_i curves. Prior to chlorophyll
2041 extraction, I used a cork borer to punch between 3 and 5 0.6 cm² disks from the
2042 leaf. Separate images of each punched leaf and set of leaf disks were curated using
2043 a flat-bed scanner to determine wet leaf area, again quantified using the 'LeafArea'

2044 R package (Katabuchi 2015). The punched leaf was dried and weighed after at
2045 least 65°C in the drying oven to determine M_{area} of the chlorophyll leaf.

2046 Leaf disks were shuttled into a test tube containing 10mL dimethyl sul-
2047 foxide, vortexed, and incubated at 65degreeC for 120 minutes (Barnes et al.
2048 1992). Incubated test tubes were vortexed again before loaded in 150 μL trip-
2049 licate aliquots to a 96-well plate. Dimethyl sulfoxide was also loaded in a 150
2050 μL triplicate aliquot as a blank. Absorbance measurements at 649.1 nm ($A_{649.1}$)
2051 and 665.1 nm ($A_{665.1}$) were read in each well using a plate reader (Biotek Synergy
2052 H1; Biotek Instruments, Winooski, VT USA) (Wellburn 1994), with triplicates
2053 subsequently averaged and corrected by the mean of the blank absorbance value.
2054 Blank-corrected absorbance values were used to estimate Chl_a ($\mu\text{g mL}^{-1}$) and
2055 Chl_b ($\mu\text{g mL}^{-1}$) following equations from Wellburn (1994):

$$Chl_a = 12.47A_{665.1} - 3.62A_{649.1} \quad (5.1)$$

2056 and

$$Chl_b = 25.06A_{665.1} - 6.50A_{649.1} \quad (5.2)$$

2057 Chl_a and Chl_b were converted to mmol mL^{-1} using the molar mass of chlorophyll a
2058 (893.51 g mol^{-1}) and the molar mass of chlorophyll b (907.47 g mol^{-1}), then added
2059 together to calculate total chlorophyll content in the dimethyl sulfoxide extractant
2060 (mmol mL^{-1}). Total chlorophyll content was multiplied by the volume of the
2061 dimethyl sulfoxide extractant (10 mL) and converted to area-based chlorophyll
2062 content by dividing by the total area of the leaf disks (Chl_{area} ; mmol m^{-2}). Mass-
2063 based chlorophyll content (Chl_{mass} ; mmol g^{-1}) was calculated by dividing Chl_{area}

2064 by the leaf mass per area of the punched leaf.

2065 5.2.5 *A/C_i curve fitting and parameter estimation*

2066 I fit A_{net}/C_i curves of each individual using the ‘fitaci’ function in the
2067 ‘plantecophys’ R package (Duursma 2015). This function estimates the maxi-
2068 mum rate of Rubisco carboxylation (V_{cmax} ; $\mu\text{mol m}^{-2} \text{s}^{-1}$) and maximum rate
2069 of electron transport for RuBP regeneration (J_{max} ; $\mu\text{mol m}^{-2} \text{s}^{-1}$) based on the
2070 Farquhar biochemical model of C₃ photosynthesis (Farquhar et al. 1980). Triose
2071 phosphate utilization (TPU) limitation was included in all curve fits, and all curve
2072 fits included measured dark respiration values. As A_{net}/C_i curves were generated
2073 using a common leaf temperature, curves were fit using Michaelis-Menten coeffi-
2074 cients for Rubisco affinity to CO₂ (K_c ; $\mu\text{mol mol}^{-1}$) and O₂ (K_o ; $\mu\text{mol mol}^{-1}$), and
2075 the CO₂ compensation point (Γ^* ; $\mu\text{mol mol}^{-1}$) reported in Bernacchi et al. (2001).
2076 Specifically, K_c was set to 404.9 $\mu\text{mol mol}^{-1}$, K_o was set to 278.4 $\mu\text{mol mol}^{-1}$, and
2077 Γ^* was set to 42.75 $\mu\text{mol mol}^{-1}$. The use of a common leaf temperature across
2078 curves and dark respiration measurements also eliminated the need to manually
2079 temperature standardize rate estimates. For clarity, I reference V_{cmax} , J_{max} , and
2080 R_d estimates throughout the rest of the paper as $V_{\text{cmax}25}$, $J_{\text{max}25}$, and R_{d25} .

2081 5.2.6 Stomatal limitation

2082 I quantified the extent by which stomatal conductance limited photosynthe-
2083 sis (l; unitless) following equations originally described in Farquhar and Sharkey
2084 (1982). Stomatal limitation was calculated as:

$$l = 1 - \frac{A_{net}}{A_{mod}} \quad (5.3)$$

2085 where A_{mod} represents the photosynthetic rate where $C_i = C_a$. A_{mod} was calcu-

2086 lated as:

$$A_{mod} = V_{cmax25} - \frac{420 - \Gamma^*}{420 + K_m} - R_{d25} \quad (5.4)$$

2087 K_m is the Michaelis-Menten coefficient for Rubisco-limited photosynthesis, calcu-

2088 lated as:

$$K_m = K_c \cdot \left(1 + \frac{O_i}{K_o}\right) \quad (5.5)$$

2089 where O_i refers to leaf intercellular O_2 concentrations, set to $210 \mu\text{mol mol}^{-1}$.

2090 5.2.7 *Proportion of leaf nitrogen allocated to photosynthesis and structure*

2091 I used equations from Niinemets and Tenhunen (1997) to estimate the
2092 proportion of leaf N content allocated to Rubisco bioenergetics, and light harvest-
2093 ing proteins. The proportion of leaf N allocated to Rubisco (ρ_{rub} ; gN gN^{-1}) was
2094 calculated as a function of V_{cmax25} and N_{area} :

$$\rho_{rubisco} = \frac{V_{cmax25} N_r}{V_{cr} N_{area}} \quad (5.6)$$

2095 where N_r is the amount of nitrogen in Rubisco, set to $0.16 \text{ gN (gN in Rubisco)}^{-1}$
2096 and V_{cr} is the maximum rate of RuBP carboxylation per unit Rubisco protein,
2097 set to $20.5 \mu\text{mol CO}_2 (\text{g Rubisco})^{-1}$. The proportion of leaf nitrogen allocated to
2098 bioenergetics (ρ_{bioe} ; gN gN^{-1}) was similarly calculated as a function of J_{max25} and

2099 N_{area} :

$$\rho_{\text{bioe}} = \frac{J_{\text{max}25} N_b}{J_{\text{mc}} N_{\text{area}}} \quad (5.7)$$

2100 where N_b is the amount of nitrogen in cytochrome f, set to 0.12407 gN (μmol
2101 cytochrome f) $^{-1}$ assuming a constant 1: 1: 1.2 cytochrome f: ferredoxin NADP
2102 reductase: coupling factor molar ratio (Evans and Seemann 1989; Niinemets and
2103 Tenhunen 1997), and J_{mc} is the capacity of electron transport per cytochrome f,
2104 set to 156 μmol electron (μmol cytochrome f) $^{-1}\text{s}^{-1}$.

2105 The proportion of leaf nitrogen allocated to light harvesting proteins was

2106 calculated as a function of Chl_{mass} and N_{mass} :

$$\rho_{\text{light}} = \frac{Chl_{\text{mass}}}{N_{\text{mass}} c_b} \quad (5.8)$$

2107 where c_b is the stoichiometry of the light-harvesting chlorophyll complexes of
2108 photosystem II, set to 2.75 mmol chlorophyll (gN in chlorophyll) $^{-1}$. We used the
2109 N_{mass} value of the focal leaf used to generate A_{net}/C_i curves instead of the leaf
2110 used to extract chlorophyll content, as the two leaves are from the same trifoliolate
2111 leaf set and are highly correlated with each other (Figure SX).

2112 The proportion of leaf nitrogen content allocated to photosynthetic tissue

2113 (ρ_{photo} ; gN gN $^{-1}$) was estimated as the sum of ρ_{rubisco} , ρ_{bioe} , and ρ_{light} .

2114 Finally, the proportion of leaf N content allocated to structural tissue (ρ_{str} ;

2115 gN gN $^{-1}$) was estimated as:

$$\rho_{\text{structure}} = \frac{N_{\text{cw}}}{N_{\text{area}}} \quad (5.9)$$

2116 where N_{cw} is the leaf N content allocated to cell walls (gN m^{-2}), calculated as a
2117 function of M_{area} using an empirical equation from Onoda et al. (2017):

$$N_{cw} = 0.000355 * M_{area}^{1.39} \quad (5.10)$$

2118 5.2.8 *Whole plant traits*

2119 Seven weeks after experiment initiation and immediately following gas ex-
2120 change measurements, I harvested all experimental individuals and separated
2121 biomass of each experimental individual into major organ types (leaves, stems,
2122 roots, and nodules when present). Fresh leaf area of all harvested leaves was mea-
2123 sured using an LI-3100C (Li-COR Biosciences, Lincoln, Nebraska, USA). Total
2124 fresh leaf area (cm^2) was calculated as the sum of all leaf areas, including the focal
2125 leaf used to collect gas exchange data and the focal leaf used to extract chlorophyll
2126 content. All harvested material was dried in an oven set to 65°C for at least 48
2127 hours, weighed, and ground to homogeneity. Leaves and nodules were manually
2128 ground either with a mortar and pestle, while stems and roots were ground using
2129 a Wiley mill (E3300 Mini Mill; Eberbach Corp., MI, USA). Total dry biomass (g)
2130 was calculated as the sum of dry leaf (including focal leaf for both the A_{net}/C_i
2131 curve and leaf used to extract chlorophyll content), stem, root, and root nodule
2132 biomass. I quantified carbon and nitrogen content of each respective organ type
2133 through elemental combustion (Costech-4010, Costech, Inc., Valencia, CA, USA)
2134 using subsamples of ground and homogenized organ tissue.

2135 Following the approach explained in the first experimental chapter, I calcu-
2136 lated structural carbon costs to acquire nitrogen as the ratio of total belowground

2137 carbon biomass to whole plant nitrogen biomass (N_{cost} ; gC gN⁻¹). Belowground
2138 carbon biomass (C_{bg} ; gC) was calculated as the sum of root carbon biomass
2139 and root nodule carbon biomass. Root carbon biomass and root nodule carbon
2140 biomass was calculated as the product of the organ biomass and the respective
2141 organ carbon content. Whole plant nitrogen biomass (N_{wp} ; gN) was similarly
2142 calculated as the sum of total leaf, stem, root, and root nodule nitrogen biomass,
2143 including the focal leaf used for A_{net}/C_i curve and chlorophyll extractions. Leaf,
2144 stem, root, and root nodule nitrogen biomass was calculated as the product of
2145 the organ biomass and the respective organ nitrogen content. This calculation
2146 only quantifies plant structural carbon costs to acquire nitrogen and does not
2147 include any additional costs of nitrogen acquisition associated with respiration,
2148 root exudation, or root turnover. An explicit explanation of the limitations for
2149 interpreting this calculation can be found in Perkowski et al. (2021) and Terrer
2150 et al. (2018).

2151 Finally, plant investments in nitrogen fixation were calculated as the ra-
2152 tio of root nodule biomass to root biomass, where increasing values indicate an
2153 increase in plant investments to nitrogen fixation (Dovrat et al. 2018; Dovrat
2154 et al. 2020; Perkowski et al. 2021). I also calculated the percent of leaf nitrogen
2155 acquired from the atmosphere (% N_{dfa}) using leaf $\delta^{15}\text{N}$ and the following equation
2156 from Andrews et al. (2011):

$$\%N_{\text{dfa}} = \frac{\delta^{15}N_{\text{reference}} - \delta^{15}N_{\text{sample}}}{\delta^{15}N_{\text{reference}} - B} \quad (5.11)$$

2157 where $\delta^{15}\text{N}_{\text{reference}}$ refers to a reference plant that exclusively acquires nitrogen via

2158 direct uptake, $\delta^{15}\text{N}_{\text{sample}}$ refers to an individual's leaf $\delta^{15}\text{N}$, and B refers to individuals
2159 that are entirely reliant on nitrogen fixation. Within each unique nitrogen
2160 fertilization treatment-by-CO₂ treatment combination, I calculated the mean leaf
2161 $\delta^{15}\text{N}$ for individuals growing in the non-inoculated treatment for $\delta^{15}\text{N}_{\text{reference}}$. Any
2162 individuals with visual confirmation of root nodule formation or nodule initiation
2163 were omitted from the calculation of $\delta^{15}\text{N}_{\text{reference}}$. Following recommendations
2164 from Andrews et al. (2011) I calculated B within each CO₂ treatment using
2165 the mean leaf $\delta^{15}\text{N}$ of inoculated individuals that received 0 ppm N. I did not
2166 calculate B within each unique soil nitrogen-by-CO₂ treatment combination, as
2167 previous studies suggest decreased reliance on nitrogen fixation with increasing
2168 soil nitrogen availability (Perkowski et al. 2021). This approach for estimating
2169 nitrogen fixation standardizes values such that approaching 1 indicates increasing
2170 reliance on nitrogen fixation.

2171 5.2.9 *Statistical analyses*

2172 Any uninoculated pots that had substantial root nodule formation (nodule
2173 biomass: root biomass values greater than 0.05 g g⁻¹) were removed from analyses.
2174 This was because they were assumed to have been colonized by symbiotic nitrogen-
2175 fixing bacteria from outside sources. This decision resulted in the removal of
2176 sixteen pots from our analysis: two pots in the elevated CO₂ treatment that
2177 received 35 ppm N, three pots in the elevated CO₂ treatment that received 70
2178 ppm N, one pot in the elevated CO₂ treatment that received 210 ppm N, two pots
2179 in the elevated CO₂ treatment that received 280 ppm N, two pots in the ambient
2180 CO₂ treatment that received 0 ppm N, three pots in the ambient CO₂ treatment

2181 that received 70 ppm N, two pots in the ambient CO₂ treatment that received
2182 105 ppm N, and one pot in the ambient CO₂ treatment that received 280 ppm N.

2183 I built a series of linear mixed effects models to investigate the impacts of
2184 CO₂ concentration, soil nitrogen fertilization, and inoculation with *B. japonicum*
2185 on *G. max* gas exchange, tradeoffs between nitrogen and water use, whole plant
2186 growth, and investment in nitrogen fixation. All models included CO₂ treatment
2187 as a categorical fixed effect, inoculation treatment as a categorical fixed effect,
2188 soil nitrogen fertilization as a continuous fixed effect, with interaction terms be-
2189 tween all three fixed effects. All models also accounted for climatic difference
2190 between chambers across experiment iterations by including a random intercept
2191 term that nested starting chamber rack by CO₂ treatment. Models with this
2192 independent variable structure were created for each of the following dependent
2193 variables: N_{area} , M_{area} , N_{mass} , Chl_{area} , V_{cmax25} , J_{max25} , $J_{\text{max25}}:V_{\text{cmax25}}$, R_{d25} , g_{sw} ,
2194 stomatal limitation, ρ_{rubisco} , ρ_{bioe} , ρ_{light} , ρ_{photo} , $\rho_{\text{structure}}$, N_{cost} , C_{bg} , N_{wp} , total
2195 biomass, total leaf area, nodule biomass, and the ratio of nodule biomass to root
2196 biomass.

2197 I used Shapiro-Wilk tests of normality to determine whether linear mixed
2198 effects models satisfied residual normality assumptions. If residual normality as-
2199 sumptions were not met (Shapiro-Wilk: $p < 0.05$), then models were fit using
2200 dependent variables that were natural log transformed. All residual normality
2201 assumptions that did not originally satisfy residual normality assumptions were
2202 met with either a natural log or square root data transformation (Shapiro-Wilk:
2203 $p > 0.05$ in all cases). Specifically, models for N_{area} , N_{mass} , Chl_{area} , V_{cmax25} ,
2204 J_{max25} , $J_{\text{max25}}:V_{\text{cmax25}}$, g_{sw} , stomatal limitation, ρ_{rubisco} , ρ_{bioe} , ρ_{light} , ρ_{photo} , and to-

2205 tal leaf area satisfied residual normality assumptions without data transformation.

2206 Models for M_{area} , $\rho_{\text{structure}}$, N_{cost} , C_{bg} , N_{wp} , and total biomass satisfied residual

2207 normality assumptions with a natural log data transformation, while models for

2208 nodule biomass and nodule biomass: root biomass satisfied residual normality

2209 assumptions with a square root data transformation.

2210 In all statistical models, I used the 'lmer' function in the 'lme4' R package

2211 (Bates et al. 2015) to fit each model and the 'Anova' function in the 'car' R

2212 package (Fox and Weisberg 2019) to calculate Type II Wald's χ^2 and determine

2213 the significance ($\alpha = 0.05$) of each fixed effect coefficient. I used the 'emmeans'

2214 R package (Lenth 2019) to conduct post-hoc comparisons using Tukey's tests,

2215 where degrees of freedom were approximated using the Kenward-Roger approach

2216 (Kenward and Roger 1997). All analyses and plots were conducted in R version

2217 4.2.0 (R Core Team 2021).

2218 5.3 Results

2219 5.3.1 *Leaf nitrogen and chlorophyll content*

2220 Elevated CO₂ reduced N_{area} , N_{mass} , and Chl_{area} by 29%, 50%, and 31%,

2221 respectively, and stimulated M_{area} by 44% ($p < 0.001$ in all cases; Table 5.1). An

2222 interaction between fertilization and CO₂ (CO₂-by-fertilization interaction: $p_{N_{\text{area}}}$

2223 = 0.017, $p_{N_{\text{mass}}} < 0.001$, $p_{M_{\text{area}}} = 0.006$, $p_{Chl_{\text{area}}} = 0.083$; Table 5.1) indicated

2224 that the general positive effect of increasing fertilization on N_{area} , N_{mass} , and

2225 Chl_{area} ($p < 0.001$ in all cases; Table 5.1) was generally stronger under ambient

2226 CO₂ (Tukey _{N_{area}} : $p = 0.026$; Tukey _{N_{mass}} : $p < 0.001$; Tukey _{M_{area}} : $p = 0.009$;

2227 Tukey _{Chl_{area}} : $p = 0.065$; Table 5.1; Figs. 5.1a-d). This pattern resulted in a

2228 stronger reduction in N_{area} , N_{mass} , and Chl_{area} as well as a stronger stimulation
2229 in M_{area} under elevated CO₂ with increasing fertilization. An additional interac-
2230 tion between inoculation and CO₂ on N_{area} (CO₂-by-inoculation interaction: $p =$
2231 0.030; Table 5.1) indicated that the general positive effect of inoculation on N_{area}
2232 ($p < 0.001$; Table 5.1) was stronger under elevated CO₂ (45% increase; Tukey: p
2233 < 0.001) than under ambient CO₂ (18% increase; Tukey: $p < 0.001$), a result that
2234 increased the reduction in N_{area} in inoculated pots under elevated CO₂. Inocula-
2235 tion treatment did not modify the downregulation in N_{mass} (CO₂-by-inoculation
2236 interaction: $p = 0.148$; Table 5.1) and Chl_{area} ($p = 0.147$; Table 5.1) or the stimu-
2237 lation in M_{area} ($p = 0.866$; Table 5.1) under elevated CO₂. However, interactions
2238 between fertilization and inoculation on N_{area} (fertilization-by-inoculation inter-
2239 action: $p < 0.001$; Table 5.1; Fig. 5.1a), N_{mass} ($p = 0.001$; Table 5.1; Fig. 5.1b),
2240 M_{area} ($p = 0.025$; Table 5.1; Fig. 5.1c), and Chl_{area} ($p < 0.001$; Table 5.1; Fig.
2241 5.1d) indicated that the general positive effect of increasing fertilization on each
2242 trait was stronger in uninoculated pots (Tukey _{N_{area}} : $p < 0.001$; Tukey _{N_{mass}} : $p =$
2243 0.001; Tukey _{M_{area}} : $p = 0.031$; Tukey _{Chl_{area}} : $p < 0.001$).

Table 5.1. Effects of soil nitrogen fertilization, inoculation, and CO₂ treatments on N_{area} , N_{mass} , M_{area} , and Chl_{area}

	N_{area}			N_{mass}			M_{area}^a			
	df	Coefficient	χ^2	p	Coefficient	χ^2	p	Coefficient	χ^2	p
(Intercept)	-	1.10E+00	-	-	3.05E-02	-	-	3.64E+00	-	-
CO ₂	1	-5.67E-01	155.908	<0.001	-1.80E-02	272.362	<0.001	3.04E-01	151.319	<0.001
Inoculation (I)	1	6.21E-01	86.029	<0.001	7.54E-03	15.576	<0.001	1.81E-01	19.158	<0.001
Fertilization (N)	1	3.06E-03	316.408	<0.001	5.78E-05	106.659	<0.001	3.10E-04	21.440	<0.001
CO ₂ *I	1	2.63E-01	4.729	0.030	3.96E-03	2.025	0.155	-3.37E-02	0.029	0.866
CO ₂ *N	1	-3.68E-04	5.723	0.017	-2.85E-05	22.542	<0.001	2.80E-04	7.619	0.006
I*N	1	-1.36E-03	43.381	<0.001	-2.00E-05	11.137	0.001	-3.36E-04	5.022	0.025
CO ₂ *I*N	1	-3.23E-04	0.489	0.484	-2.59E-06	0.041	0.839	1.15E-04	0.208	0.649
	Chl_{area}									
	df	Coefficient	χ^2	p						
(Intercept)	-	2.13E-02	-	-						
CO ₂	1	-1.33E-02	69.233	<0.001						
Inoculation (I)	1	1.24E-01	136.341	<0.001						
Fertilization (N)	1	3.35E-04	163.111	<0.001						
CO ₂ *I	1	-3.18E-02	2.102	0.147						
CO ₂ *N	1	-8.79E-05	2.999	<i>0.083</i>						
I*N	1	-2.65E-04	75.769	<0.001						
CO ₂ *I*N	1	7.68E-05	2.144	0.147						

131

2244 *Significance determined using Type II Wald χ^2 tests ($\alpha = 0.05$). P -values < 0.05 are in bold, while p -values between
 2245 0.05 and 0.1 are italicized. A superscript “a” is included after trait labels to indicate if models were fit with natural
 2246 log transformed response variables. Key: df = degrees of freedom, N_{area} = leaf nitrogen content per unit leaf area,
 2247 N_{mass} = leaf nitrogen content, M_{area} = leaf mass per unit leaf area.

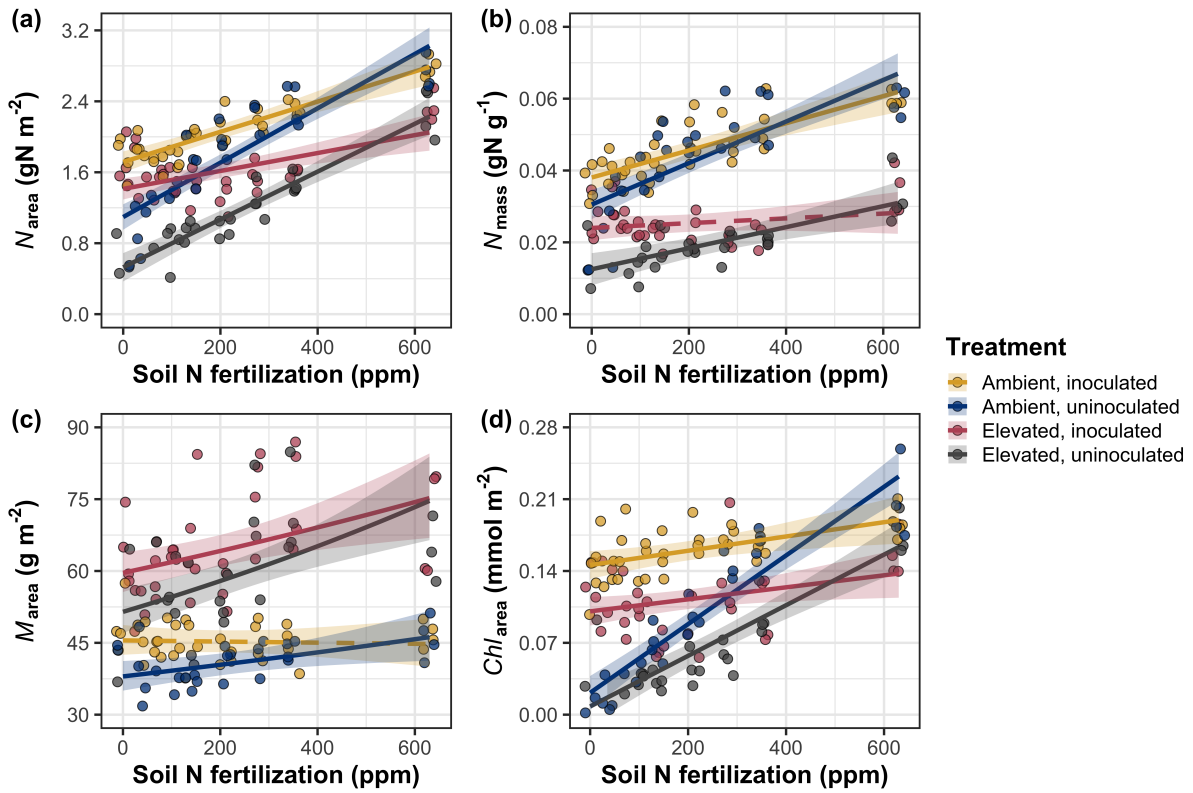


Figure 5.1. Effects of CO_2 , fertilization, and inoculation on leaf nitrogen per unit leaf area (a), leaf nitrogen content (b), leaf mass per unit leaf area (c), and chlorophyll content per unit leaf area (d). Soil nitrogen fertilization is represented on the x-axis in all panels. Yellow points and trendlines indicate inoculated individuals grown under ambient CO_2 , blue points and trendlines indicate uninoculated individuals grown under ambient CO_2 , red points and trendlines indicate inoculated individuals grown under elevated CO_2 , and grey points indicate uninoculated individuals grown under elevated CO_2 . Solid trendlines indicate regression slopes that are different from zero ($p < 0.05$), while dashed trendlines indicate slopes that are not distinguishable from zero ($p > 0.05$).

2248 5.3.2 *Leaf biochemistry and stomatal conductance*

2249 Elevated CO₂ resulted in plants with 16% lower V_{cmax25} ($p < 0.001$; Table
2250 5.2) and 10% lower J_{max25} ($p = 0.014$; Table 5.2) as compared to those grown under
2251 ambient CO₂. However, CO₂ concentration did not influence R_{d25} ($p = 0.613$;
2252 Table 5.2). A relatively stronger downregulation in V_{cmax25} than J_{max25} resulted
2253 in an 8% stimulation in $J_{max25}:V_{cmax25}$ under elevated CO₂ ($p < 0.001$; Table 5.2;
2254 Fig. 2E). The downregulatory effect of CO₂ on V_{cmax25} and J_{max25} was not modified
2255 across the fertilization gradient (CO₂-by-fertilization interaction: $p = 0.185$, $p =$
2256 0.389 for V_{cmax25} and J_{max25} , respectively; Table 5.2; Fig. 5.2a-b) or between
2257 inoculation treatments (CO₂-by-inoculation interaction: $p = 0.799$ and $p = 0.714$
2258 for V_{cmax25} and J_{max25} , respectively; Table 5.2). However, a strong interaction
2259 between fertilization and inoculation (fertilization-by-inoculation interaction: $p \leq$
2260 0.001 in all cases; Table 5.2) indicated that the general positive effect of increasing
2261 fertilization on V_{cmax25} ($p < 0.001$; Table 5.2), J_{max25} ($p < 0.001$; Table 5.2), and
2262 R_{d25} ($p = 0.015$; Table 2) was only observed in uninoculated pots (Tukey: p
2263 ≤ 0.001 in all cases), as there was no apparent effect of fertilization on V_{cmax25}
2264 (Tukey: $p = 0.456$), J_{max25} (Tukey: $p = 0.180$), or R_{d25} (Tukey: $p = 0.443$) in
2265 inoculated pots (Figs. 5.2a-d). A relatively stronger positive effect of increasing
2266 fertilization on V_{cmax25} than J_{max25} resulted in a general reduction in $J_{max25}:V_{cmax25}$
2267 with increasing fertilization ($p < 0.001$), though this pattern was only seen in
2268 uninoculated pots (Tukey: $p = 0.003$) and not inoculated plants (Tukey: $p >$
2269 0.05).

2270 Elevated CO₂ reduced stomatal conductance by 20% ($p < 0.001$; Table
2271 5.2; Fig. 5.2e) compared to ambient CO₂, but this downregulation did not influ-

ence stomatal limitation of photosynthesis ($p = 0.355$; Table 5.2; Fig. 5.2f). As with V_{cmax25} and J_{max25} , the downregulation of stomatal conductance due to elevated CO₂ was not modified across the fertilization gradient (CO₂-by-fertilization interaction: $p = 0.141$; Table 5.2) or between inoculation treatments (CO₂-by-inoculation interaction: $p = 0.179$; Table 5.2). Fertilization also did not modify the general null effect of CO₂ on stomatal limitation (CO₂-by-fertilization interaction: $p = 0.554$; Table 5.2), although an interaction between CO₂ and inoculation (CO₂-by-inoculation interaction: $p = 0.043$; Table 5.2) indicated that inoculation increased stomatal limitation under ambient CO₂ (Tukey: $p = 0.021$), but not under elevated CO₂ (Tukey: $p > 0.999$). An interaction between inoculation and fertilization on stomatal conductance (fertilization-by-inoculation interaction: $p < 0.001$; Table 5.2) indicated that increasing fertilization increased stomatal conductance in uninoculated pots (Tukey: $p = 0.003$) but decreased stomatal conductance in inoculated pots (Tukey: $p = 0.021$). The similar in magnitude, but opposite direction, trend in the effect of increasing fertilization on stomatal conductance between inoculation treatments likely drove a null general response of stomatal conductance to increasing fertilization ($p = 0.642$; Table 5.2).

Table 5.2. Effects of soil nitrogen fertilization, inoculation, and CO₂ on leaf biochemistry

	<i>V_{cmax25}</i>			<i>J_{max25}</i>			<i>R_{d25}</i>			
	df	Coefficient	χ^2	p	Coefficient	χ^2	p	Coefficient	χ^2	p
(Intercept)	-	4.36E+01	-	-	8.30E+01	-	-	1.69E+00	-	-
CO ₂	1	-7.05E+00	18.039	<0.001	-9.11E+00	6.042	0.014	4.53E-01	0.256	0.613
Inoculation (I)	1	5.87E+01	98.579	<0.001	9.62E+01	85.064	<0.001	1.04E+00	3.094	0.079
Fertilization (N)	1	1.32E-01	37.053	<0.001	2.09E-01	25.356	<0.001	2.86E-03	5.965	0.015
CO ₂ *I	1	-4.65E+00	0.065	0.799	7.84E-01	0.667	0.414	-5.71E-01	2.563	0.109
CO ₂ *N	1	-3.58E-02	1.758	0.185	-4.33E-02	0.742	0.389	-1.55E-03	2.675	0.102
I*N	1	-1.35E-01	60.394	<0.001	-2.30E-01	57.410	<0.001	-2.84E-03	12.083	0.001
CO ₂ *I*N	1	2.73E-02	0.748	0.387	3.46E-02	0.377	0.539	7.21E-04	0.244	0.622

	<i>J_{max25}:V_{cmax25}</i>			<i>g_{sw}</i>			Stomatal limitation			
	df	Coefficient	χ^2	p	Coefficient	χ^2	p	Coefficient	χ^2	p
(Intercept)	-	1.92E+00	-	-	1.95E-01	-	-	2.12E-01	-	-
CO ₂	1	5.71E-02	92.010	<0.001	-6.23E-02	9.718	0.002	3.91E-02	0.856	0.355
Inoculation (I)	1	-1.79E-01	27.768	<0.001	1.30E-01	22.351	<0.001	7.87E-02	4.582	0.032
Fertilization (N)	1	-4.61E-04	28.147	<0.001	2.50E-04	0.066	0.797	2.60E-04	32.218	<0.001
CO ₂ *I	1	8.94E-02	2.916	0.088	6.69E-02	1.810	0.179	-7.84E-02	4.093	0.043
CO ₂ *N	1	2.35E-04	3.210	0.073	-8.50E-05	2.165	0.141	-1.24E-04	0.350	0.554
I*N	1	3.27E-04	9.607	0.002	-3.09E-04	14.696	<0.001	-1.67E-04	2.547	0.110
CO ₂ *I*N	1	-1.66E-04	1.102	0.294	-8.89E-05	0.234	0.629	1.67E-04	2.231	0.135

135

2289 *Significance determined using Type II Wald χ^2 tests ($\alpha = 0.05$). *P*-values < 0.05 are in bold, while *p*-values between
 2290 0.05 and 0.1 are italicized. Key: *V_{cmax25}* = maximum rate of Rubisco carboxylation at 25°C; *J_{max25}* = maximum rate
 2291 of electron transport for RuBP regeneration at 25°C, *R_{d25}* = dark respiration at 25°C; *J_{max25}:V_{cmax25}* = the ratio of
 2292 *J_{max25}* to *V_{cmax25}*; *g_{sw}* = stomatal conductance.

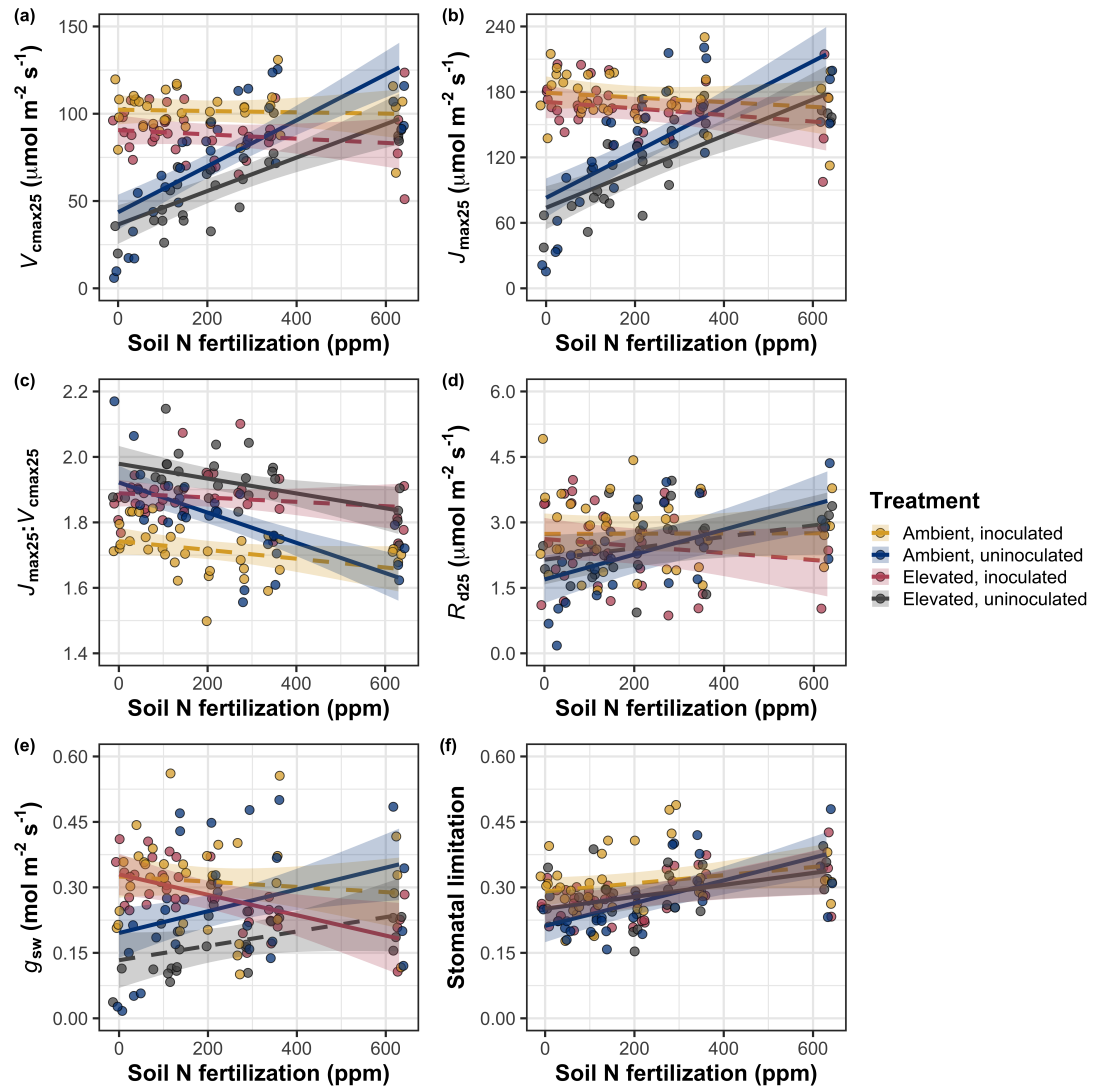


Figure 5.2. Effects of CO₂, fertilization, and inoculation on maximum rate of Rubisco carboxylation (a), the maximum rate of RuBP regeneration (b), and the ratio of the maximum rate of RuBP regeneration to the maximum rate of Rubisco carboxylation leaf mass per unit leaf area (c), dark respiration (d), stomatal conductance (e), and stomatal limitation (f). Soil nitrogen fertilization is represented on the x-axis in all panels. Colored points and trendlines are as explained in Figure 1.

2293 5.3.3 *Leaf nitrogen allocation*

2294 A relatively stronger downregulation in N_{area} than $V_{\text{cmax}25}$ or $J_{\text{max}25}$ resulted
2295 in an 20% and 29% respective stimulation in ρ_{rubisco} and ρ_{bioe} under elevated CO₂
2296 ($p < 0.001$ in both cases; Table 5.3). There was no apparent CO₂ effect on ρ_{light}
2297 ($p = 0.700$; Table 5.3), but the strong stimulation in ρ_{rubisco} and ρ_{bioe} resulted
2298 in a 21% stimulation of ρ_{photo} under elevated CO₂ ($p < 0.001$; Table 5.3; Fig.
2299 5.3a). The stimulation of ρ_{rubisco} , ρ_{bioe} , and ρ_{photo} due to elevated CO₂ was not
2300 modified across the fertilization gradient (CO₂-by-fertilization interaction: p_{rubisco}
2301 = 0.269, $p_{\text{bioe}} = 0.298$, $p_{\text{photo}} = 0.281$; Table 5.3). A marginal interaction between
2302 inoculation and CO₂ on ρ_{rubisco} and ρ_{photo} (CO₂-by-inoculation interaction: p_{rubisco}
2303 = 0.057, $p_{\text{photo}} = 0.057$; Table 5.3) indicated that the general positive effect of
2304 inoculation on ρ_{rubisco} and ρ_{photo} ($p < 0.001$ in both cases; Table 5.3) was only
2305 apparent under ambient CO₂ (Tukey: $p < 0.001$ in both cases), with no apparent
2306 effect of inoculation under elevated CO₂ (Tukey_{rubisco}: $p = 0.200$; Tukey_{photo}: p
2307 = 0.147). Inoculation did not modify the stimulation of ρ_{bioe} under elevated CO₂
2308 (CO₂-by-inoculation interaction: $p = 0.122$; Table 5.3) or the null effect of CO₂ on
2309 ρ_{bioe} (CO₂-by-inoculation interaction: $p = 0.298$; Table 5.3). Strong interactions
2310 between fertilization and inoculation on ρ_{rubisco} , ρ_{bioe} , and ρ_{photo} (fertilization-
2311 by-inoculation interaction: $p < 0.001$ in all cases; Table 5.3) indicated that the
2312 general negative effect of increasing fertilization ($p < 0.001$ in all cases; Table
2313 5.3) was only observed in inoculated pots (Tukey: $p < 0.001$ in all cases), with
2314 no apparent effect of fertilization on ρ_{rubisco} (Tukey: $p = 0.612$), ρ_{bioe} (Tukey:
2315 $p = 0.544$), or ρ_{photo} (Tukey: $p = 0.521$; Fig 5.3a) in uninoculated pots. An
2316 additional interaction between fertilization and inoculation on ρ_{light} (fertilization-

2317 by-inoculation interaction: $p < 0.001$; Table 5.3) indicated a negative effect of
2318 increasing fertilization on ρ_{light} in inoculated pots (Tukey: $p = 0.041$), but a
2319 positive effect of increasing fertilization in uninoculated pots (Tukey: $p < 0.001$).

2320 The stimulation in M_{area} resulted in an 133% stimulation of $\rho_{\text{structure}}$ under
2321 elevated CO₂ ($p < 0.001$; Table 5.3; Fig 5.3b). An interaction between fertiliza-
2322 tion and CO₂ (CO₂-by-fertilization interaction: $p = 0.039$; Table 5.3) indicated
2323 that the general negative effect of increasing fertilization ($p < 0.001$; Table 5.3) on
2324 $\rho_{\text{structure}}$ was marginally stronger under ambient CO₂ (Tukey: $p = 0.055$), resulting
2325 in a stronger stimulation in $\rho_{\text{structure}}$ under elevated CO₂ with increasing fertiliza-
2326 tion. A marginal interaction between inoculation and CO₂ (CO₂-by-inoculation
2327 interaction: $p = 0.057$; Table 5.3) indicated that the general positive effect of
2328 inoculation on $\rho_{\text{structure}}$ ($p < 0.001$; Table 5.3) was only observed under elevated
2329 CO₂ (Tukey: $p < 0.001$), with no apparent inoculation effect observed under am-
2330 bient CO₂ (Tukey: $p = 0.513$). Finally, an interaction between fertilization and
2331 inoculation (fertilization-by-inoculation interaction: $p < 0.001$; Table 5.3) indi-
2332 cated that, while increasing fertilization generally increased $\rho_{\text{structure}}$ ($p < 0.001$;
2333 Table 5.3), this response was generally stronger in uninoculated pots (Tukey: p
2334 = 0.001; Fig. 5.3b).

Table 5.3. Effects of soil N availability, soil pH, species, and N_{area} on leaf nitrogen allocation

		ρ_{rubisco}		ρ_{bioe}		ρ_{light}				
	df	Coefficient	χ^2	p	Coefficient	χ^2	p	Coefficient	χ^2	p
(Intercept)	-	2.70E-01	-	-	5.26E-02	-	-	8.48E-03	-	-
CO_2	1	1.42E-01	23.510	<0.001	3.00E-02	53.899	<0.001	2.03E-03	0.149	0.700
Inoculation (I)	1	1.83E-01	23.475	<0.001	2.80E-02	13.860	<0.001	2.04E-02	147.234	<0.001
Fertilization (N)	1	1.35E-04	16.609	<0.001	1.22E-05	26.827	<0.001	3.22E-05	19.378	<0.001
CO_2*I	1	-1.07E-01	3.629	<i>0.057</i>	-1.67E-02	2.390	0.122	-5.33E-03	0.684	0.408
CO_2*N	1	-2.16E-04	1.223	0.269	-3.59E-05	1.085	0.298	-7.01E-06	0.351	0.553
$I*N$	1	-4.26E-04	20.045	<0.001	-6.87E-05	15.458	<0.001	-4.37E-05	64.042	<0.001
CO_2*I*N	1	2.50E-04	3.327	<i>0.068</i>	4.08E-05	2.651	0.103	1.74E-05	3.735	<i>0.053</i>

		ρ_{photo}		$\rho_{\text{structure}}^a$			
	df	Coefficient	χ^2	p	Coefficient	χ^2	p
(Intercept)	-	3.32E-01	-	-	-2.93E+00	-	-
CO_2	1	1.81E-01	27.651	<0.001	8.77E-01	229.571	<0.001
Inoculation (I)	1	2.31E-01	26.238	<0.001	-2.55E-01	13.872	<0.001
Fertilization (N)	1	1.76E-04	15.899	<0.001	-1.51E-03	38.128	<0.001
CO_2*I	1	-1.36E-01	3.671	<i>0.055</i>	-2.99E-01	3.622	<i>0.057</i>
CO_2*N	1	-2.72E-04	1.163	0.281	3.14E-04	4.266	0.039
$I*N$	1	-5.37E-04	21.355	<0.001	7.00E-04	11.025	0.001
CO_2*I*N	1	3.29E-04	4.009	0.045	4.52E-04	0.669	0.413

139

2335 *Significance determined using Type II Wald χ^2 tests ($\alpha = 0.05$). P -values < 0.05 are in bold, while p -values
 2336 between 0.05 and 0.1 are italicized. A superscript “a” is included after trait labels to indicate if models were fit with
 2337 natural log transformed response variables. Key: df=degrees of freedom, ρ_{rubisco} = proportion of leaf N allocated
 2338 to photosynthesis, ρ_{bioe} = proportion of leaf N allocated to bioenergetics, ρ_{light} = proportion of leaf N allocated to
 2339 light harvesting proteins, ρ_{photo} = proportion of leaf N allocated to photosynthesis, $\rho_{\text{structure}}$ = proportion of leaf N
 2340 allocated to cell wall structural tissue

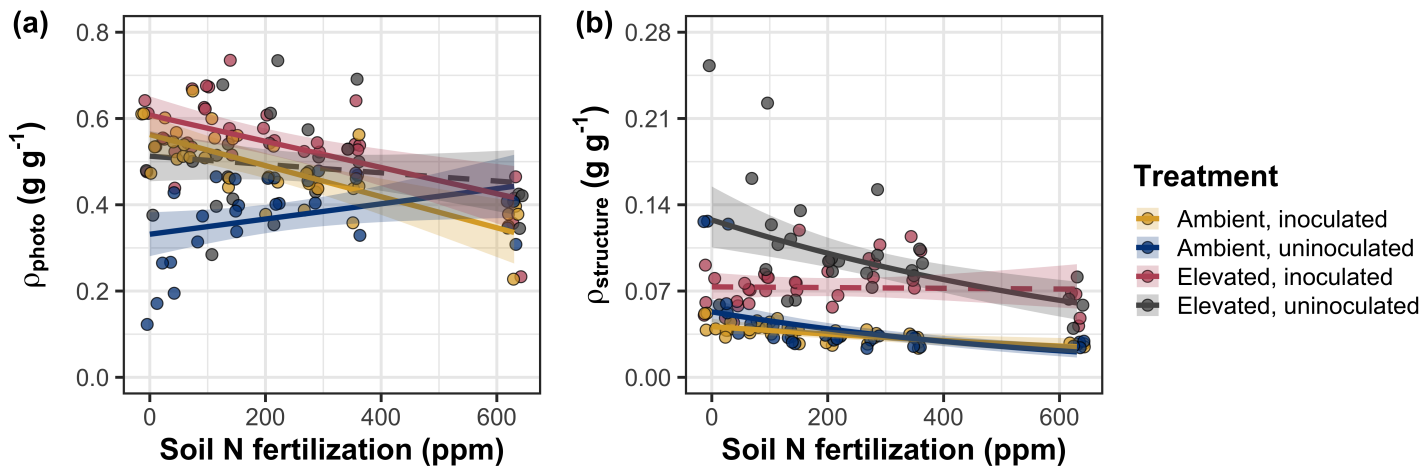


Figure 5.3. Effects of CO_2 , fertilization, and inoculation on the relative fraction of leaf nitrogen allocated to photosynthesis (a) and the fraction of leaf nitrogen allocated to structure (b). Soil nitrogen fertilization is represented on the x-axis in both panels. Colored points and trendlines are as explained in Figure 1.

2341 5.3.4 *Whole plant traits*

2342 Total leaf area was 51% greater and total biomass was 102% greater under
2343 elevated CO₂ ($p < 0.001$ in both cases; Table 5.4), a pattern that was enhanced
2344 by fertilization (CO₂-by-fertilization interaction: $p < 0.001$ in both cases; Table
2345 5.4; Figs. 5.4a-b) but was not modified across inoculation treatments (CO₂-by-
2346 inoculation interaction: $p_{total_leaf_area} = 0.151$, $p_{total_biomass} = 0.472$; Table 5.4).
2347 Specifically, the general positive effect of increasing fertilization on total leaf area
2348 and whole plant biomass ($p < 0.001$ in both cases; Table 5.4) was stronger under
2349 elevated CO₂ (Tukey: $p < 0.001$ in both cases). The general positive effect of
2350 increasing fertilization on total leaf area was modified by inoculation treatment
2351 (fertilization-by-inoculation interaction: $p < 0.001$ in both cases; Table 5.4), in-
2352 dicating a stronger positive effect of increasing fertilization in uninoculated pots
2353 (Tukey: $p_{total_leaf_area} = 0.002$, $p_{total_biomass} = 0.001$, Fig. 5.4a).

2354 A 62% stimulation in N_{cost} under elevated CO₂ was modified through a
2355 strong three-way interaction between CO₂, fertilization, and inoculation (CO₂-
2356 by-inoculation-by-fertilization interaction: $p < 0.001$; Table 5.4; Fig. 5.4). This
2357 interaction revealed a general negative effect of increasing fertilization on N_{cost}
2358 ($p < 0.001$; Table 5.4) that was observed in all treatment combinations (Tukey:
2359 $p < 0.001$ in all cases) except for inoculated pots grown under elevated CO₂
2360 (Tukey: $p = 0.779$; Fig. 5.4c). This response also resulted in generally stronger
2361 negative effects of increasing fertilization on N_{cost} in uninoculated pots grown
2362 under elevated CO₂ than uninoculated pots grown under ambient CO₂ (Tukey:
2363 $p = 0.001$) and inoculated pots grown under either ambient CO₂ (Tukey: $p <$
2364 0.001) or elevated CO₂ (Tukey: $p < 0.001$), while uninoculated pots grown under

2365 ambient CO₂ had generally stronger negative effects of increasing fertilization on
2366 N_{cost} than inoculated pots grown under elevated CO₂ (Tukey: $p = 0.002$), but
2367 not inoculated pots grown under ambient CO₂ (Tukey: $p = 0.216$; Fig. 5.4).
2368 The general reduction in N_{cost} with increasing fertilization and in uninoculated
2369 pots were driven by a stronger positive effect of increasing fertilization on N_{wp}
2370 (denominator of N_{cost}) than C_{bg} (numerator of N_{cost}), while the general stimulation
2371 in N_{cost} under elevated CO₂ was driven by a stronger positive effect of elevated
2372 CO₂ on C_{bg} than N_{wp} (Table 5.4).

Table 5.4. Effects of soil N availability, soil pH, species, and N_{area} on total leaf area, whole plant biomass, and carbon costs to acquire nitrogen

	Total leaf area			Total biomass			N_{cost}			
	df	Coefficient	χ^2	p	Coefficient	χ^2	p	Coefficient	χ^2	p
(Intercept)	-	8.78E+01	-	-	9.96E-01	-	-	8.67E+00	-	-
CO_2	1	3.36E+01	69.291	<0.001	5.07E-01	131.477	<0.001	8.75E+00	88.189	<0.001
Inoculation (I)	1	1.88E+02	35.715	<0.001	7.96E-01	34.264	<0.001	-1.68E+00	136.343	<0.001
Fertilization (N)	1	9.35E-01	274.199	<0.001	3.14E-03	269.046	<0.001	-8.50E-03	80.501	<0.001
$\text{CO}_2 * \text{I}$	1	6.44E+01	2.064	0.151	-7.69E-02	0.518	0.472	-8.38E+00	85.237	<0.001
$\text{CO}_2 * \text{N}$	1	5.05E-01	18.655	<0.001	1.61E-03	16.877	<0.001	-9.17E-03	1.050	0.306
$\text{I} * \text{N}$	1	-3.84E-01	10.804	0.001	-1.45E-03	15.779	<0.001	4.20E-03	46.489	<0.001
$\text{CO}_2 * \text{I} * \text{N}$	1	-2.97E-03	<0.001	0.990	-1.14E-04	0.023	0.880	1.32E-02	18.125	<0.001

	C_{bg}			N_{wp}			
	df	Coefficient	χ^2	p	Coefficient	χ^2	p
(Intercept)	-	-1.70E+00	-	-	1.24E-01	-	-
CO_2	1	9.21E-01	84.134	<0.001	-3.41E-03	23.890	<0.001
Inoculation (I)	1	1.18E+00	41.030	<0.001	1.68E-01	134.460	<0.001
N fertilization (N)	1	3.38E-03	152.248	<0.001	6.69E-04	529.021	<0.001
$\text{CO}_2 * \text{I}$	1	-6.18E-01	8.965	0.003	3.68E-02	1.190	0.275
$\text{CO}_2 * \text{N}$	1	-3.66E-05	1.188	0.276	1.58E-04	5.915	0.015
$\text{I} * \text{N}$	1	-2.22E-03	22.648	<0.001	-3.20E-04	55.562	<0.001
$\text{CO}_2 * \text{I} * \text{N}$	1	8.09E-04	1.109	0.292	-7.54E-05	0.620	0.431

143

2373 *Significance determined using Type II Wald χ^2 tests ($\alpha = 0.05$). P-values < 0.05 are in bold, while p-values between
 2374 0.05 and 0.1 are italicized. Key: df = degrees of freedom; N_{cost} = structural carbon cost to acquire nitrogen; C_{bg} =
 2375 belowground carbon biomass; N_{wp} = whole plant nitrogen biomass

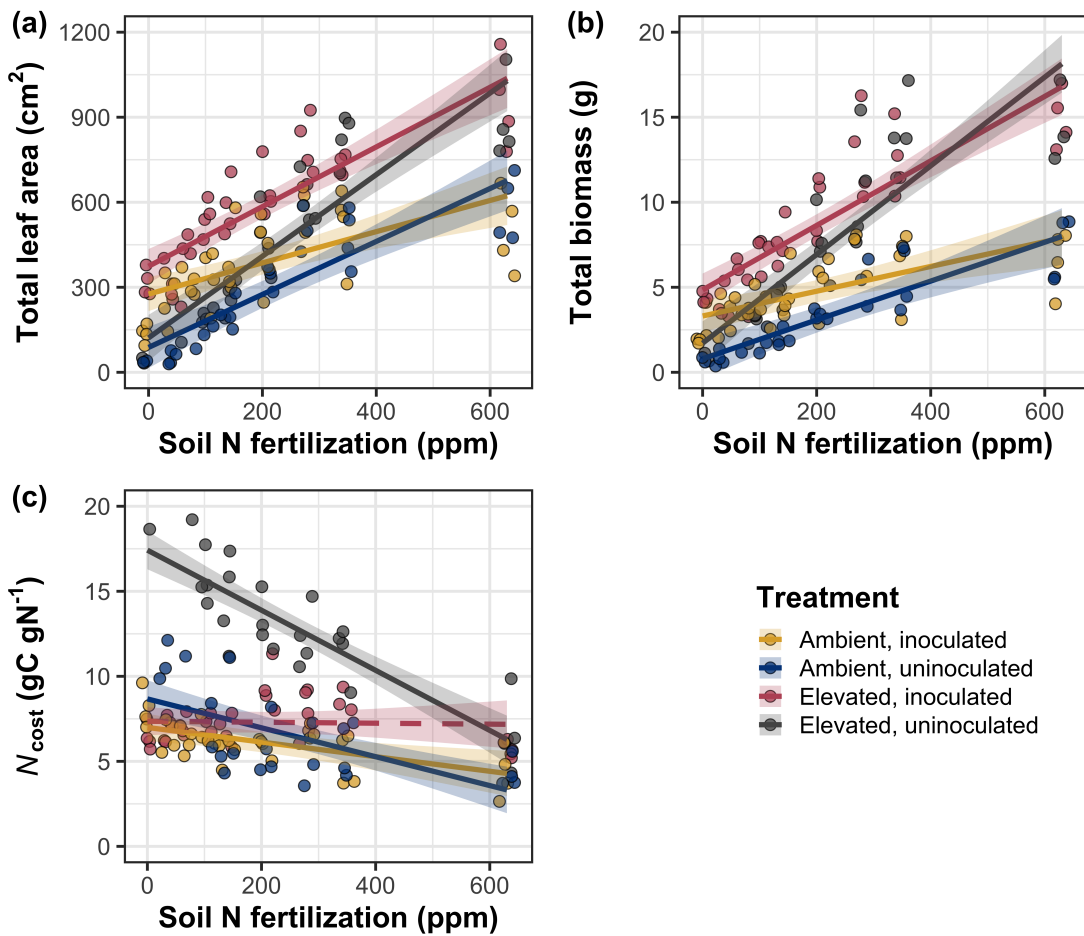


Figure 5.4. Effects of CO_2 , fertilization, and inoculation on total leaf area (a), total biomass (b), and structural carbon costs to acquire nitrogen (c). Soil nitrogen fertilization is represented continuously on the x-axis in all panels. Colored points and trendlines are as explained in Figure 1.

2376 5.3.5 *Nitrogen fixation*

2377 Nodule biomass was stimulated by 30% under elevated CO₂ ($p < 0.001$;
2378 Table 5.5), a pattern that was modified across the fertilization gradient (CO₂-
2379 by-fertilization interaction: $p = 0.479$; Table 5.5), but not between inoculation
2380 treatments (CO₂-by-inoculation interaction: $p = 0.404$; Table 5.5). Specifically,
2381 the general negative effect of increasing fertilization on nodule biomass ($p < 0.001$;
2382 Table 5.5) was stronger under elevated CO₂ than ambient CO₂ (Tukey: $p <$
2383 0.001; Fig. 5.5a), which reduced the stimulation in nodule biomass under elevated
2384 CO₂ with increasing fertilization. A strong interaction between fertilization and
2385 inoculation (fertilization-by-inoculation interaction: $p < 0.001$; Table 5.5) was
2386 driven by a stronger negative effect of increasing fertilization in inoculated pots
2387 (Tukey: $p < 0.001$; Fig. 5.5a).

2388 There was no effect of CO₂ on nodule: root biomass ($p = 0.767$; Table
2389 5.5), although an interaction between CO₂ and inoculation (CO₂-by-inoculation
2390 interaction: $p < 0.001$; Table 5.5) indicated that the general positive effect of in-
2391 oculation on nodule: root biomass ($p < 0.001$; Table 5.5) was stronger under am-
2392 bient CO₂ (3129% increase; Tukey: $p < 0.001$) than elevated CO₂ (379% increase;
2393 Tukey: $p < 0.001$; Fig. 5.5b). The null effect of CO₂ on nodule: root biomass
2394 was consistently observed across the fertilization gradient ($p = 0.183$; Table 5.5;
2395 Fig. 5.5b). An interaction between fertilization and inoculation (fertilization-by-
2396 inoculation interaction: $p < 0.001$; Table 5.5) indicated that the general negative
2397 effect of increasing fertilization on nodule: root biomass ($p < 0.001$; Table 5.5)
2398 was stronger in inoculated pots (Tukey: $p < 0.001$; Fig. 5.5b).

2399 There was no effect of CO₂ on %N_{dfa} ($p = 0.472$; Table 5.5), a pattern

2400 that was not modified by inoculation (CO_2 -by-inoculation interaction: $p = 0.156$;
2401 Table 5.5) or fertilization (CO_2 -by-fertilization interaction: $p = 0.099$; Table 5.5).
2402 An interaction between fertilization and inoculation (fertilization-by-inoculation
2403 interaction: $p < 0.001$; Table 5.5) indicated that the general negative effect of
2404 increasing fertilization on $\%N_{dfa}$ ($p < 0.001$; Table 5.5) was only observed in
2405 inoculated pots (Tukey: $p < 0.001$), with no apparent effect of fertilization on
2406 $\%N_{dfa}$ in uninoculated pots (Tukey: $p = 0.651$; Table 5.5; Fig. 5.5c).

Table 5.5. Effects of soil N availability, soil pH, species, and N_{area} on root nodule biomass and plant investments in symbiotic nitrogen fixation

	Root nodule biomass ^b			Root nodule: root biomass ^b			% N_{dfa}^b			
	df	Coefficient	χ^2	p	Coefficient	χ^2	p	Coefficient	χ^2	p
(Intercept)	-	9.41E-03	-	-	1.33E-02	-	-	7.48E-01	-	-
CO ₂	1	1.20E-01	19.258	<0.001	9.94E-02	0.087	0.768	-1.00E-01	0.518	0.472
Inoculation (I)	1	5.74E-01	755.020	<0.001	5.40E-01	903.691	<0.001	9.01E+00	955.570	<0.001
Fertilization (N)	1	7.71E-06	84.376	<0.001	-5.99E-06	258.099	<0.001	3.64E-04	292.938	<0.001
CO ₂ *I	1	-4.68E-02	0.950	0.330	-1.38E-01	20.614	<0.001	-1.44E-01	2.010	0.156
CO ₂ *N	1	-1.59E-04	2.106	0.147	-1.73E-04	1.773	0.183	-6.21E-05	2.716	0.099
I*N	1	-5.82E-04	44.622	<0.001	-7.45E-04	133.918	<0.001	-1.58E-02	231.290	<0.001
CO ₂ *I*N	1	7.26E-05	0.196	0.658	1.76E-04	2.359	0.125	2.77E-03	2.119	0.145

2407 *Significance determined using Type II Wald χ^2 tests ($\alpha = 0.05$). P-values < 0.05 are in bold, while p-values between
2408 0.05 and 0.1 are italicized. Superscript letters indicate model coefficients fit to square-root (^b) transformed data.
2409 Key: df = degrees of freedom % N_{dfa} = percent nitrogen fixed from the atmosphere.

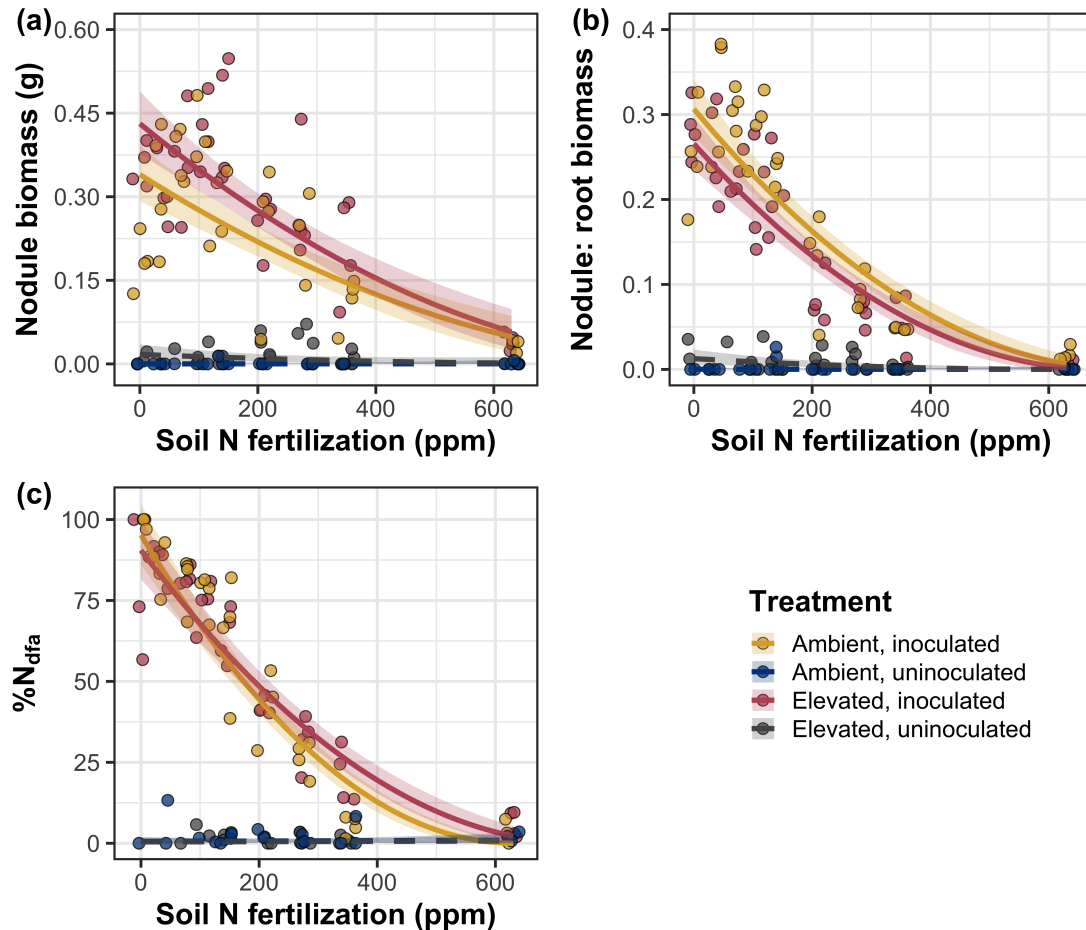


Figure 5.5. Effects of CO₂, fertilization, and inoculation on nodule biomass (a), nodule: root biomass (b), and percent nitrogen fixed from the atmosphere (c). Soil nitrogen fertilization is represented on the x-axis. Yellow points and trendlines indicate inoculated individuals grown under ambient CO₂, blue points and trendlines indicate uninoculated individuals grown under ambient CO₂, red points and trendlines indicate inoculated individuals grown under elevated CO₂, and grey points indicate uninoculated individuals grown under elevated CO₂. Solid trendlines indicate slopes that are different from zero ($p < 0.05$), while dashed trendlines indicate slopes that are not different from zero ($p > 0.05$). Curvilinear trendlines occur as a result of back-transforming models where response variables received either a natural log or square root transformation prior to fitting.

2410 5.4 Discussion

2411 In this study, I determined leaf and whole plant acclimation responses of
2412 7-week *G. max* seedlings grown under two CO₂ concentrations, two inoculation
2413 treatments, and nine soil nitrogen fertilization treatments in a full-factorial growth
2414 chamber experiment. In support of my hypotheses and patterns expected from
2415 theory, elevated CO₂ reduced N_{area} , V_{cmax25} , and J_{max25} . The relatively stronger
2416 downregulation in V_{cmax25} than J_{max25} under elevated CO₂ resulted in a stimulation
2417 in $J_{\text{max25}}:V_{\text{cmax25}}$ under elevated CO₂. The downregulation of V_{cmax25} and J_{max25}
2418 under elevated CO₂ was similar across fertilization and inoculation treatments,
2419 indicating that the CO₂ responses were not due to nitrogen limitation. Interest-
2420 ingly, results indicate that elevated CO₂ increased the fraction of leaf nitrogen
2421 allocated to photosynthesis and structure, leading to a stimulation in nitrogen
2422 use efficiency under elevated CO₂ despite the apparent downregulation in N_{area} ,
2423 V_{cmax25} , and J_{max25} . The downregulation in leaf photosynthetic processes under
2424 elevated CO₂ also corresponded with a strong stimulation in total leaf area and to-
2425 tal biomass. Strong stimulations in whole plant growth due to elevated CO₂ were
2426 generally enhanced with increasing fertilization and were negatively related to
2427 structural carbon costs to acquire nitrogen. Inoculation generally did not modify
2428 whole plant responses to elevated CO₂ across the fertilization gradient, likely due
2429 to a strong reduction in root nodulation with increasing fertilization. However,
2430 strong positive effects of inoculation on whole plant growth were observed under
2431 low fertilization, consistent with our hypothesis. Overall, observed leaf and whole
2432 plant acclimation responses to CO₂ support hypotheses and patterns expected
2433 from photosynthetic least-cost theory, showing that leaf acclimation responses to

2434 CO₂ were decoupled from soil nitrogen availability and ability to acquire nitro-
2435 gen via symbiotic nitrogen fixation. Instead, leaf and whole plant acclimation
2436 responses to CO₂ were driven by optimal resource investment to photosynthetic
2437 capacity, where optimal resource investment at the leaf level maximized nitrogen
2438 allocation to structures that support whole plant growth.

2439 5.4.1 *Soil nitrogen fertilization has divergent effects on leaf and whole plant
2440 acclimation responses to CO₂*

2441 Elevated CO₂ reduced N_{area} , V_{cmax25} , J_{max25} , and stomatal conductance by
2442 29%, 16%, 10%, and 20%, respectively (Table 5.2). The larger downregulation in
2443 V_{cmax25} than J_{max25} led to an 8% stimulation in $J_{\text{max25}}:V_{\text{cmax25}}$ (Table 5.2), while
2444 the larger downregulation in N_{area} than V_{cmax25} resulted in a 21% stimulation
2445 in the fraction of leaf nitrogen allocated to photosynthesis under elevated CO₂.
2446 These acclimation responses are directionally consistent with previous studies that
2447 have investigated or reviewed leaf acclimation responses to CO₂ (Drake et al.
2448 1997; Makino et al. 1997; Ainsworth et al. 2002; Ainsworth and Long 2005;
2449 Ainsworth and Rogers 2007; Smith and Dukes 2013; Smith and Keenan 2020;
2450 Poorter et al. 2022), and follow patterns expected from photosynthetic least-cost
2451 theory (Wright et al. 2003; Prentice et al. 2014; Smith et al. 2019; Smith and
2452 Keenan 2020). Together, the stimulation in $J_{\text{max25}}:V_{\text{cmax25}}$ and the fraction of leaf
2453 nitrogen allocated to photosynthesis, and nitrogen use efficiency under elevated
2454 CO₂ provide strong support for the idea that leaves were downregulating V_{cmax25}
2455 in response to elevated CO₂ in order to optimally coordinate photosynthesis such
2456 that net photosynthesis rates approached becoming equally co-limited by Rubisco

2457 carboxylation and RuBP regeneration (Chen et al. 1993; Maire et al. 2012).

2458 Increasing fertilization and inoculation induced strong positive effects on
2459 N_{area} (Fig. 1a), $V_{\text{cmax}25}$ (Fig. 5.2a), $J_{\text{max}25}$ (Fig. 5.2b). The general positive
2460 response of N_{area} to increasing fertilization and in inoculated pots was enhanced
2461 under ambient CO₂, which, paired with the general downregulation in N_{area} un-
2462 der elevated CO₂, resulted in a stronger downregulation of N_{area} under elevated
2463 CO₂ with increasing fertilization and in inoculated pots (Fig. 5.1a). These pat-
2464 terns suggest that N_{area} responses to CO₂ were at least partially dependent on
2465 soil nitrogen fertilization and nitrogen acquisition strategy. However, the general
2466 stimulation in the fraction of leaf nitrogen allocated to Rubisco, bioenergetics,
2467 or photosynthesis under elevated CO₂ was not modified across the fertilization
2468 gradient and was only marginally enhanced in inoculated pots. These patterns
2469 suggest that the increased downregulation of Narea under elevated CO₂ with in-
2470 creasing fertilization was not associated with a change in relative investment to
2471 photosynthetic tissue. Instead, a stronger downregulation in the fraction of leaf
2472 nitrogen allocated to structure under ambient CO₂ resulted in a stronger stim-
2473 ulation in $\rho_{\text{structure}}$ under elevated CO₂ with increasing fertilization (Fig. 5.3b),
2474 indicating that fertilization shifted relative investment in leaf structural tissue un-
2475 der elevated CO₂. These results, combined with a stimulation in PNUE (Fig. SX)
2476 and iWUE (Fig. SX) under elevated CO₂ that was independent of fertilization
2477 or inoculation treatment, provide additional support for the hypothesis that leaf
2478 acclimation photosynthetic responses to CO₂ were independent of fertilization;
2479 though fertilization may contribute to changes in leaf morphology under elevated
2480 CO₂ through shifts in M_{area} (Onoda et al. 2017; Wang et al. 2017; Dong et al.

2481 2022).

2482 The downregulation in N_{area} , $V_{\text{cmax}25}$, and $J_{\text{max}25}$ under elevated CO₂ cor-
2483 responded with a respective 62% and 100% stimulation in total leaf area (Fig.
2484 5.4a) and total biomass (Fig. 5.4b). The stimulation in total leaf area and total
2485 biomass under elevated CO₂ also corresponded with generally higher structural
2486 carbon costs to acquire nitrogen (Fig. 5.4c), a pattern driven by a stimulation
2487 in belowground carbon biomass and reduction in whole plant nitrogen biomass.
2488 Alone, this result suggests that elevated CO₂ reduces plant nitrogen uptake effi-
2489 ciency, which does not explain why plants grown under elevated CO₂ generally had
2490 higher biomass and total leaf area. However, a strong negative effect of increasing
2491 fertilization on structural carbon costs to acquire nitrogen, which were generally
2492 similar between CO₂ concentrations, was driven by a stronger increase in whole
2493 plant nitrogen biomass than belowground carbon biomass. Thus, increases in the
2494 positive response of whole plant growth and total leaf area under elevated CO₂
2495 with increasing fertilization were likely driven by an increase in nitrogen uptake
2496 efficiency, allowing plants to satisfy any increase in whole plant nitrogen demand
2497 associated with increased CO₂.

2498 Interestingly, these results indicate that the general stimulation in total
2499 leaf area and whole plant growth under elevated CO₂ was not modified by inoc-
2500 ulation despite an apparent general negative effect of inoculation on N_{cost} . This
2501 response could have been due to strong negative effect of increasing fertilization on
2502 nodulation (Fig. 5.5), which may have caused the strong increase in the positive
2503 effect of elevated CO₂ on whole plant growth with increasing fertilization to mask
2504 any increase in the positive effect of elevated CO₂ on whole plant growth due to

2505 inoculation. Reductions in nodulation with increasing fertilization are commonly
2506 observed patterns that have been inferred to be a response that allows species
2507 optimize nitrogen uptake efficiency as costs to acquire nitrogen via direct uptake
2508 become more similar (Fig. 5.4c) (Gibson and Harper 1985; Rastetter et al. 2001).
2509 In this study, pairwise comparisons indicated strong positive effects of inocula-
2510 tion on total leaf area and total biomass (158% increase in total leaf area, 119%
2511 increase in total biomass) under elevated CO₂ at 0 ppm N, but no observable
2512 inoculation effect on total leaf area or total biomass under elevated CO₂ at 350
2513 ppm N or 630 ppm N. While these responses did not generally differ from those
2514 observed under ambient CO₂, they do confirm the hypothesis that positive effects
2515 of inoculation on whole plant growth responses to elevated CO₂ would decrease
2516 with increasing fertilization.

2517 Combined, results reported here suggest that soil nitrogen availability has
2518 a divergent role in modifying leaf and whole plant acclimation responses to CO₂.
2519 Leaf acclimation responses were generally decoupled from fertilization, while whole
2520 plant acclimation responses relied heavily on an increase in nitrogen uptake ef-
2521 ficiency and consequent reduction in costs of acquiring nitrogen associated with
2522 increasing fertilization. However, whole plant responses to CO₂ indicated that
2523 fertilization may play a more important role in determining whole plant acclima-
2524 tion responses to CO₂ than nitrogen acquisition strategy, although these patterns
2525 were likely driven by reductions in nodulation with increasing fertilization. These
2526 results suggest that plants acclimate to CO₂ in nitrogen-limited systems by mini-
2527 mizing the number of optimally coordinated leaves, and that the downregulation
2528 in leaf nitrogen content under elevated CO₂ is not a direct response to changes in

2529 soil nitrogen availability as previously implied.

2530 5.4.2 *Implications for future model development*

2531 Many terrestrial biosphere models predict photosynthetic capacity through
2532 plant functional group-specific linear regressions between N_{area} and V_{cmax} (Rogers
2533 2014; Rogers et al. 2017), which assumes that leaf nitrogen-photosynthesis rela-
2534 tionships are constant across growing environments. Our results build on previ-
2535 ous work suggesting that leaf nitrogen-photosynthesis relationships dynamically
2536 change across growing environments (Luo et al. 2021; Dong et al. 2022). Specif-
2537 ically, results from this experiment indicate that CO_2 concentration increased
2538 the fraction of leaf nitrogen content allocated to photosynthesis, while a general
2539 negative effect of increasing fertilization on the fraction of leaf nitrogen content
2540 allocated to photosynthesis was dependent on inoculation treatment. Similar in-
2541 creases in N_{area} , $V_{\text{cmax}25}$, and $J_{\text{max}25}$ with increasing fertilization resulted in no
2542 change in the fraction of leaf nitrogen allocated to photosynthesis in uninoculated
2543 pots, while larger increases in N_{area} than $V_{\text{cmax}25}$ and $J_{\text{max}25}$ with increasing fertil-
2544 ization decreased the fraction of leaf nitrogen allocated to photosynthesis in inoc-
2545 ulated pots (Fig. 5.3a). As inoculated pots were able to access less finite supply of
2546 nitrogen across the fertilization gradient, these patterns suggest that constant leaf
2547 nitrogen-photosynthesis relationships may only apply in environments where ni-
2548 trogen is limiting and will likely change with increasing CO_2 concentrations. Thus,
2549 terrestrial biosphere models that parameterize photosynthetic capacity through
2550 linear relationships between N_{area} and V_{cmax} (Rogers 2014; Rogers et al. 2017)
2551 may be overestimating photosynthetic capacity in systems where nitrogen is not

2552 as limiting and may contribute to erroneous model simulations under future CO₂
2553 concentrations.

2554 These results also demonstrate that optimal resource investment to photo-
2555 synthetic capacity defines leaf acclimation responses to elevated CO₂, and that
2556 these responses were independent of fertilization or inoculation treatment. Cur-
2557 rent approaches for simulating photosynthetic responses to CO₂ generally invoke
2558 patterns expected from progressive nitrogen limitation, where the downregulation
2559 in N_{area} , and therefore photosynthetic capacity, due to elevated CO₂ are com-
2560 monly a function of progressive reductions in soil nitrogen availability. Results
2561 reported here contradict this formulation, suggesting that the leaf acclimation re-
2562 sponse is driven by optimal resource investment to photosynthetic capacity and
2563 is independent of soil resource supply. Optimality models that leverage prin-
2564 ciples from optimal coordination and photosynthetic least-cost theories (Wang
2565 et al. 2017; Stocker et al. 2020; Scott and Smith 2022) are capable of capturing
2566 such acclimation responses to CO₂ (Smith and Keenan 2020), suggesting that the
2567 implementation of these models may improve the simulation of photosynthetic
2568 processes in terrestrial biosphere models under increasing CO₂ concentrations.

2569 5.4.3 *Study limitations and future directions*

2570 There are two study limitations that must be addressed to contextualize
2571 patterns observed in this study. First, restricting the volume of belowground
2572 substrate via a potted experiment does not adequately replicate belowground en-
2573 vironments of natural systems, and therefore may modify effects of soil resource
2574 availability and inoculation on plant nitrogen uptake, particularly if pot size limits

2575 whole plant growth (Poorter et al. 2012). I attempted to minimize the extent of
2576 pot size limitation experienced in the first experimental chapters while account-
2577 ing for the expected stimulation in whole plant growth under elevated CO₂ by
2578 using 6-liter pots. Despite attempts to minimize growth limitation imposed by
2579 pot volume, fertilization and CO₂ treatments increased the biomass: pot volume
2580 ratio such that all treatment combinations to exceed 1 g L⁻¹ biomass: pot volume
2581 under high fertilization. The 1 g L⁻¹ biomass: pot volume recommendation from
2582 Poorter et al. (2012) was designated to avoid growth limitation imposed by pot
2583 volume. However, if pot size limitation indeed limited whole plant growth, then
2584 structural carbon costs to acquire nitrogen, belowground carbon biomass, whole
2585 plant nitrogen biomass, and whole plant biomass should each exhibit strong sat-
2586 uration points with increasing fertilization, which was not observed here. Addi-
2587 tionally, a second set of photosynthetic measurements from one week prior to the
2588 harvest (6 weeks post-germination) revealed ... As pot limitation is expected
2589 to decrease net photosynthesis, and focal leaves were of similar ages between the
2590 sixth and seventh week, one might expect growth limitation induced by constricted
2591 pot volume to result in a dampened effect of inoculation and fertilization on net
2592 photosynthesis, V_{cmax} , and J_{max25} . Analyses from the sixth week of development
2593 revealed ... Additionally, analyses revealed a stronger/weaker downregulation in
2594 V_{cmax25} and J_{max25} on week 7, though disentangling the causality of this response
2595 (i.e. whether due to pot size limitation or simply a stronger acclimation response)
2596 would be difficult.

2597 Second, this study evaluated leaf and whole plant responses to CO₂ in 7-
2598 week seedlings. Given the long-term scale of the progressive nitrogen limitation

2599 hypothesis, patterns observed here should be validated in longer-term nitrogen
2600 manipulation experiments. Previous work in free air CO₂ enrichment experiments
2601 show some support for patterns expected from the progressive nitrogen limitation
2602 hypothesis (Reich et al. 2006; Norby et al. 2010), although results are not consis-
2603 tent across experimental sites (Finzi et al. 2006; Moore et al. 2006; Liang et al.
2604 2016). We found some support for patterns expected by the progressive nitrogen
2605 limitation hypothesis, namely an increase in plant nitrogen uptake under elevated
2606 CO₂ (Luo et al. 2004), though leaf acclimation responses to CO₂ were strongly
2607 indicative of optimal resource investment to photosynthetic capacity as expected
2608 from photosynthetic least-cost theory (Prentice et al. 2014; Smith et al. 2019;
2609 Smith and Keenan 2020).

2610 5.4.4 *Conclusions*

2611 This study provides strong evidence suggesting that leaf acclimation re-
2612 sponds to elevated CO₂ did not vary with soil nitrogen fertilization or ability
2613 to acquire nitrogen through symbiotic nitrogen fixation. However, whole plant
2614 acclimation responses to CO₂ were dependent on fertilization, where increasing
2615 fertilization increased the positive effect of whole plant growth under elevated
2616 CO₂. Results also indicate that fertilization played a relatively more important
2617 role in modifying whole plant responses to CO₂, perhaps due to a reduction in
2618 nodulation across the fertilization gradient. These patterns strongly support the
2619 hypothesis that leaf and whole plant acclimation responses are driven by opti-
2620 mal resource investment to photosynthetic capacity, and that leaf acclimation
2621 responses to CO₂ were not modified by changes in soil nitrogen availability. Ad-

2622 ditionally, strong interactions between fertilization and inoculation on leaf and
2623 whole plant traits indicated positive effects of fertilization on leaf and whole plant
2624 traits in uninoculated pots, but null effects of fertilization on leaf and whole plant
2625 traits in inoculated pots. These results build on previous work suggesting that
2626 constant leaf nitrogen-photosynthesis relationships are dynamic and change across
2627 growing environments, calling the use of constant relationships by terrestrial bio-
2628 sphere models into question.

2629

Chapter 6

2630

Conclusions

2631 Experiments included in this dissertation leverage patterns expected from
2632 photosynthetic least-cost theory to investigate effects of soil resource availability
2633 and aboveground climate on costs of nitrogen acquisition, leaf nitrogen-water use
2634 tradeoffs, and plant acclimation responses to elevated CO₂. Photosynthetic least-
2635 cost theory provides a contemporary framework for understanding impacts of
2636 climatic and edaphic characteristics on plant ecophysiological processes, namely
2637 leaf nitrogen allocation and photosynthetic capacity. When I began planning
2638 experiments for this dissertation in August 2018,, empirical tests of the theory
2639 were sparse and model development was just beginning with a goal of eventually
2640 implementing the theory in terrestrial biosphere models. At the time, it was
2641 critical that experimentation be done to test underlying assumptions of the theory
2642 and validate its suitability for implementing in terrestrial biosphere models.

2643 Early iterations of model development held the unit cost of acquiring ni-
2644 trogen relative to water constant (Wang et al. 2017), in part because limited data
2645 existed to evaluate how this parameter changes across spatiotemporal scales and
2646 different environmental gradients. However, the Fixation and Uptake of Nitrogen
2647 model (Fisher et al. 2010; Brzostek et al. 2014) indicates that costs of nitro-
2648 gen acquisition decreased with increasing soil nitrogen availability and varies in
2649 species with different nitrogen acquisition strategies, suggesting that the unit cost
2650 of acquiring nitrogen relative to water should change across nitrogen availability
2651 gradients. Additionally,

2652 All experimental chapters in this dissertation provide strong and consist-
2653 ent support for patterns expected from the theory across different experimental
2654 approaches, spatiotemporal scales, and different plant functional groups. In this
2655 chapter, I first summarize experimental approaches and primary findings of each
2656 experimental chapter. Then, I use findings from the four experimental chapters
2657 to synthesize recommendations for future photosynthetic least-cost theory model
2658 development, and propose experiments that will allow for further understanding
2659 of mechanisms that drive patterns expected from photosynthetic least-cost theory
2660 across environmental gradients.

2661

References

- 2662** Abrams, M. D. and S. A. Mostoller (1995). Gas exchange, leaf structure and
2663 nitrogen in contrasting successional tree species growing in open and under-
2664 story sites during a drought. *Tree Physiology* 15(6), 361–370.
- 2665** Adams, M. A., T. L. Turnbull, J. I. Sprent, and N. Buchmann (2016). Legumes
2666 are different: Leaf nitrogen, photosynthesis, and water use efficiency. *Pro-
2667 ceedings of the National Academy of Sciences of the United States of Amer-
2668 ica* 113(15), 4098–4103.
- 2669** Ainsworth, E. A., P. A. Davey, C. J. Bernacchi, O. C. Dermody, E. A. Heaton,
2670 D. J. Moore, P. B. Morgan, S. L. Naidu, H. S. Y. Ra, X. G. Zhu, P. S. Curtis,
2671 and S. P. Long (2002). A meta-analysis of elevated [CO₂] effects on soybean
2672 (*Glycine max*) physiology, growth and yield. *Global Change Biology* 8(8),
2673 695–709.
- 2674** Ainsworth, E. A. and S. P. Long (2005). What have we learned from 15 years of
2675 free-air CO₂ enrichment (FACE)? A meta-analytic review of the responses
2676 of photosynthesis, canopy properties and plant production to rising CO₂.
2677 *New Phytologist* 165(2), 351–372.
- 2678** Ainsworth, E. A. and A. Rogers (2007). The response of photosynthesis and
2679 stomatal conductance to rising [CO₂]: mechanisms and environmental in-
2680 teractions. *Plant, Cell and Environment* 30(3), 258–270.
- 2681** Allen, K., J. B. Fisher, R. P. Phillips, J. S. Powers, and E. R. Brzostek (2020).
2682 Modeling the carbon cost of plant nitrogen and phosphorus uptake across
2683 temperate and tropical forests. *Frontiers in Forests and Global Change* 3,

- 2684** 1–12.
- 2685** Allison, S. D., C. I. Czimczik, and K. K. Treseder (2008). Microbial activity
- 2686** and soil respiration under nitrogen addition in Alaskan boreal forest. *Global*
- 2687** *Change Biology* 14(5), 1156–1168.
- 2688** Andersen, M. K., H. Hauggaard-Nielsen, P. Ambus, and E. S. Jensen (2005).
- 2689** Biomass production, symbiotic nitrogen fixation and inorganic N use in dual
- 2690** and tri-component annual intercrops. *Plant and Soil* 266(1-2), 273–287.
- 2691** Andrews, M., E. K. James, J. I. Sprent, R. M. Boddey, E. Gross, and F. B. dos
- 2692** Reis (2011). Nitrogen fixation in legumes and actinorhizal plants in natural
- 2693** ecosystems: Values obtained using ^{15}N natural abundance. *Plant Ecology*
- 2694** and *Diversity* 4(2-3), 117–130.
- 2695** Arndal, M. F., A. Tolver, K. S. Larsen, C. Beier, and I. K. Schmidt (2018). Fine
- 2696** root growth and vertical distribution in response to elevated CO₂, warming
- 2697** and drought in a mixed heathland–grassland. *Ecosystems* 21(1), 15–30.
- 2698** Arnone, J. A. (1997). Indices of plant N availability in an alpine grassland under
- 2699** elevated atmospheric CO₂. *Plant and Soil* 190(1), 61–66.
- 2700** Arora, V. K., A. Katavouta, R. G. Williams, C. D. Jones, V. Brovkin,
- 2701** P. Friedlingstein, J. Schwinger, L. Bopp, O. Boucher, P. Cadule, M. A.
- 2702** Chamberlain, J. R. Christian, C. Delire, R. A. Fisher, T. Hajima, T. Ilyina,
- 2703** E. Joetzjer, M. Kawamiya, C. D. Koven, J. P. Krasting, R. M. Law, D. M.
- 2704** Lawrence, A. Lenton, K. Lindsay, J. Pongratz, T. Raddatz, R. Séférian,
- 2705** K. Tachiiri, J. F. Tjiputra, A. Wiltshire, T. Wu, and T. Ziehn (2020).
- 2706** Carbon-concentration and carbon-climate feedbacks in CMIP6 models and
- 2707** their comparison to CMIP5 models. *Biogeosciences* 17(16), 4173–4222.

- 2708 Bae, K., T. J. Fahey, R. D. Yanai, and M. Fisk (2015). Soil nitrogen availability affects belowground carbon allocation and soil respiration in northern
2709 hardwood forests of New Hampshire. *Ecosystems* 18(7), 1179–1191.
- 2710
- 2711 Barber, S. A. (1962). A diffusion and mass-flow concept of soil nutrient availability. *Soil Science* 93(1), 39–49.
- 2712
- 2713 Barnes, J. D., L. Balaguer, E. Manrique, S. Elvira, and A. W. Davison (1992).
2714 A reappraisal of the use of DMSO for the extraction and determination
2715 of chlorophylls a and b in lichens and higher plants. *Environmental and
2716 Experimental Botany* 32(2), 85–100.
- 2717 Bates, D., M. Mächler, B. Bolker, and S. Walker (2015). Fitting linear mixed-
2718 effects models using lme4. *Journal of Statistical Software* 67(1), 1–48.
- 2719 Beaudette, D., J. Skovlin, S. Roeker, and A. Brown (2022). soilDB: Soil
2720 Database Interface.
- 2721 Bengtson, P., J. Barker, and S. J. Grayston (2012). Evidence of a strong cou-
2722 pling between root exudation, C and N availability, and stimulated SOM
2723 decomposition caused by rhizosphere priming effects. *Ecology and Evolu-
2724 tion* 2(8), 1843–1852.
- 2725 Bernacchi, C. J., E. L. Singsaas, C. Pimentel, A. R. Portis, and S. P. Long
2726 (2001). Improved temperature response functions for models of Rubisco-
2727 limited photosynthesis. *Plant, Cell and Environment* 24(2), 253–259.
- 2728 Bialic-Murphy, L., N. G. Smith, P. Voothuluru, R. M. McElderry, M. D.
2729 Roche, S. T. Cassidy, S. N. Kivlin, and S. Kalisz (2021). Invasion-induced
2730 root–fungal disruptions alter plant water and nitrogen economies. *Ecology*

- 2731** *Letters* 24(6), 1145–1156.
- 2732** Bloom, A. J., F. S. Chapin, and H. A. Mooney (1985). Resource limitation
2733 in plants - an economic analogy. *Annual Review of Ecology and Systemat-*
2734 *ics* 16(1), 363–392.
- 2735** Bloomfield, K. J., B. D. Stocker, T. F. Keenan, and I. C. Prentice (2023).
2736 Environmental controls on the light use efficiency of terrestrial gross primary
2737 production. *Global Change Biology* 29(4), 0–2.
- 2738** Bonan, G. B., M. D. Hartman, W. J. Parton, and W. R. Wieder (2013). Eval-
2739 uating litter decomposition in earth system models with long-term litter
2740 bag experiments: an example using the Community Land Model version 4
2741 (CLM4). *Global Change Biology* 19(3), 957–974.
- 2742** Bonan, G. B., P. J. Lawrence, K. W. Oleson, S. Levis, M. Jung, M. Reich-
2743 stein, D. M. Lawrence, and S. C. Swenson (2011). Improving canopy pro-
2744 cesses in the Community Land Model version 4 (CLM4) using global flux
2745 fields empirically inferred from FLUXNET data. *Journal of Geophysical Re-*
2746 *search* 116(G2), G02014.
- 2747** Booth, B. B. B., C. D. Jones, M. Collins, I. J. Totterdell, P. M. Cox, S. Sitch,
2748 C. Huntingford, R. A. Betts, G. R. Harris, and J. Lloyd (2012). High sen-
2749 sitivity of future global warming to land carbon cycle processes. *Environ-*
2750 *mental Research Letters* 7(2), 024002.
- 2751** Borer, E. T., W. S. Harpole, P. B. Adler, E. M. Lind, J. L. Orrock, E. W.
2752 Seabloom, and M. D. Smith (2014). Finding generality in ecology: A model
2753 for globally distributed experiments. *Methods in Ecology and Evolution* 5(1),
2754 65–73.

- 2755** Braghieri, R. K., J. B. Fisher, K. Allen, E. Brzostek, M. Shi, X. Yang, D. M.
- 2756** Ricciuto, R. A. Fisher, Q. Zhu, and R. P. Phillips (2022). Modeling global
- 2757** carbon costs of plant nitrogen and phosphorus acquisition. *Journal of Ad-*
- 2758** *vances in Modeling Earth Systems* 14(8), 1–23.
- 2759** Brix, H. (1971). Effects of nitrogen fertilization on photosynthesis and respi-
- 2760** ration in Douglas-fir. *Forest Science* 17(4), 407–414.
- 2761** Brzostek, E. R., J. B. Fisher, and R. P. Phillips (2014). Modeling the carbon
- 2762** cost of plant nitrogen acquisition: Mycorrhizal trade-offs and multipath
- 2763** resistance uptake improve predictions of retranslocation. *Journal of Geo-*
- 2764** *physical Research: Biogeosciences* 119, 1684–1697.
- 2765** Bubier, J. L., R. Smith, S. Juutinen, T. R. Moore, R. Minocha, S. Long, and
- 2766** S. Minocha (2011). Effects of nutrient addition on leaf chemistry, morphol-
- 2767** ogy, and photosynthetic capacity of three bog shrubs. *Oecologia* 167(2),
- 2768** 355–368.
- 2769** Cernusak, L. A., N. Ubierna, K. Winter, J. A. M. Holtum, J. D. Marshall, and
- 2770** G. D. Farquhar (2013). Environmental and physiological determinants of
- 2771** carbon isotope discrimination in terrestrial plants. *New Phytologist* 200(4),
- 2772** 950–965.
- 2773** Chen, J.-L., J. F. Reynolds, P. C. Harley, and J. D. Tenhunen (1993). Coor-
- 2774** dination theory of leaf nitrogen distribution in a canopy. *Oecologia* 93(1),
- 2775** 63–69.
- 2776** Clark, D. B., L. M. Mercado, S. Sitch, C. D. Jones, N. Gedney, M. J. Best,
- 2777** M. Pryor, G. G. Rooney, R. L. H. Essery, E. Blyth, O. Boucher, R. J.
- 2778** Harding, C. Huntingford, and P. M. Cox (2011). The Joint UK Land Envi-

- 2779 ronment Simulator (JULES), model description. Part 2: Carbon fluxes and
2780 vegetation dynamics. *Geoscientific Model Development* 4(3), 701–722.
- 2781 Cornwell, W. K., J. H. C. Cornelissen, K. Amatangelo, E. Dorrepaal, V. T.
2782 Eviner, O. Godoy, S. E. Hobbie, B. Hoorens, H. Kurokawa, N. Pérez-
2783 Harguindeguy, H. M. Quested, L. S. Santiago, D. A. Wardle, I. J. Wright,
2784 R. Aerts, S. D. Allison, P. van Bodegom, V. Brovkin, A. Chatain, T. V.
2785 Callaghan, S. Díaz, E. Garnier, D. E. Gurvich, E. Kazakou, J. A. Klein,
2786 J. Read, P. B. Reich, N. A. Soudzilovskaia, M. V. Vaieretti, and M. Westoby
2787 (2008). Plant species traits are the predominant control on litter decompo-
2788 sition rates within biomes worldwide. *Ecology Letters* 11(10), 1065–1071.
- 2789 Cornwell, W. K., I. J. Wright, J. Turner, V. Maire, M. M. Barbour, L. A.
2790 Cernusak, T. E. Dawson, D. S. Ellsworth, G. D. Farquhar, H. Griffiths,
2791 C. Keitel, A. Knohl, P. B. Reich, D. G. Williams, R. Bhaskar, J. H. C. Cor-
2792 nelissen, A. Richards, S. Schmidt, F. Valladares, C. Körner, E.-D. Schulze,
2793 N. Buchmann, and L. S. Santiago (2018). Climate and soils together regulate
2794 photosynthetic carbon isotope discrimination within C₃ plants worldwide.
2795 *Global Ecology and Biogeography* 27(9), 1056–1067.
- 2796 Cramer, W. and I. C. Prentice (1988). Simulation of regional soil moisture
2797 deficits on a European scale. *Norsk Geografisk Tidsskrift - Norwegian Jour-*
2798 *nal of Geography* 42(2-3), 149–151.
- 2799 Curtis, P. S. (1996). A meta-analysis of leaf gas exchange and nitrogen in trees
2800 grown under elevated carbon dioxide. *Plant, Cell and Environment* 19(2),
2801 127–137.
- 2802 Daly, C., M. Halbleib, J. I. Smith, W. P. Gibson, M. K. Doggett, G. H. Taylor,

- 2803** J. Curtis, and P. P. Pasteris (2008). Physiographically sensitive mapping
2804 of climatological temperature and precipitation across the conterminous
2805 United States. *International Journal of Climatology* 28(15), 2031–2064.
- 2806** Davies-Barnard, T., J. Meyerholt, S. Zaehle, P. Friedlingstein, V. Brovkin,
2807 Y. Fan, R. A. Fisher, C. D. Jones, H. Lee, D. Peano, B. Smith, D. Wårlind,
2808 and A. J. Wiltshire (2020). Nitrogen cycling in CMIP6 land surface models:
2809 progress and limitations. *Biogeosciences* 17(20), 5129–5148.
- 2810** Davis, T. W., I. C. Prentice, B. D. Stocker, R. T. Thomas, R. J. Whitley,
2811 H. Wang, B. J. Evans, A. V. Gallego-Sala, M. T. Sykes, and W. Cramer
2812 (2017). Simple process-led algorithms for simulating habitats (SPLASH
2813 v.1.0): robust indices of radiation, evapotranspiration and plant-available
2814 moisture. *Geoscientific Model Development* 10, 689–708.
- 2815** Delaire, M., E. Frak, M. Sigogne, B. Adam, F. Beaujard, and X. Le Roux
2816 (2005). Sudden increase in atmospheric CO₂ concentration reveals strong
2817 coupling between shoot carbon uptake and root nutrient uptake in young
2818 walnut trees. *Tree Physiology* 25(2), 229–235.
- 2819** Doane, T. A. and W. R. Horwáth (2003). Spectrophotometric determination of
2820 nitrate with a single reagent. *Analytical Letters* 36(12), 2713–2722.
- 2821** Dong, N., I. C. Prentice, B. J. Evans, S. Caddy-Retalic, A. J. Lowe, and I. J.
2822 Wright (2017). Leaf nitrogen from first principles: field evidence for adaptive
2823 variation with climate. *Biogeosciences* 14(2), 481–495.
- 2824** Dong, N., I. C. Prentice, I. J. Wright, B. J. Evans, H. F. Togashi, S. Caddy-
2825 Retalic, F. A. McInerney, B. Sparrow, E. Leitch, and A. J. Lowe (2020).
2826 Components of leaf-trait variation along environmental gradients. *New Phy-*

- 2827** *tologist* 228(1), 82–94.
- 2828** Dong, N., I. C. Prentice, I. J. Wright, H. Wang, O. K. Atkin, K. J. Bloomfield,
- 2829** T. F. Domingues, S. M. Gleason, V. Maire, Y. Onoda, H. Poorter, and N. G.
- 2830** Smith (2022). Leaf nitrogen from the perspective of optimal plant function.
- 2831** *Journal of Ecology* 110(11), 2585–2602.
- 2832** Dong, N., I. J. Wright, J. M. Chen, X. Luo, H. Wang, T. F. Keenan, N. G.
- 2833** Smith, and I. C. Prentice (2022). Rising CO₂ and warming reduce global
- 2834** canopy demand for nitrogen. *New Phytologist* 235(5), 1692–1700.
- 2835** Dovrat, G., H. Bakhshian, T. Masci, and E. Sheffer (2020). The nitrogen eco-
- 2836** nomic spectrum of legume stoichiometry and fixation strategy. *New Phytol-*
- 2837** *ogist* 227(2), 365–375.
- 2838** Dovrat, G., T. Masci, H. Bakhshian, E. Mayzlish Gati, S. Golan, and E. Shef-
- 2839** fer (2018). Drought-adapted plants dramatically downregulate dinitrogen
- 2840** fixation: Evidences from Mediterranean legume shrubs. *Journal of Ecol-*
- 2841** *ogy* 106(4), 1534–1544.
- 2842** Drake, B. G., M. A. Gonzàlez-Meler, and S. P. Long (1997). More efficient
- 2843** plants: a consequence of rising atmospheric CO₂? *Annual Review of Plant*
- 2844** *Biology* 48, 609–639.
- 2845** Duursma, R. A. (2015). Plantecophys - An R Package for Analyzing and Mod-
- 2846** elling Leaf Gas Exchange Data. *PLOS ONE* 10(11), e0143346.
- 2847** Eastman, B. A., M. B. Adams, E. R. Brzostek, M. B. Burnham, J. E. Carrara,
- 2848** C. Kelly, B. E. McNeil, C. A. Walter, and W. T. Peterjohn (2021). Altered
- 2849** plant carbon partitioning enhanced forest ecosystem carbon storage after 25

- 2850 years of nitrogen additions. *New Phytologist* 230(4), 1435–1448.
- 2851 Ellsworth, D. S. and P. B. Reich (1996). Photosynthesis and leaf nitrogen in five
- 2852 Amazonian tree species during early secondary succession. *Ecology* 77(2),
- 2853 581–594.
- 2854 Espelta, J. M., P. Cortés, M. Mangirón, and J. Retana (2005). Differences in
- 2855 biomass partitioning, leaf nitrogen content, and water use efficiency d13C
- 2856 result in similar performance of seedlings of two Mediterranean oaks with
- 2857 contrasting leaf habit. *Ecoscience* 12(4), 447–454.
- 2858 Evans, J. R. (1989). Photosynthesis and nitrogen relationships in leaves of C₃
- 2859 plants. *Oecologia* 78(1), 9–19.
- 2860 Evans, J. R. and V. C. Clarke (2019). The nitrogen cost of photosynthesis.
- 2861 *Journal of Experimental Botany* 70(1), 7–15.
- 2862 Evans, J. R. and H. Poorter (2001). Photosynthetic acclimation of plants to
- 2863 growth irradiance: the relative importance of specific leaf area and nitrogen
- 2864 partitioning in maximizing carbon gain. *Plant, Cell and Environment* 24(8),
- 2865 755–767.
- 2866 Evans, J. R. and J. R. Seemann (1989). The allocation of protein nitrogen in
- 2867 the photosynthetic apparatus: costs, consequences, and control. *Photosyn-*
- 2868 *thesis* 8, 183–205.
- 2869 Exbrayat, J.-F., A. A. Bloom, P. Falloon, A. Ito, T. L. Smallman, and
- 2870 M. Williams (2018). Reliability ensemble averaging of 21st century projec-
- 2871 tions of terrestrial net primary productivity reduces global and regional
- 2872 uncertainties. *Earth System Dynamics* 9(1), 153–165.

- 2873** Farquhar, G. D., J. R. Ehleringer, and K. T. Hubick (1989). Carbon Isotope
2874 Discrimination and Photosynthesis. *Annual Review of Plant Physiology and*
2875 *Plant Molecular Biology* 40(1), 503–537.
- 2876** Farquhar, G. D. and T. D. Sharkey (1982). Stomatal conductance and photo-
2877 synthesis. *Annual Review of Plant Physiology* 33(1), 317–345.
- 2878** Farquhar, G. D., S. von Caemmerer, and J. A. Berry (1980). A biochemical
2879 model of photosynthetic CO₂ assimilation in leaves of C₃ species.
2880 *Planta* 149(1), 78–90.
- 2881** Fay, P. A., S. M. Prober, W. S. Harpole, J. M. H. Knops, J. D. Bakker, E. T.
2882 Borer, E. M. Lind, A. S. MacDougall, E. W. Seabloom, P. D. Wragg, P. B.
2883 Adler, D. M. Blumenthal, Y. M. Buckley, C. Chu, E. E. Cleland, S. L.
2884 Collins, K. F. Davies, G. Du, X. Feng, J. Firn, D. S. Gruner, N. Hagenah,
2885 Y. Hautier, R. W. Heckman, V. L. Jin, K. P. Kirkman, J. A. Klein, L. M.
2886 Ladwig, Q. Li, R. L. McCulley, B. A. Melbourne, C. E. Mitchell, J. L. Moore,
2887 J. W. Morgan, A. C. Risch, M. Schütz, C. J. Stevens, D. A. Wedin, and
2888 L. H. Yang (2015). Grassland productivity limited by multiple nutrients.
2889 *Nature Plants* 1(7), 15080.
- 2890** Feng, X. (1999). Trends in intrinsic water-use efficiency of natural trees for the
2891 past 100-200 years: A response to atmospheric CO₂ concentration. *Geochim-
2892* *ica et Cosmochimica Acta* 63(13-14), 1891–1903.
- 2893** Field, C. B. and H. A. Mooney (1986). The photosynthesis-nitrogen relationship
2894 in wild plants. In T. J. Givnish (Ed.), *On the Economy of Plant Form and*
2895 *Function*, pp. 25–55. Cambridge: Cambridge University Press.
- 2896** Finzi, A. C., D. J. P. Moore, E. H. DeLucia, J. Lichter, K. S. Hofmockel, R. B.

- 2897 Jackson, H. S. Kim, R. Matamala, H. R. McCarthy, R. Oren, J. S. Pippen,
2898 and W. H. Schlesinger (2006). Progressive nitrogen limitation of ecosystem
2899 processes under elevated CO₂ in a warm-temperate forest. *Ecology* 87(1),
2900 15–25.
- 2901 Firn, J., J. M. McGree, E. Harvey, H. Flores Moreno, M. Schutz, Y. M. Buckley,
2902 E. T. Borer, E. W. Seabloom, K. J. La Pierre, A. M. MacDougall, S. M.
2903 Prober, C. J. Stevens, L. L. Sullivan, E. Porter, E. Ladouceur, C. Allen,
2904 K. H. Moromizato, J. W. Morgan, W. S. Harpole, Y. Hautier, N. Eisen-
2905 hauer, J. P. Wright, P. B. Adler, C. A. Arnillas, J. D. Bakker, L. Biederman,
2906 A. A. D. Broadbent, C. S. Brown, M. N. Bugalho, M. C. Caldeira, E. E. Cle-
2907 land, A. Ebeling, P. A. Fay, N. Hagenah, A. R. Kleinhesselink, R. Mitchell,
2908 J. L. Moore, C. Nogueira, P. L. Peri, C. Roscher, M. D. Smith, P. D. Wragg,
2909 and A. C. Risch (2019). Leaf nutrients, not specific leaf area, are consistent
2910 indicators of elevated nutrient inputs. *Nature Ecology and Evolution* 3(3),
2911 400–406.
- 2912 Fisher, J. B., S. Sitch, Y. Malhi, R. A. Fisher, C. Huntingford, and S.-Y. Tan
2913 (2010). Carbon cost of plant nitrogen acquisition: A mechanistic, globally
2914 applicable model of plant nitrogen uptake, retranslocation, and fixation.
2915 *Global Biogeochemical Cycles* 24(1), 1–17.
- 2916 Fox, J. and S. Weisberg (2019). *An R companion to applied regression* (Third
2917 edit ed.). Thousand Oaks, California: Sage.
- 2918 Franklin, O., R. E. McMurtrie, C. M. Iversen, K. Y. Crous, A. C. Finzi, D. Tis-
2919 sue, D. S. Ellsworth, R. Oren, and R. J. Norby (2009). Forest fine-root
2920 production and nitrogen use under elevated CO₂: contrasting responses

- 2921** in evergreen and deciduous trees explained by a common principle. *Global
2922 Change Biology* 15(1), 132–144.
- 2923** Friedlingstein, P., M. Meinshausen, V. K. Arora, C. D. Jones, A. Anav, S. K.
2924 Liddicoat, and R. Knutti (2014). Uncertainties in CMIP5 climate projections
2925 due to carbon cycle feedbacks. *Journal of Climate* 27(2), 511–526.
- 2926** Friel, C. A. and M. L. Friesen (2019). Legumes modulate allocation to rhizobial
2927 nitrogen fixation in response to factorial light and nitrogen manipulation.
2928 *Frontiers in Plant Science* 10, 1316.
- 2929** Fujikake, H., A. Yamazaki, N. Ohtake, K. Sueoshi, S. Matsuhashi, T. Ito,
2930 C. Mizuniwa, T. Kume, S. Hoshimoto, N.-S. Ishioka, S. Watanabe, A. Osa,
2931 T. Sekine, H. Uchida, A. Tsuji, and T. Ohyama (2003). Quick and reversible
2932 inhibition of soybean root nodule growth by nitrate involves a decrease in
2933 sucrose supply to nodules. *Journal of Experimental Botany* 54(386), 1379–
2934 1388.
- 2935** Ghannoum, O., J. R. Evans, and S. von Caemmerer (2011). Nitrogen and water
2936 use efficiency of C₄ plants. In A. S. Raghavendra and R. F. Sage (Eds.), *C₄
2937 Photosynthesis and Related CO₂ Concentrating Mechanisms*, Chapter 8, pp.
2938 129–146. Springer.
- 2939** Ghimire, B., W. J. Riley, C. D. Koven, J. Kattge, A. Rogers, P. B. Reich, and
2940 I. J. Wright (2017). A global trait-based approach to estimate leaf nitrogen
2941 functional allocation from observations:. *Ecological Applications* 27(5),
2942 1421–1434.
- 2943** Giardina, C. P., M. D. Coleman, J. E. Hancock, J. S. King, E. A. Lilleskov,
2944 W. M. Loya, K. S. Pregitzer, M. G. Ryan, and C. C. Trettin (2005). The

- 2945 response of belowground carbon allocation in forests to global change. In
2946 D. Binkley and O. Manyailo (Eds.), *Tree Species Effects on Soils: Implica-*
2947 *tions for Global Change* (Volume 55 ed.), Chapter Chapter 7, pp. 119–154.
2948 Berlin/Heidelberg: Springer-Verlag.
- 2949 Gibson, A. H. and J. E. Harper (1985). Nitrate effect on nodulation of soybean
2950 by *Bradyrhizobium japonicum*. *Crop Science* 25(3), 497–501.
- 2951 Gill, A. L. and A. C. Finzi (2016). Belowground carbon flux links biogeochemical
2952 cycles and resource-use efficiency at the global scale. *Ecology Letters* 19(12),
2953 1419–1428.
- 2954 Goll, D. S., V. Brovkin, B. R. Parida, C. H. Reick, J. Kattge, P. B. Reich, P. M.
2955 van Bodegom, and Ü. Niinemets (2012). Nutrient limitation reduces land
2956 carbon uptake in simulations with a model of combined carbon, nitrogen
2957 and phosphorus cycling. *Biogeosciences Discussions* 9(3), 3173–3232.
- 2958 Gregory, L. M., A. M. McClain, D. M. Kramer, J. D. Pardo, K. E. Smith, O. L.
2959 Tessmer, B. J. Walker, L. G. Ziccardi, and T. D. Sharkey (2021, oct). The
2960 triose phosphate utilization limitation of photosynthetic rate: Out of global
2961 models but important for leaf models. *Plant, Cell and Environment* 44(10),
2962 3223–3226.
- 2963 Grossiord, C., T. N. Buckley, L. A. Cernusak, K. A. Novick, B. Poulter, R. T. W.
2964 Siegwolf, J. S. Sperry, and N. G. McDowell (2020). Plant responses to rising
2965 vapor pressure deficit. *New Phytologist* 226(6), 1550–1566.
- 2966 Guerrieri, R., M. Mencuccini, L. J. Sheppard, M. Saurer, M. P. Perks, P. Levy,
2967 M. A. Sutton, M. Borghetti, and J. Grace (2011). The legacy of enhanced
2968 N and S deposition as revealed by the combined analysis of $\delta^{13}\text{C}$, $\delta^{18}\text{O}$ and

- 2969** $\delta^{15}\text{N}$ in tree rings. *Global Change Biology* 17(5), 1946–1962.
- 2970** Gulmon, S. L. and C. C. Chu (1981). The effects of light and nitrogen on photo-
- 2971** synthesis, leaf characteristics, and dry matter allocation in the chaparral
- 2972** shrub, *<i>Diplacus aurantiacus</i>*. *Oecologia* 49(2), 207–212.
- 2973** Gutschick, V. P. (1981). Evolved strategies in nitrogen acquisition by plants.
- 2974** *The American Naturalist* 118(5), 607–637.
- 2975** Hallik, L., Ü. Niinemets, and I. J. Wright (2009). Are species shade and drought
- 2976** tolerance reflected in leaf-level structural and functional differentiation in
- 2977** Northern Hemisphere temperate woody flora? *New Phytologist* 184(1), 257–
- 2978** 274.
- 2979** Harrison, M. T., E. J. Edwards, G. D. Farquhar, A. B. Nicotra, and J. R.
- 2980** Evans (2009). Nitrogen in cell walls of sclerophyllous leaves accounts for
- 2981** little of the variation in photosynthetic nitrogen-use efficiency. *Plant, Cell*
- 2982** and *Environment* 32(3), 259–270.
- 2983** Harrison, S. P., W. Cramer, O. Franklin, I. C. Prentice, H. Wang,
- 2984** Å. Brännström, H. de Boer, U. Dieckmann, J. Joshi, T. F. Keenan,
- 2985** A. Lavergne, S. Manzoni, G. Mengoli, C. Morfopoulos, J. Peñuelas,
- 2986** S. Pietsch, K. T. Rebel, Y. Ryu, N. G. Smith, B. D. Stocker, and I. J.
- 2987** Wright (2021). Eco-evolutionary optimality as a means to improve vegeta-
- 2988** tion and land-surface models. *New Phytologist* 231(6), 2125–2141.
- 2989** Henneron, L., P. Kardol, D. A. Wardle, C. Cros, and S. Fontaine (2020). Rhizo-
- 2990** sphere control of soil nitrogen cycling: a key component of plant economic
- 2991** strategies. *New Phytologist* 228(4), 1269–1282.

- 2992** Hijmans, R. J. (2022). terra: Spatial Data Analysis.
- 2993** Hikosaka, K. and A. Shigeno (2009). The role of Rubisco and cell walls in the
- 2994** interspecific variation in photosynthetic capacity. *Oecologia* 160(3), 443–
- 2995** 451.
- 2996** Hoagland, D. R. and D. I. Arnon (1950). The water culture method for growing
- 2997** plants without soil. *California Agricultural Experiment Station: 347* 347(2),
- 2998** 1–32.
- 2999** Hobbie, E. A. (2006). Carbon allocation to ectomycorrhizal fungi correlates
- 3000** with belowground allocation in culture studies. *Ecology* 87(3), 563–569.
- 3001** Hobbie, E. A. and J. E. Hobbie (2008). Natural abundance of ^{15}N in nitrogen-
- 3002** limited forests and tundra can estimate nitrogen cycling through mycorrhizal
- 3003** fungi: a review. *Ecosystems* 11(5), 815–830.
- 3004** Hoek, T. A., K. Axelrod, T. Biancalani, E. A. Yurtsev, J. Liu, and J. Gore
- 3005** (2016). Resource availability modulates the cooperative and competitive na-
- 3006** nature of a microbial cross-feeding mutualism. *PLOS Biology* 14(8), e1002540.
- 3007** Höglberg, M. N., M. J. I. Briones, S. G. Keel, D. B. Metcalfe, C. Campbell, A. J.
- 3008** Midwood, B. Thornton, V. Hurry, S. Linder, T. Näsholm, and P. Höglberg
- 3009** (2010). Quantification of effects of season and nitrogen supply on tree below-
- 3010** ground carbon transfer to ectomycorrhizal fungi and other soil organisms in
- 3011** a boreal pine forest. *New Phytologist* 187(2), 485–493.
- 3012** Höglberg, P., M. N. Höglberg, S. G. Göttlicher, N. R. Betson, S. G. Keel, D. B.
- 3013** Metcalfe, C. Campbell, A. Schindlbacher, V. Hurry, T. Lundmark, S. Linder,
- 3014** and T. Näsholm (2008). High temporal resolution tracing of photosynthate

- 3015 carbon from the tree canopy to forest soil microorganisms. *New Phytologist* 177(1), 220–228.
- 3016
- 3017 Houlton, B. Z., Y.-P. Wang, P. M. Vitousek, and C. B. Field (2008). A uni-
3018 fying framework for dinitrogen fixation in the terrestrial biosphere. *Nature* 454(7202), 327–330.
- 3019
- 3020 Huber, M. L., R. A. Perkins, A. Laesecke, D. G. Friend, J. V. Sengers, M. J.
3021 Assael, I. N. Metaxa, E. Vogel, R. Mareš, and K. Miyagawa (2009). New
3022 international formulation for the viscosity of H₂O. *Journal of Physical and
3023 Chemical Reference Data* 38(2), 101–125.
- 3024 Hungate, B. A., J. S. Dukes, M. R. Shaw, Y. Luo, and C. B. Field (2003).
3025 Nitrogen and climate change. *Science* 302(5650), 1512–1513.
- 3026 IPCC (2021). *Climate Change 2021: The Physical Science Basis. Contribution
3027 of Working Group I to the Sixth Assessment Report of the Intergovernmental
3028 Panel on Climate Change*, Volume In Press. Cambridge, United Kingdom
3029 and New York, NY, USA: Cambridge University Press.
- 3030 Johnson, N. C., J. H. Graham, and F. A. Smith (1997). Functioning of mycor-
3031 rhizal associations along the mutualism-parasitism continuum. *New Phytol-*
3032 *ogist* 135(4), 575–585.
- 3033 Kachurina, O. M., H. Zhang, W. R. Raun, and E. G. Krenzer (2000). Simul-
3034 taneous determination of soil aluminum, ammonium- and nitrate- nitrogen
3035 using 1 M potassium chloride. *Communications in Soil Science and Plant
3036 Analysis* 31(7-8), 893–903.
- 3037 Kaiser, C., M. R. Kilburn, P. L. Clode, L. Fuchslueger, M. Koranda, J. B. Cliff,

- 3038** Z. M. Solaiman, and D. V. Murphy (2015). Exploring the transfer of recent
3039 plant photosynthates to soil microbes: mycorrhizal pathway vs direct root
3040 exudation. *New Phytologist* 205(4), 1537–1551.
- 3041** Katabuchi, M. (2015). LeafArea: An R package for rapid digital analysis of leaf
3042 area. *Ecological Research* 30(6), 1073–1077.
- 3043** Kattge, J. and W. Knorr (2007). Temperature acclimation in a biochemical
3044 model of photosynthesis: a reanalysis of data from 36 species. *Plant, Cell*
3045 and *Environment* 30(9), 1176–1190.
- 3046** Kattge, J., W. Knorr, T. Raddatz, and C. Wirth (2009). Quantifying photosyn-
3047 thetic capacity and its relationship to leaf nitrogen content for global-scale
3048 terrestrial biosphere models. *Global Change Biology* 15(4), 976–991.
- 3049** Kayler, Z., A. Gessler, and N. Buchmann (2010). What is the speed of link
3050 between aboveground and belowground processes? *New Phytologist* 187(4),
3051 885–888.
- 3052** Kayler, Z., C. Keitel, K. Jansen, and A. Gessler (2017). Experimental evi-
3053 dence of two mechanisms coupling leaf-level C assimilation to rhizosphere
3054 CO₂ release. *Environmental and Experimental Botany* 135,
3055 21–26.
- 3056** Keeling, C. D., W. G. Mook, and P. P. Tans (1979, jan). Recent trends in the
3057 ¹³C/¹²C ratio of atmospheric carbon dioxide.
3058 *Nature* 277(5692), 121–123.
- 3059** Kenward, M. G. and J. H. Roger (1997). Small sample inference for fixed effects
3060 from restricted maximum likelihood. *Biometrics* 53(3), 983.

- 3061** Knapp, A. K., M. L. Avolio, C. Beier, C. J. W. Carroll, S. L. Collins, J. S.
3062 Dukes, L. H. Fraser, R. J. Griffin-Nolan, D. L. Hoover, A. Jentsch, M. E.
3063 Loik, R. P. Phillips, A. K. Post, O. E. Sala, I. J. Slette, L. Yahdjian, and
3064 M. D. Smith (2017). Pushing precipitation to the extremes in distributed
3065 experiments: recommendations for simulating wet and dry years. *Global
Change Biology* 23(5), 1774–1782.
- 3067** Knorr, W. (2000). Annual and interannual CO₂ exchanges of the
3068 terrestrial biosphere: process-based simulations and uncertainties. *Global
Ecology and Biogeography* 9(3), 225–252.
- 3070** Knorr, W. and M. Heimann (2001). Uncertainties in global terrestrial biosphere
3071 modeling: 1. A comprehensive sensitivity analysis with a new photosynthesis
3072 and energy balance scheme. *Global Biogeochemical Cycles* 15(1), 207–225.
- 3073** Kulmatiski, A., P. B. Adler, J. M. Stark, and A. T. Tredennick (2017). Water
3074 and nitrogen uptake are better associated with resource availability than
3075 root biomass. *Ecosphere* 8(3), e01738.
- 3076** Lavergne, A., D. Sandoval, V. J. Hare, H. Graven, and I. C. Prentice (2020).
3077 Impacts of soil water stress on the acclimated stomatal limitation of pho-
3078 tosynthesis: Insights from stable carbon isotope data. *Global Change Biol-
ogy* 26(12), 7158–7172.
- 3080** Lawrence, D. M., R. A. Fisher, C. D. Koven, K. W. Oleson, S. C. Swen-
3081 son, G. B. Bonan, N. Collier, B. Ghimire, L. Kampenhout, D. Kennedy,
3082 E. Kluzek, P. J. Lawrence, F. Li, H. Li, D. L. Lombardozzi, W. J. Riley,
3083 W. J. Sacks, M. Shi, M. Vertenstein, W. R. Wieder, C. Xu, A. A. Ali,
3084 A. M. Badger, G. Bisht, M. Broeke, M. A. Brunke, S. P. Burns, J. Buzan,

- 3085 M. Clark, A. Craig, K. M. Dahlin, B. Drewniak, J. B. Fisher, M. Flanner,
3086 A. M. Fox, P. Gentine, F. M. Hoffman, G. Keppel-Aleks, R. Knox, S. Ku-
3087 mar, J. Lenaerts, L. R. Leung, W. H. Lipscomb, Y. Lu, A. Pandey, J. D.
3088 Pelletier, J. Perket, J. T. Randerson, D. M. Ricciuto, B. M. Sanderson,
3089 A. Slater, Z. M. Subin, J. Tang, R. Q. Thomas, M. Val Martin, and X. Zeng
3090 (2019). The Community Land Model Version 5: description of new features,
3091 benchmarking, and impact of forcing uncertainty. *Journal of Advances in*
3092 *Modeling Earth Systems* 11(12), 4245–4287.
- 3093 LeBauer, D. S. and K. K. Treseder (2008). Nitrogen limitation of net primary
3094 productivity. *Ecology* 89(2), 371–379.
- 3095 Lefcheck, J. S. (2016). piecewiseSEM: Piecewise structural equation modelling
3096 in r for ecology, evolution, and systematics. *Methods in Ecology and Evolu-*
3097 *tion* 7(5), 573–579.
- 3098 Lenth, R. (2019). emmeans: estimated marginal means, aka least-squares
3099 means.
- 3100 Li, W., H. Zhang, G. Huang, R. Liu, H. Wu, C. Zhao, and N. G. McDowell
3101 (2020). Effects of nitrogen enrichment on tree carbon allocation: A global
3102 synthesis. *Global Ecology and Biogeography* 29(3), 573–589.
- 3103 Liang, J., X. Qi, L. Souza, and Y. Luo (2016). Processes regulating progressive
3104 nitrogen limitation under elevated carbon dioxide: a meta-analysis. *Biogeosciences*
3105 13(9), 2689–2699.
- 3106 Liang, X., T. Zhang, X. Lu, D. S. Ellsworth, H. BassiriRad, C. You, D. Wang,
3107 P. He, Q. Deng, H. Liu, J. Mo, and Q. Ye (2020). Global response patterns of
3108 plant photosynthesis to nitrogen addition: A meta-analysis. *Global Change*

- 3109** *Biology* 26(6), 3585–3600.
- 3110** López, J., D. A. Way, and W. Sadok (2021). Systemic effects of rising atmo-
3111 spheric vapor pressure deficit on plant physiology and productivity. *Global*
3112 *Change Biology* 27(9), 1704–1720.
- 3113** Lu, J., J. Yang, C. Keitel, L. Yin, P. Wang, W. Cheng, and F. A. Dijkstra
3114 (2022). Belowground Carbon Efficiency for Nitrogen and Phosphorus Ac-
3115 quisition Varies Between *Lolium perenne* and *Trifolium repens* and Depends
3116 on Phosphorus Fertilization. *Frontiers in Plant Science* 13, 1–9.
- 3117** Luo, X., T. F. Keenan, J. M. Chen, H. Croft, I. C. Prentice, N. G. Smith,
3118 A. P. Walker, H. Wang, R. Wang, C. Xu, and Y. Zhang (2021). Global
3119 variation in the fraction of leaf nitrogen allocated to photosynthesis. *Nature*
3120 *Communications* 12(1), 4866.
- 3121** Luo, Y., W. S. Currie, J. S. Dukes, A. C. Finzi, U. A. Hartwig, B. A. Hungate,
3122 R. E. McMurtrie, R. Oren, W. J. Parton, D. E. Pataki, R. M. Shaw, D. R.
3123 Zak, and C. B. Field (2004). Progressive nitrogen limitation of ecosystem
3124 responses to rising atmospheric carbon dioxide. *BioScience* 54(8), 731–739.
- 3125** Maire, V., P. Martre, J. Kattge, F. Gastal, G. Esser, S. Fontaine, and J.-F.
3126 Soussana (2012). The coordination of leaf photosynthesis links C and N
3127 fluxes in C₃ plant species. *PLoS ONE* 7(6), e38345.
- 3128** Makino, A. (2003). Rubisco and nitrogen relationships in rice: leaf photosyn-
3129 thesis and plant growth. *Soil Science and Plant Nutrition* 49(3), 319–327.
- 3130** Makino, A., M. Harada, T. Sato, H. Nakano, and T. Mae (1997). Growth and N
3131 Allocation in Rice Plants under CO₂ Enrichment. *Plant Physiology* 115(1),

- 3132** 199–203.
- 3133** Markham, J. H. and C. Zekveld (2007). Nitrogen fixation makes biomass al-
- 3134** location to roots independent of soil nitrogen supply. *Canadian Journal of*
- 3135** *Botany* (9), 787–793.
- 3136** Marschner, H. and B. Dell (1994). Nutrient uptake in mycorrhizal symbiosis.
- 3137** *Plant and Soil* 159(1), 89–102.
- 3138** Matamala, R. and W. H. Schlesinger (2000). Effects of elevated atmospheric
- 3139** CO₂ on fine root production and activity in an intact tem-
- 3140** perate forest ecosystem. *Global Change Biology* 6(8), 967–979.
- 3141** Medlyn, B. E., E. Dreyer, D. S. Ellsworth, M. Forstreuter, P. C. Harley,
- 3142** M. U. F. Kirschbaum, X. Le Roux, P. Montpied, J. Strassmeyer, A. Wal-
- 3143** croft, K. Wang, and D. Loustau (2002). Temperature response of parameters
- 3144** of a biochemically based model of photosynthesis. II. A review of experimen-
- 3145** tal data. *Plant, Cell and Environment* 25(9), 1167–1179.
- 3146** Menge, D. N. L., S. A. Levin, and L. O. Hedin (2008). Evolutionary tradeoffs can
- 3147** select against nitrogen fixation and thereby maintain nitrogen limitation.
- 3148** *Proceedings of the National Academy of Sciences* 105(5), 1573–1578.
- 3149** Menne, M. J., I. Durre, R. S. Vose, B. E. Gleason, and T. G. Houston (2012).
- 3150** An overview of the global historical climatology network-daily database.
- 3151** *Journal of Atmospheric and Oceanic Technology* 29(7), 897–910.
- 3152** Meyerholt, J., K. Sickel, and S. Zaehle (2020). Ensemble projections elucidate
- 3153** effects of uncertainty in terrestrial nitrogen limitation on future carbon up-
- 3154** take. *Global Change Biology* 26(7), 3978–3996.

- 3155** Meyerholt, J., S. Zaehle, and M. J. Smith (2016). Variability of pro-
3156 jected terrestrial biosphere responses to elevated levels of atmospheric
3157 CO₂ due to uncertainty in biological nitrogen fixation. *Bio-*
3158 *geosciences* 13(5), 1491–1518.
- 3159** Minocha, R., S. Long, A. H. Magill, J. D. Aber, and W. H. McDowell (2000).
3160 Foliar free polyamine and inorganic ion content in relation to soil and soil
3161 solution chemistry in two fertilized forest stands at the Harvard Forest,
3162 Massachusetts. *Plant and Soil* 222(1-2), 119–137.
- 3163** Moore, D. J., S. Aref, R. M. Ho, J. S. Pippen, J. G. Hamilton, and E. H. De
3164 Lucia (2006). Annual basal area increment and growth duration of *Pinus*
3165 *taeda* in response to eight years of free-air carbon dioxide enrichment. *Global*
3166 *Change Biology* 12(8), 1367–1377.
- 3167** Morgan, J. A., D. E. Pataki, C. Körner, H. Clark, S. J. Del Grosso, J. M.
3168 Grünzweig, A. K. Knapp, A. R. Mosier, P. C. D. Newton, P. A. Niklaus,
3169 J. B. Nippert, R. S. Nowak, W. J. Parton, H. W. Polley, and M. R. Shaw
3170 (2004). Water relations in grassland and desert ecosystems exposed to ele-
3171 vated atmospheric CO₂. *Oecologia* 140(1), 11–25.
- 3172** Muñoz, N., X. Qi, M. W. Li, M. Xie, Y. Gao, M. Y. Cheung, F. L. Wong, and
3173 H.-M. Lam (2016). Improvement in nitrogen fixation capacity could be part
3174 of the domestication process in soybean. *Heredity* 117(2), 84–93.
- 3175** Nadelhoffer, K. J. and J. W. Raich (1992). Fine root production estimates and
3176 belowground carbon allocation in forest ecosystems. *Ecology* 73(4), 1139–
3177 1147.
- 3178** Niinemets, Ü. and J. D. Tenhunen (1997). A model separating leaf struc-

- 3179 tural and physiological effects on carbon gain along light gradients for the
3180 shade-tolerant species *< i>Acer saccharum</i>*. *Plant, Cell and Environment* 20(7), 845–866.
- 3182 Norby, R. J., J. Ledford, C. D. Reilly, N. E. Miller, and E. G. O'Neill
3183 (2004). Fine-root production dominates response of a deciduous forest to
3184 atmospheric CO₂ enrichment. *Proceedings of the National Academy of Sci-*
3185 *ences* 101(26), 9689–9693.
- 3186 Norby, R. J., J. M. Warren, C. M. Iversen, B. E. Medlyn, and R. E. Mc-
3187 Murtrie (2010). CO₂ enhancement of forest productivity constrained by
3188 limited nitrogen availability. *Proceedings of the National Academy of Sci-*
3189 *ences* 107(45), 19368–19373.
- 3190 Novick, K. A., D. L. Ficklin, P. C. Stoy, C. A. Williams, G. Bohrer, A. C.
3191 Oishi, S. A. Papuga, P. D. Blanken, A. Noormets, B. N. Sulman, R. L.
3192 Scott, L. Wang, and R. P. Phillips (2016). The increasing importance of
3193 atmospheric demand for ecosystem water and carbon fluxes. *Nature Climate
3194 Change* 6(11), 1023–1027.
- 3195 Noyce, G. L., M. L. Kirwan, R. L. Rich, and J. P. Megonigal (2019). Asyn-
3196 chronous nitrogen supply and demand produce nonlinear plant allocation
3197 responses to warming and elevated CO₂. *Proceedings of the*
3198 *National Academy of Sciences* 116(43), 21623–21628.
- 3199 Onoda, Y., K. Hikosaka, and T. Hirose (2004). Allocation of nitrogen to
3200 cell walls decreases photosynthetic nitrogen-use efficiency. *Functional Ecol-*
3201 *ogy* 18(3), 419–425.
- 3202 Onoda, Y., I. J. Wright, J. R. Evans, K. Hikosaka, K. Kitajima, Ü. Niinemets,

- 3203** H. Poorter, T. Tosens, and M. Westoby (2017). Physiological and structural
3204 trade-offs underlying the leaf economics spectrum. *New Phytologist* 214(4),
3205 1447–1463.
- 3206** Oren, R., J. S. Sperry, G. G. Katul, D. E. Pataki, B. E. Ewers, N. Phillips,
3207 and K. V. R. Schäfer (1999). Survey and synthesis of intra- and interspecific
3208 variation in stomatal sensitivity to vapor pressure deficit. *Plant, Cell and*
3209 *Environment* 22(12), 1515–1526.
- 3210** Oreskes, N., K. Shrader-Frechette, and K. Belitz (1994). Verification, vali-
3211 dation, and confirmation of numerical models in the Earth sciences. *Sci-
ence* 263(5147), 641–646.
- 3213** Paillassa, J., I. J. Wright, I. C. Prentice, S. Pepin, N. G. Smith, G. Ethier,
3214 A. C. Westerband, L. J. Lamarque, H. Wang, W. K. Cornwell, and V. Maire
3215 (2020). When and where soil is important to modify the carbon and water
3216 economy of leaves. *New Phytologist* 228(1), 121–135.
- 3217** Parvin, S., S. Uddin, S. Tausz Posch, R. Armstrong, and M. Tausz (2020). Car-
3218 bon sink strength of nodules but not other organs modulates photosynthesis
3219 of faba bean (*Vicia faba*) grown under elevated [CO₂] and different
3220 water supply. *New Phytologist* 227(1), 132–145.
- 3221** Paul, K. I., P. J. Polglase, A. M. O'Connell, J. C. Carlyle, P. J. Smethurst, and
3222 P. K. Khanna (2003). Defining the relation between soil water content and
3223 net nitrogen mineralization. *European Journal of Soil Science* 54(1), 39–48.
- 3224** Peng, Y., K. J. Bloomfield, L. A. Cernusak, T. F. Domingues, and I. C. Pre-
3225 nttice (2021). Global climate and nutrient controls of photosynthetic capacity.
3226 *Communications Biology* 4(1), 462.

- 3227** Perkowski, E. A., E. F. Waring, and N. G. Smith (2021). Root mass carbon
3228 costs to acquire nitrogen are determined by nitrogen and light availability
3229 in two species with different nitrogen acquisition strategies. *Journal of*
3230 *Experimental Botany* 72(15), 5766–5776.
- 3231** Phillips, R. P., E. R. Brzostek, and M. G. Midgley (2013). The mycorrhizal-
3232 associated nutrient economy: a new framework for predicting carbon-
3233 nutrient couplings in temperate forests. *New Phytologist* 199(1), 41–51.
- 3234** Phillips, R. P., A. C. Finzi, and E. S. Bernhardt (2011). Enhanced root ex-
3235 udation induces microbial feedbacks to N cycling in a pine forest under
3236 long-term CO₂ fumigation. *Ecology Letters* 14(2), 187–194.
- 3237** Pinheiro, J. and D. Bates (2022). nlme: linear and nonlinear mixed effects
3238 models.
- 3239** Poggio, L., L. M. De Sousa, N. H. Batjes, G. B. M. Heuvelink, B. Kempen,
3240 E. Ribeiro, and D. Rossiter (2021). SoilGrids 2.0: Producing soil information
3241 for the globe with quantified spatial uncertainty. *Soil* 7(1), 217–240.
- 3242** Pons, T. L. and R. W. Pearcy (1994). Nitrogen reallocation and photosynthetic
3243 acclimation in response to partial shading in soybean plants. *Physiologia*
3244 *Plantarum* 92(4), 636–644.
- 3245** Poorter, H., J. Bühler, D. Van Dusschoten, J. Climent, and J. A. Postma (2012).
3246 Pot size matters: A meta-analysis of the effects of rooting volume on plant
3247 growth. *Functional Plant Biology* 39(11), 839–850.
- 3248** Poorter, H., O. Knopf, I. J. Wright, A. A. Temme, S. W. Hogewoning, A. Graf,
3249 L. A. Cernusak, and T. L. Pons (2022). A meta-analysis of responses of C₃

- 3250 plants to atmospheric CO₂: dose-response curves for 85 traits ranging from
3251 the molecular to the whole-plant level. *New Phytologist* 233(4), 1560–1596.
- 3252 Prentice, I. C., N. Dong, S. M. Gleason, V. Maire, and I. J. Wright (2014).
3253 Balancing the costs of carbon gain and water transport: testing a new theo-
3254 retical framework for plant functional ecology. *Ecology Letters* 17(1), 82–91.
- 3255 Prentice, I. C., X. Liang, B. E. Medlyn, and Y.-P. Wang (2015). Reliable, ro-
3256 bust and realistic: The three R's of next-generation land-surface modelling.
3257 *Atmospheric Chemistry and Physics* 15, 5987–6005.
- 3258 Priestley, C. H. B. and R. J. Taylor (1972). On the Assessment of Surface
3259 Heat Flux and Evaporation Using Large-Scale Parameters. *Monthly Weather
3260 Review* 100(2), 81–92.
- 3261 Querejeta, J. I., I. Prieto, C. Armas, F. Casanoves, J. S. Diémé, M. Diouf,
3262 H. Yossi, B. Kaya, F. I. Pugnaire, and G. M. Rusch (2022). Higher leaf
3263 nitrogen content is linked to tighter stomatal regulation of transpiration
3264 and more efficient water use across dryland trees. *New Phytologist* 235(4),
3265 1351–1364.
- 3266 R Core Team (2021). R: A language and environment for statistical computing.
- 3267 Raich, J. W., D. A. Clark, L. Schwendenmann, and T. E. Wood (2014). Above-
3268 ground tree growth varies with belowground carbon allocation in a tropical
3269 rainforest environment. *PLoS ONE* 9(6), e100275.
- 3270 Rastetter, E. B., P. M. Vitousek, C. B. Field, G. R. Shaver, D. Herbert, and
3271 G. I. Ågren (2001). Resource optimization and symbiotic nitrogen fixation.
3272 *Ecosystems* 4(4), 369–388.

- 3273** Reich, P. B. (2014). The world-wide 'fast-slow' plant economics spectrum: a
3274 traits manifesto. *Journal of Ecology* 102(2), 275–301.
- 3275** Reich, P. B., S. E. Hobbie, T. Lee, D. S. Ellsworth, J. B. West, D. Tilman,
3276 J. M. H. Knops, S. Naeem, and J. Trost (2006). Nitrogen limitation con-
3277 strains sustainability of ecosystem response to CO₂. *Nature* 440(7086), 922–925.
- 3278**
- 3279** Reichman, G. A., D. L. Grunes, and F. G. Viets (1966). Effect of Soil Mois-
3280 ture on Ammonification and Nitrification in Two Northern Plains Soils. *Soil*
3281 *Science Society of America Journal* 30(3), 363–366.
- 3282** Rhine, E. D., R. L. Mulvaney, E. J. Pratt, and G. K. Sims (1998). Improving
3283 the Berthelot reaction for determining ammonium in soil extracts and water.
3284 *Soil Science Society of America Journal* 62(2), 473.
- 3285** Rogers, A. (2014). The use and misuse of V_{cmax} in Earth System Models. *Pho-*
3286 *tosynthesis Research* 119(1-2), 15–29.
- 3287** Rogers, A., B. E. Medlyn, J. S. Dukes, G. B. Bonan, S. Caemmerer, M. C.
3288 Dietze, J. Kattge, A. D. B. Leakey, L. M. Mercado, Ü. Niinemets, I. C.
3289 Prentice, S. P. Serbin, S. Sitch, D. A. Way, and S. Zaehle (2017). A roadmap
3290 for improving the representation of photosynthesis in Earth system models.
3291 *New Phytologist* 213(1), 22–42.
- 3292** Saathoff, A. J. and J. Welles (2021). Gas exchange measurements in the un-
3293 steady state. *Plant Cell and Environment* 44(11), 3509–3523.
- 3294** Sage, R. F. and R. W. Pearcy (1987). The nitrogen use efficiency of C₃ and C₄
3295 plants: I. Leaf nitrogen, growth, and biomass partitioning in *Chenopodium*

- 3296 *album* (L.) and *Amaranthus retroflexus* (L.). *Plant Physiology* 84(3), 954–
3297 958.
- 3298 Saleh, A. M., M. Abdel-Mawgoud, A. R. Hassan, T. H. Habeeb, R. S. Yehia,
3299 and H. AbdElgawad (2020). Global metabolic changes induced by arbuscular
3300 mycorrhizal fungi in oregano plants grown under ambient and elevated levels
3301 of atmospheric CO₂. *Plant Physiology and Biochemistry* 151, 255–263.
- 3302 Saxton, K. E. and W. J. Rawls (2006). Soil water characteristic estimates by
3303 texture and organic matter for hydrologic solutions. *Soil Science Society of
3304 America Journal* 70(5), 1569–1578.
- 3305 Schaefer, K., C. R. Schwalm, C. Williams, M. A. Arain, A. Barr, J. M. Chen,
3306 K. J. Davis, D. Dimitrov, T. W. Hilton, D. Y. Hollinger, E. Humphreys,
3307 B. Poulter, B. M. Racza, A. D. Richardson, A. Sahoo, P. Thornton, R. Var-
3308 gas, H. Verbeeck, R. Anderson, I. Baker, T. A. Black, P. Bolstad, J. Chen,
3309 P. S. Curtis, A. R. Desai, M. C. Dietze, D. Dragoni, C. M. Gough, R. F.
3310 Grant, L. Gu, A. K. Jain, C. Kucharik, B. E. Law, S. Liu, E. Lokipitiya,
3311 H. A. Margolis, R. Matamala, J. H. McCaughey, R. Monson, J. W. Munger,
3312 W. Oechel, C. Peng, D. T. Price, D. Ricciuto, W. J. Riley, N. Roulet,
3313 H. Tian, C. Tonitto, M. Torn, E. Weng, and X. Zhou (2012). A model-
3314 data comparison of gross primary productivity: Results from the North
3315 American Carbon Program site synthesis. *Journal of Geophysical Research:
3316 Biogeosciences* 117(G3), G03010.
- 3317 Schmitt, M. R. and G. E. Edwards (1981). Photosynthetic capacity and nitrogen
3318 use efficiency of maize, wheat, and rice: A comparison between C₃ and C₄
3319 photosynthesis. *Journal of Experimental Botany* 32(3), 459–466.

- 3320** Schneider, C. A., W. S. Rasband, and K. W. Eliceiri (2012). NIH Image to
3321 ImageJ: 25 years of image analysis. *Nature Methods* 9(7), 671–675.
- 3322** Scott, H. G. and N. G. Smith (2022). A Model of C4 Photosynthetic Acclimation
3323 Based on Least-Cost Optimality Theory Suitable for Earth System Model
3324 Incorporation. *Journal of Advances in Modeling Earth Systems* 14(3), 1–16.
- 3325** Shi, M., J. B. Fisher, E. R. Brzostek, and R. P. Phillips (2016). Carbon cost
3326 of plant nitrogen acquisition: Global carbon cycle impact from an improved
3327 plant nitrogen cycle in the Community Land Model. *Global Change Biology*
3328 22(3), 1299–1314.
- 3329** Shi, M., J. B. Fisher, R. P. Phillips, and E. R. Brzostek (2019). Neglecting
3330 plant–microbe symbioses leads to underestimation of modeled climate im-
3331 pacts. *Biogeosciences* 16(2), 457–465.
- 3332** Smith, B., D. Wärldin, A. Arneth, T. Hickler, P. Leadley, J. Siltberg, and
3333 S. Zaehle (2014). Implications of incorporating N cycling and N limitations
3334 on primary production in an individual-based dynamic vegetation model.
3335 *Biogeosciences* 11(7), 2027–2054.
- 3336** Smith, N. G. and J. S. Dukes (2013). Plant respiration and photosynthesis in
3337 global-scale models: incorporating acclimation to temperature and CO₂.
3338 *Global Change Biology* 19(1), 45–63.
- 3339** Smith, N. G. and T. F. Keenan (2020). Mechanisms underlying leaf photosyn-
3340 thetic acclimation to warming and elevated CO₂ as inferred from least-cost
3341 optimality theory. *Global Change Biology* 26(9), 5202–5216.
- 3342** Smith, N. G., T. F. Keenan, I. C. Prentice, H. Wang, I. J. Wright, Ü. Niinemets,

- 3343** K. Y. Crous, T. F. Domingues, R. Guerrieri, F. oko Ishida, J. Kattge, E. L.
3344 Kruger, V. Maire, A. Rogers, S. P. Serbin, L. Tarvainen, H. F. Togashi,
3345 P. A. Townsend, M. Wang, L. K. Weerasinghe, and S.-X. Zhou (2019).
3346 Global photosynthetic capacity is optimized to the environment. *Ecology*
3347 *Letters* 22(3), 506–517.
- 3348** Smith, N. G., D. L. Lombardozzi, A. Tawfik, G. B. Bonan, and J. S. Dukes
3349 (2017). Biophysical consequences of photosynthetic temperature acclimation
3350 for climate. *Journal of Advances in Modeling Earth Systems* 9(1), 536–547.
- 3351** Smith, N. G., S. L. Malyshev, E. Shevliakova, J. Kattge, and J. S. Dukes
3352 (2016). Foliar temperature acclimation reduces simulated carbon sensitivity
3353 to climate. *Nature Climate Change* 6(4), 407–411.
- 3354** Smith, S. E. and D. J. Read (2008). *Mycorrhizal Symbiosis*. Academic Press.
- 3355** Soil Survey Staff (2022). Web Soil Survey.
- 3356** Soudzilovskaia, N. A., J. C. Douma, A. A. Akhmetzhanova, P. M. van Bode-
3357 gom, W. K. Cornwell, E. J. Moens, K. K. Treseder, and J. H. C. Cornelissen
3358 (2015). Global patterns of plant root colonization intensity by mycorrhizal
3359 fungi explained by climate and soil chemistry. *Global Ecology and Biogeogra-*
3360 *phy* 24(3), 371–382.
- 3361** Stark, J. M. and M. K. Firestone (1995). Mechanisms for soil moisture ef-
3362 fects on activity of nitrifying bacteria. *Applied and Environmental Microbi-*
3363 *ology* 61(1), 218–221.
- 3364** Stocker, B. D., H. Wang, N. G. Smith, S. P. Harrison, T. F. Keenan, D. San-
3365 doval, T. Davis, and I. C. Prentice (2020). P-model v1.0: An optimality-

- 3366** based light use efficiency model for simulating ecosystem gross primary pro-
3367 duction. *Geoscientific Model Development* 13(3), 1545–1581.
- 3368** Stocker, B. D., J. Zscheischler, T. F. Keenan, I. C. Prentice, J. Peñuelas, and
3369 S. I. Seneviratne (2018). Quantifying soil moisture impacts on light use
3370 efficiency across biomes. *New Phytologist* 218(4), 1430–1449.
- 3371** Sulman, B. N., D. T. Roman, K. Yi, L. Wang, R. P. Phillips, and K. A.
3372 Novick (2016). High atmospheric demand for water can limit forest car-
3373 bon uptake and transpiration as severely as dry soil. *Geophysical Research*
3374 *Letters* 43(18), 9686–9695.
- 3375** Sulman, B. N., E. Shevliakova, E. R. Brzostek, S. N. Kivlin, S. L. Malyshev,
3376 D. N. L. Menge, and X. Zhang (2019). Diverse mycorrhizal associations
3377 enhance terrestrial C storage in a global model. *Global Biogeochemical Cy-
3378 cles* 33(4), 501–523.
- 3379** Sweet, S. K., D. W. Wolfe, A. DeGaetano, and R. Benner (2017). Anatomy
3380 of the 2016 drought in the Northeastern United States: Implications for
3381 agriculture and water resources in humid climates. *Agricultural and Forest*
3382 *Meteorology* 247, 571–581.
- 3383** Taylor, B. N. and D. N. L. Menge (2018). Light regulates tropical symbiotic
3384 nitrogen fixation more strongly than soil nitrogen. *Nature Plants* 4(9), 655–
3385 661.
- 3386** Terrer, C., S. Vicca, B. A. Hungate, R. P. Phillips, and I. C. Prentice (2016).
3387 Mycorrhizal association as a primary control of the CO₂ fertilization effect.
3388 *Science* 353(6294), 72–74.

- 3389 Terrer, C., S. Vicca, B. D. Stocker, B. A. Hungate, R. P. Phillips, P. B. Reich,
3390 A. C. Finzi, and I. C. Prentice (2018). Ecosystem responses to elevated CO₂
3391 governed by plant–soil interactions and the cost of nitrogen acquisition. *New
3392 Phytologist* 217(2), 507–522.
- 3393 Thieurmel, B. and A. Elmarhraoui (2019). suncalc: Compute sun position,
3394 sunlight phases, moon position, and lunar phase.
- 3395 Thomas, R. Q., E. N. J. Brookshire, and S. Gerber (2015). Nitrogen limita-
3396 tion on land: how can it occur in Earth system models? *Global Change
3397 Biology* 21(5), 1777–1793.
- 3398 Thomas, R. Q., S. Zaehle, P. H. Templer, and C. L. Goodale (2013). Global pat-
3399 terns of nitrogen limitation: confronting two global biogeochemical models
3400 with observations. *Global Change Biology* 19(10), 2986–2998.
- 3401 Thornton, P. E., J.-F. Lamarque, N. A. Rosenbloom, and N. M. Mahowald
3402 (2007). Influence of carbon-nitrogen cycle coupling on land model response
3403 to CO₂ fertilization and climate variability. *Global Bioge-
3404 ochemical Cycles* 21(4), GB4018.
- 3405 Tingey, D. T., D. L. Phillips, and M. G. Johnson (2000). Elevated CO₂ and
3406 conifer roots: effects on growth, life span and turnover. *New Phytolo-
3407 gist* 147(1), 87–103.
- 3408 Udvardi, M. and P. S. Poole (2013). Transport and metabolism in legume-
3409 rhizobia symbioses. *Annual Review of Plant Biology* 64, 781–805.
- 3410 USDA NRCS (2022). The PLANTS Database.
- 3411 Uselman, S. M., R. G. Qualls, and R. B. Thomas (2000). Effects of increased

- 3412** atmospheric CO₂, temperature, and soil N availability on root exudation
3413 of dissolved organic carbon by an N-fixing tree (*Robinia pseudoacacia* L.).
3414 *Plant and Soil* 222, 191–202.
- 3415** van Diepen, L. T. A., E. A. Lilleskov, K. S. Pregitzer, and R. M. Miller (2007).
3416 Decline of arbuscular mycorrhizal fungi in northern hardwood forests ex-
3417 posed to chronic nitrogen additions. *New Phytologist* 176(1), 175–183.
- 3418** Vance, C. P. and G. H. Heichel (1991). Carbon in N₂ fixation: Limitation or
3419 exquisite adaptation. *Annual Review of Plant Physiology and Plant Molec-*
3420 *ular Biology* 42(1), 373–392.
- 3421** Viet, H. D., J.-H. Kwak, K.-S. Lee, S.-S. Lim, M. Matsushima, S. X. Chang,
3422 K.-H. Lee, and W.-J. Choi (2013). Foliar chemistry and tree ring δ¹³C of
3423 *Pinus densiflora* in relation to tree growth along a soil pH gradient. *Plant*
3424 *and Soil* 363(1-2), 101–112.
- 3425** Vitousek, P. M., K. Cassman, C. C. Cleveland, T. Crews, C. B. Field, N. B.
3426 Grimm, R. W. Howarth, R. Marino, L. Martinelli, E. B. Rastetter, and
3427 J. I. Sprent (2002). Towards an ecological understanding of biological nitro-
3428 gen fixation. In *The Nitrogen Cycle at Regional to Global Scales*, pp. 1–45.
3429 Springer Netherlands.
- 3430** Vitousek, P. M. and R. W. Howarth (1991). Nitrogen limitation on land and in
3431 the sea: How can it occur? *Biogeochemistry* 13(2), 87–115.
- 3432** Vitousek, P. M., S. Porder, B. Z. Houlton, and O. A. Chadwick (2010).
3433 Terrestrial phosphorus limitation: mechanisms, implications, and nitro-
3434 gen–phosphorus interactions. *Ecological Applications* 20(1), 5–15.

- 3435** Walker, A. P., A. P. Beckerman, L. Gu, J. Kattge, L. A. Cernusak, T. F.
3436 Domingues, J. C. Scales, G. Wohlfahrt, S. D. Wullschleger, and F. I. Woodward (2014). The relationship of leaf photosynthetic traits - V_{cmax} and J_{max} - to leaf nitrogen, leaf phosphorus, and specific leaf area: a meta-analysis and modeling study. *Ecology and Evolution* 4(16), 3218–3235.
- 3440** Wang, H., I. C. Prentice, T. F. Keenan, T. W. Davis, I. J. Wright, W. K.
3441 Cornwell, B. J. Evans, and C. Peng (2017). Towards a universal model for
3442 carbon dioxide uptake by plants. *Nature Plants* 3(9), 734–741.
- 3443** Wang, H., I. C. Prentice, I. J. Wright, D. I. Warton, S. Qiao, X. Xu, J. Zhou,
3444 Kikuzawa, and N. C. Stenseth (2023). Leaf economics fundamentals explained by optimality principles. *Science Advances* 9(3), eadd566.
- 3446** Wang, J., J. M. Knops, C. E. Brassil, and C. Mu (2017). Increased productivity
3447 in wet years drives a decline in ecosystem stability with nitrogen additions
3448 in arid grasslands. *Ecology* 98(7), 1779–1786.
- 3449** Wang, W., Y. Wang, G. Hoch, Z. Wang, and J. Gu (2018). Linkage of root mor-
3450 phology to anatomy with increasing nitrogen availability in six temperate
3451 tree species. *Plant and Soil* 425(1-2), 189–200.
- 3452** Weatherburn, M. W. (1967). Phenol-hypochlorite reaction for determination of
3453 ammonia. *Analytical Chemistry* 39(8), 971–974.
- 3454** Wellburn, A. R. (1994). The spectral determination of chlorophylls a and b, as
3455 well as total carotenoids, using various solvents with spectrophotometers of
3456 different resolution. *Journal of Plant Physiology* 144(3), 307–313.
- 3457** Wen, Z., P. J. White, J. Shen, and H. Lambers (2022). Linking root exuda-

- 3458** tion to belowground economic traits for resource acquisition. *New Phytologist* 233(4), 1620–1635.
- 3459**
- 3460** Westerband, A. C., I. J. Wright, V. Maire, J. Paillassa, I. C. Prentice, O. K.
- 3461** Atkin, K. J. Bloomfield, L. A. Cernusak, N. Dong, S. M. Gleason, C. Guil-
- 3462** herme Pereira, H. Lambers, M. R. Leishman, Y. Malhi, and R. H. Nolan
- 3463** (2023). Coordination of photosynthetic traits across soil and climate gradi-
- 3464** ents. *Global Change Biology* 29(3), 1–29.
- 3465** Wieder, W. R., C. C. Cleveland, W. K. Smith, and K. Todd-Brown (2015).
- 3466** Future productivity and carbon storage limited by terrestrial nutrient avail-
- 3467** ability. *Nature Geoscience* 8(6), 441–444.
- 3468** Wieder, W. R., D. M. Lawrence, R. A. Fisher, G. B. Bonan, S. J. Cheng, C. L.
- 3469** Goodale, A. S. Grandy, C. D. Koven, D. L. Lombardozzi, K. W. Oleson,
- 3470** and R. Q. Thomas (2019). Beyond static benchmarking: using experimental
- 3471** manipulations to evaluate land model assumptions. *Global Biogeochemical*
- 3472** *Cycles* 33(10), 1289–1309.
- 3473** Wright, I. J., P. B. Reich, and M. Westoby (2003). Least-cost input mixtures
- 3474** of water and nitrogen for photosynthesis. *The American Naturalist* 161(1),
- 3475** 98–111.
- 3476** Wright, I. J., P. B. Reich, M. Westoby, D. D. Ackerly, Z. Baruch, F. Bongers,
- 3477** J. Cavender-Bares, T. Chapin, J. H. C. Cornelissen, M. Diemer, J. Flexas,
- 3478** E. Garnier, P. K. Groom, J. Gulias, K. Hikosaka, B. B. Lamont, T. Lee,
- 3479** W. Lee, C. Lusk, J. J. Midgley, M.-L. Navas, Ü. Niinemets, J. Oleksyn,
- 3480** N. Osada, H. Poorter, P. Poot, L. Prior, V. I. Pyankov, C. Roumet, S. C.
- 3481** Thomas, M. G. Tjoelker, E. J. Veneklaas, and R. Villar (2004). The world-

- 3482 wide leaf economics spectrum. *Nature* 428(6985), 821–827.
- 3483 Xu-Ri and I. C. Prentice (2017). Modelling the demand for new nitrogen fixation
- 3484 by terrestrial ecosystems. *Biogeosciences* 14(7), 2003–2017.
- 3485 Yahdjian, L., L. A. Gherardi, and O. E. Sala (2011). Nitrogen limitation in
- 3486 arid-subhumid ecosystems: A meta-analysis of fertilization studies. *Journal*
- 3487 *of Arid Environments* 75(8), 675–680.
- 3488 Zaehle, S., B. E. Medlyn, M. G. De Kauwe, A. P. Walker, M. C. Dietze, T. Hick-
- 3489 ler, Y. Luo, Y. P. Wang, B. El-Masri, P. Thornton, A. Jain, S. Wang,
- 3490 D. Warlind, E. Weng, W. Parton, C. M. Iversen, A. Gallet-Budynek, H. Mc-
- 3491 carthy, A. C. Finzi, P. J. Hanson, I. C. Prentice, R. Oren, and R. J. Norby
- 3492 (2014). Evaluation of 11 terrestrial carbon-nitrogen cycle models against
- 3493 observations from two temperate Free-Air CO₂ Enrichment studies. *New*
- 3494 *Phytologist* 202(3), 803–822.
- 3495 Zaehle, S., S. Sitch, B. Smith, and F. Hatterman (2005). Effects of parame-
- 3496 ter uncertainties on the modeling of terrestrial biosphere dynamics. *Global*
- 3497 *Biogeochemical Cycles* 19(3), GB3020.
- 3498 Zhu, Q., W. J. Riley, J. Tang, N. Collier, F. M. Hoffman, X. Yang, and G. Bisht
- 3499 (2019). Representing nitrogen, phosphorus, and carbon interactions in the
- 3500 E3SM land model: development and global benchmarking. *Journal of Ad-*
- 3501 *vances in Modeling Earth Systems* 11(7), 2238–2258.
- 3502 Ziegler, C., M. E. Dusenge, B. Nyirambangutse, E. Zibera, G. Wallin, and
- 3503 J. Uddling (2020). Contrasting Dependencies of Photosynthetic Capacity
- 3504 on Leaf Nitrogen in Early- and Late-Successional Tropical Montane Tree
- 3505 Species. *Frontiers in Plant Science* 11, 1–12.

- 3506** Ziehn, T., J. Kattge, W. Knorr, and M. Scholze (2011). Improving the pre-
3507 dictability of global CO₂ assimilation rates under climate change. *Geophysical Research Letters* 38(10), L10404.
3508